

DISSERTATION

CHARACTERIZING THE ROLE OF THE HEC1 TAIL DOMAIN AT THE  
KINETOCHORE-MICROTUBULE INTERFACE IN HUMAN CELLS

Submitted by

Robert T. Wimbish

Department of Biochemistry and Molecular Biology

In partial fulfillment of the requirements

For the Degree of Doctor of Philosophy

Colorado State University

Fort Collins, Colorado

Fall 2020

Doctoral Committee:

Advisor: Jennifer DeLuca

Steven Markus  
Anireddy Reddy  
Eric Ross

Copyright by Robert T. Wimbish 2020

All Rights Reserved

## ABSTRACT

### CHARACTERIZING THE ROLE OF THE HEC1 TAIL DOMAIN AT THE KINETOCHORE-MICROTUBULE INTERFACE IN HUMAN CELLS

Chromosome segregation is powered by interactions between the mitotic spindle and kinetochores. Kinetochores – large, protein-rich machines built on the centromere of each sister chromatid – must bind to spindle microtubules and harness the forces from their dynamic instability to drive chromosome movement. This interaction must be robust enough to ensure chromosomes remain bound to the growing and shrinking microtubule polymers, yet must also be reversible: incorrectly oriented kinetochore-microtubule attachments can cause chromosome mis-segregation leading to aneuploidy, which can be catastrophic for the newly formed cell. Thus, cells must be able to actively regulate the strength with which kinetochores bind to spindle microtubules – such a regulatory scheme ensures that incorrect attachments can be released, and correct attachments can be preferentially stabilized. The direct linkage between kinetochores and microtubules is the highly conserved, kinetochore-anchored NDC80 complex. This complex is also an effector of attachment strength regulation; specifically, the N-terminal “tail” region of the NDC80 complex subunit Highly expressed in cancer 1 (Hec1) is a target for phosphorylation by the Aurora family of kinases, which ultimately weakens kinetochore-microtubule attachments.

Here, we investigate the molecular basis for kinetochore-microtubule attachment regulation in human cells. We find that Hec1 tail phosphorylation regulates kinetochore-microtubule attachments independently of the spindle and kinetochore associated (Ska)

complex, a critical factor for attachment stability, contrary to previous reports that the two pathways are functionally coupled. We additionally map the domains of the NDC80 complex required for its coordination with Ska complexes to strengthen attachments. We also find that the Hec1 tail domain is dispensable for the initial formation of kinetochore-microtubule attachments, but provide evidence it plays a role in force generation. We further interrogate this role and how phosphorylation of the tail regulates attachment formation and force generation, and find that the length requirements for these functions of the tail are different. Moreover, we demonstrate that the phosphoregulatory pathway for attachment regulation is deficient for short tails, suggesting a new model for the means by which attachments are regulated. Together these results provide novel insight into how attachments between chromosomes and the spindle are formed and regulated, and how errors in this process can lead to chromosome mis-segregation.

## ACKNOWLEDGEMENTS

I am immensely grateful to Jennifer DeLuca for investing and believing in me through both my successes and failures in the lab. The countless meetings in her office drawing NDC80 diagrams on her whiteboard, texting her about an exciting result, or speculating about the dynamics of a specific protein-protein interaction, are some of my most fond memories from the lab. She has been instrumental to my development as both a scientist and a professional, and I owe much of the way I think about molecular biology to her mentorship.

Throughout this process, I have been fortunate to have worked alongside so many talented and helpful people in the DeLuca lab. Keith DeLuca taught me many technical skills that I will carry with me through my career, Jack Himes made me realize how much you can learn about yourself when you are training someone (in addition to being a great help during a time when experiments were piling up), and I always had incredible emotional support from Amanda Broad and Hazheen Shirnekhi – they were like sisters to me throughout this process, and I am grateful that we transitioned from co-workers to friends. The contributions of Jeanne Mick cannot be understated – she was alongside me (if not out in front of me) for many cloning and protein purification projects, and I am especially indebted to her for her help and kindness in these final few months.

In the biochemistry department, I am grateful to my committee members Steven, Eric, and Reddy for their helpful contributions to my research and for helping me grow as a scientist and orator. Additionally, I want to thank my rotation mentors, Santiago Di Pietro, Andrea Ambrosio, and Tim Stasevich, for being some of my first exposure into the cell biology world and investing their time into my development.

In addition to my co-workers, I have been lucky to have the most incredible support system throughout this process. Ciccio and Tatsuya have both been wonderful examples of dedication to science while living to the fullest; I am lucky to call them my friends and will reminisce fondly on our time together in the lab and the mountains. Lydia has always felt like my “big sister” in science, and living with her and Sam has truly been one of the highlights of my time in Colorado – they are the closest thing to family that I have here.

Finally, I have to thank my family. My “G mama”, Dorothy Wimbish, has been a huge support to me in many ways, and her kindness and generosity are an example I hope to one day emulate. My siblings Emily, David, and Christiane have been vocally supportive since day one, and their passions have been an inspiration that drives my own ambition. My parents, John and Sandra, have been most impacted by the collateral that comes with doing a PhD – I am grateful to them for being understanding amidst all of the canceled plans, missed holidays, and unanswered phone calls. I could not have done this without their love and support.

## TABLE OF CONTENTS

ABSTRACT.....	ii
ACKNOWLEDGEMENTS.....	v
CHAPTER 1: INTRODUCTION.....	1
1.1: Mitotic Cell Division and the Chromosome Segregation Machinery.....	1
1.2: Kinetochore-Microtubule Attachments and the NDC80 Complex.....	4
1.3: Phospho-regulation of Kinetochore-Microtubule Attachments.....	6
1.4: The Hec1 Tail Domain and Microtubule Dynamics.....	10
1.5: Hec1 Tail Contribution to NDC80 Complex-Microtubule Binding <i>in vitro</i> .....	14
1.6: Hec1 Tail Contribution to Kinetochore-Microtubule Attachments in Cells....	16
1.7: Compensation for Hec1 Tail Function by Co-factors.....	18
1.8: Mechanistic Perspectives of Hec1 Tail-Mediated Attachment Stabilization and Regulation.....	19
1.8a: Models for Attachment Stabilization and Regulation by Direct Tail Domain-Microtubule Binding.....	20
1.8b: Models for Attachment Stabilization and Regulation by NDC80 Complex Oligomerization.....	23
1.8c: Models for Attachment Stabilization and Regulation by Co-factor Recruitment.....	25
1.9 Thesis Rationale.....	28

CHAPTER 2: MULTI-DOMAIN REQUIREMENTS FOR FORCE GENERATION AND SKA RECRUITMENT TO KINETOCHORES BY THE NDC80 COMPLEX.....	30
2.1: Introduction.....	30
2.2: Results.....	35
2.3: Discussion.....	75
2.4: Methods.....	86
 CHAPTER 3: REQUIREMENTS FOR ATTACHMENT REGULATION AND TENSION GENERATION BY THE HEC1 TAIL DOMAIN.....	97
3.1: Introduction.....	97
3.2: Results.....	101
3.3: Discussion.....	124
3.4: Methods.....	138
 CHAPTER 4: CONCLUSIONS AND FUTURE DIRECTIONS.....	146
4.1: Summary and Relevance.....	146
4.2: Insight into NDC80-Ska complex coordination and future directions.....	146
4.3: Insight into Hec1 loop domain function and future directions.....	150
4.4: Insight into Hec1 tail domain function and future directions.....	152
4.5: Insight into regulation of attachment strength by the Hec1 tail domain and future directions.....	154
4.6: Insight into the effects of blocking Hec1 tail phosphorylation and future directions.....	155
4.7: Evolutionary perspective on Hec1/Ndc80 tail function.....	157

REFERENCES.....162

## CHAPTER 1: INTRODUCTION

1

### **1.1 Mitotic Cell Division and the Chromosome Segregation Machinery**

Mitotic cell division is required for the health and proliferation of all eukaryotic life: single- and multi-cellular organisms alike depend on the formation of new cells to grow, regenerate, and propagate their genes. Critical to this process is the ability of the dividing mother cell to equally partition its duplicated genome between two newly formed daughter cells, thus ensuring each new cell has a full complement of DNA. Prior to mitotic entry, the duplicated genome compacts into dense, highly ordered structures called chromosomes. Simultaneously, the cellular cytoskeleton undergoes a dramatic rearrangement to form the mitotic spindle, a large microtubule-based machine specialized for moving chromosomes. Successful division of the genome requires that the duplicated chromosomes congress to the equator of the cell where they are poised to be segregated. The mitotic spindle then exerts forces on the chromosomes as the identical sister chromatids separate, moving them toward opposite ends of the spindle and ultimately resulting in equal partitioning of the genetic material into daughter cells.

---

<sup>1</sup> The majority of this chapter was published as a review in February 2020 under the title, “Hec1/Ndc80 Tail Domain Function at the Kinetochores-Microtubule Interface.” I have added new sections and removed parts of the published manuscript where appropriate for clarity.

JGD and I researched, wrote, and edited the manuscript together.

Wimbish RT, and DeLuca, JG. 2020. Hec1/Ndc80 tail domain function at the kinetochores-microtubule interface. *Frontiers Reviews Cell and Developmental Biology*, 31: 1453-1473

Congression and segregation of mitotic chromosomes relies on interactions between spindle microtubules and kinetochores, which are comprised of a large number of proteins and multi-protein complexes assembled on regions of centromeric heterochromatin within each sister chromatid (Figure 1.1 A and B). Kinetochores face the challenging task of directly binding to the highly dynamic microtubule plus ends and tracking with them as they undergo cycles of polymerization and depolymerization. By doing so, kinetochores are able to harness the forces generated by microtubule dynamics to power chromosome movements that result in their alignment at the spindle equator in metaphase, and their subsequent movement toward the spindle poles in anaphase. Critically, kinetochore-microtubule attachments of a specific orientation must form in order for chromosomes to be equally divided into the daughter cells. Early in mitosis, microtubules stochastically “probe” for chromosomes, which are scattered throughout the cytoplasm in a disordered array. As a result, incorrect attachments often form between kinetochores and microtubules – for example, both kinetochores of a pair of sister chromatids may bind to microtubules emanating from the same spindle pole (Figure 1.2 A). If such erroneous attachments were to persist into anaphase, they would result in mis-segregation of chromosomes. It is therefore critical that kinetochores regulate the strength with which they bind microtubules to ensure that incorrect attachments are released, and correct attachments are stabilized, thereby preventing chromosome mis-segregation at mitotic exit (Figure 1.2 B). Thus, two critical functions of kinetochores are to form force-transducing attachments to spindle microtubules, and to temporally regulate the strength with which they bind to microtubules to facilitate error correction.

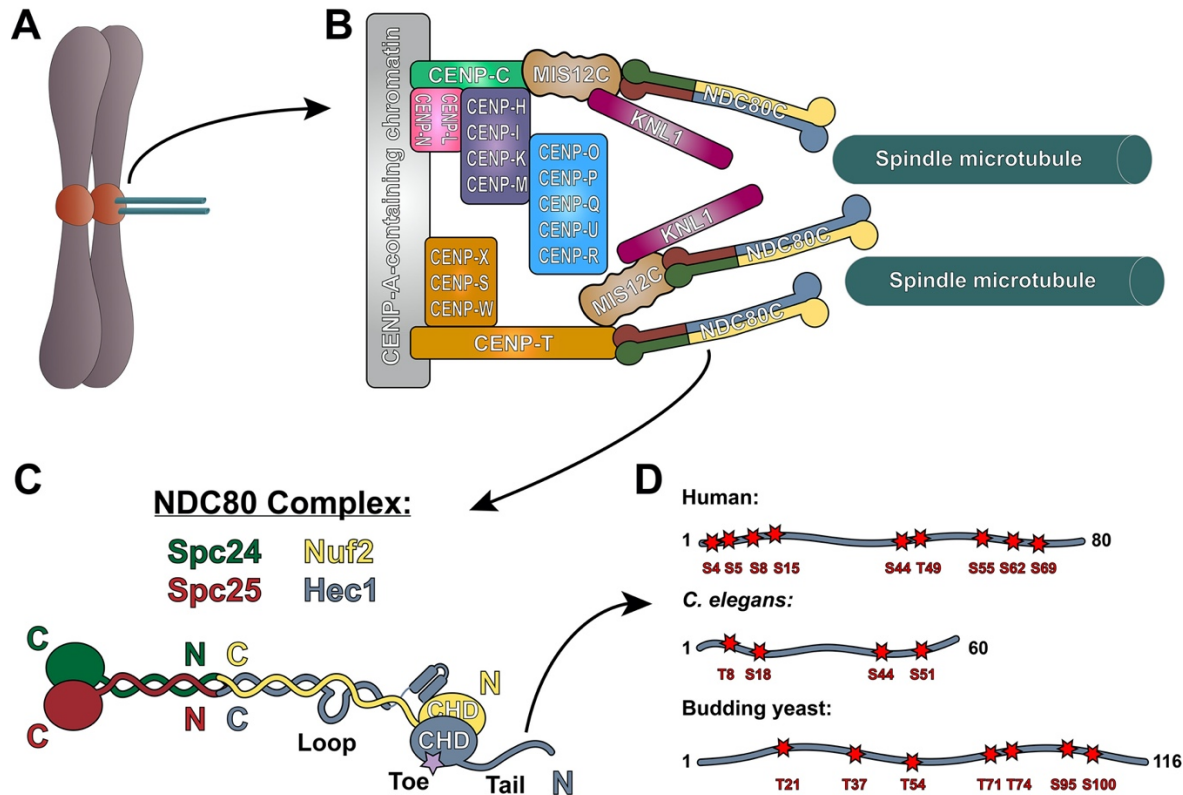


**Figure 1.1. The NDC80 complex at the kinetochore-microtubule interface.** (A) Mitotic chromosome. (B) Organization of the kinetochore-microtubule interface in vertebrate cells. The foundation of the kinetochore is the CCAN, or the Constitutive Centromere Associated Network, which binds to CENP-A-containing centromeric chromatin. The CCAN is composed of 16 subunits, organized in multiple subcomplexes including: CENP-L/N; CENP-O/P/Q/U/R; CENP-H/I/K/M; CENP-T/W/S/X; and CENP-C. CENP-C recruits the KMN “network” (composed of KNL1, the MIS12 complex, and the NDC80 complex) through its direct association with the MIS12 complex. CENP-T also recruits the NDC80 complex alone, as well as the KMN network through binding the MIS12 complex. (C) Architecture of the NDC80 complex. The C-termini of Spc24 (green) and Spc25 (red) form the kinetochore-targeting domain which binds either the MIS12 complex or CENP-T. The N-terminal regions of Spc24 and Spc25 form a coiled-coil domain that tetramerizes with the C-termini of Nuf2 (yellow) and Hec1 (blue). The N-terminus of Hec1 is comprised of a well-ordered CH domain, which contains the high affinity microtubule-binding “toe” region, and the tail domain which is also implicated in microtubule binding. The ~40 amino acid loop domain of Hec1 is also indicated on the schematic. (D) Representation of the Hec1/Ndc80 tail domains from human, *Caenorhabditis elegans*, and the budding yeast *Saccharomyces cerevisiae*. Shown are the mapped and putative Aurora kinase phosphorylation sites. The human sites shown are Ser4, Ser5, Ser8, Ser15, Ser44, Thr49, Ser55, Ser62, and Ser69. The *C. elegans* sites shown are Thr8, Ser18, Ser44, and Ser51. The budding yeast sites shown are Thr21, Ser37, Thr54, Thr71, Thr74, Ser95, and Ser100 (see text for references).

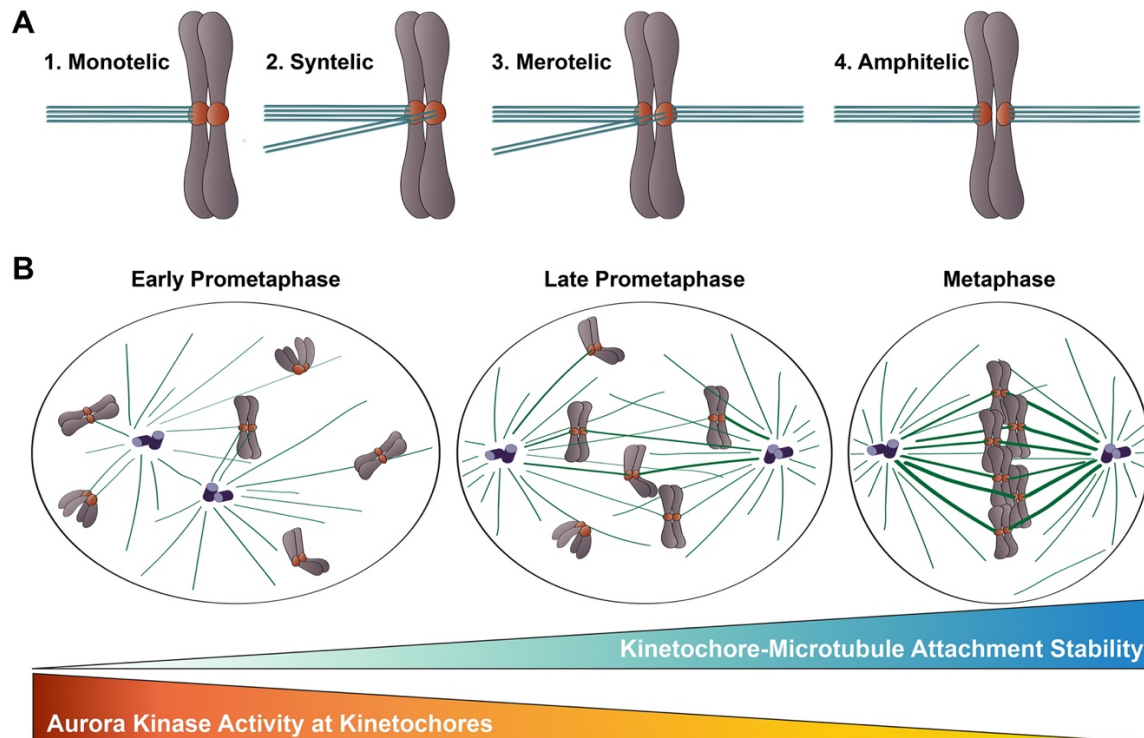


**Figure 1.2. Kinetochores-microtubule attachments during mitosis.** (A) Types of kinetochores-microtubule attachments. (1) Monotelic attachment: one sister kinetochore is attached to microtubules from one spindle pole and one sister is unattached; (2) Syntelic attachment: both sister kinetochores are attached to microtubules emanating from the same spindle pole; (3) Merotelic attachment: one sister kinetochore is attached to microtubules from both spindle poles; and (4) Amphitelic attachment (correct): one sister kinetochore is attached to microtubules from one pole and one sister kinetochore is attached to microtubules from the opposite pole. (B) Chromosome congression during mitotic progression. In early prometaphase, kinetochores-microtubule attachments errors are common, kinetochores-microtubule attachments are short-lived and labile, and Aurora B kinase activity at kinetochores is high. As mitosis progresses, erroneous kinetochores-microtubule attachments are corrected, kinetochores-microtubule attachments become long-lived and stable, and Aurora B kinase activity at kinetochores decreases.

## 1.2 Kinetochores-Microtubule Attachments and the NDC80 Complex

At the core of the kinetochore's force-transducing microtubule binding activity is the NDC80 complex, a hetero-tetrameric protein complex comprised of Hec1 (also called Ndc80), Nuf2, Spc24, and Spc25. Extending roughly 60 nm in length, the NDC80 complex is a dumbbell-shaped structure with two globular domains on each end,

connected by a central coiled-coil shaft (Ciferri et al., 2005, 2008; Wei et al., 2005, 2006; Wang et al., 2008; Figure 1.1 C). At one end of the complex, the C-terminal domains of Spc24 and Spc25 each adopt a RWD (RING finger, WD repeat, DEAD-like helicase) fold, through which they associate with either the Mis12 complex (bound to CENP-C or CENP-T) or CDK1-phosphorylated CENP-T to anchor the NDC80 complex to the kinetochore (Wei et al., 2006; Ciferri et al., 2008; Petrovic et al., 2010; Malvezzi et al., 2013; Nishino et al., 2013; Huis in't Veld et al., 2016; Hara et al., 2018; Figure 1.1 B). The N-terminal regions of Spc24 and Spc25 form a coiled-coil domain, which associates with the long coiled-coil domain of the Hec1/Nuf2 dimer at a tetramerization junction (Ciferri et al., 2005; Wei et al., 2005; Valverde et al., 2016). The Hec1/Nuf2 coiled-coil domain, which accounts for nearly 40 nm of the NDC80 complex's length, is interrupted briefly by a ~40 amino acid region in Hec1, termed the "loop" domain (Figure 1.1 C; Maiolica et al., 2007). At the end of the NDC80 complex opposite the kinetochore-docking region, the N-termini of Hec1 and Nuf2 fold into a dimerized pair of globular calponin-homology (CH) domains (Wei et al., 2007; Ciferri et al., 2008), a conserved fold found in both actin and microtubule binding proteins (Slep et al., 2005; Sjöblom et al., 2008). The Hec1 CH domain contains a high-affinity microtubule binding site – termed the "toe" – that docks into the microtubule lattice between tubulin monomers at both the inter- and intra-dimer interfaces (Wilson-Kubalek et al., 2008; Alushin et al., 2010; Figure 1.1 C). In all organisms tested to date, mutations in this region – even single point mutations – abolish kinetochore-microtubule interactions in cells and significantly weaken NDC80 complex-microtubule binding *in vitro* (Ciferri et al., 2008; Sundin et al., 2011; Tooley et al., 2011; Cheerambathur et al., 2013; Lampert

et al., 2013). At its extreme N-terminus, Hec1 contains a positively charged, unstructured region that varies in length from ~60–116 amino acids, depending on the organism (Figure 1.1 D). A large body of work in cells and *in vitro* has demonstrated that this N-terminal region – termed the Hec1 “tail” domain – plays at least two distinct roles in kinetochore function: (1) phosphorylation of the tail by the Aurora family of kinases regulates kinetochore-microtubule attachment stability; and (2) the tail contributes to the establishment and maintenance of force-generating kinetochore-microtubule attachments in cells. Evidence for these two functions of the Hec1 tail domain is summarized in the sections below, and key questions pertaining to the rationale behind this thesis are highlighted. Broadly, it has remained unclear if these two functions of the Hec1 tail are conserved across species, as its contribution to these processes appears to differ between organisms. Additionally, key outstanding questions remain regarding how the Hec1 tail contributes to kinetochore-microtubule attachments and how these attachments are mechanistically regulated.

### **1.3 Phospho-regulation of Kinetochore-Microtubule Attachments**

As mentioned above, a critical function of kinetochores is to adjust the strength with which they bind to spindle microtubules to control kinetochore-microtubule attachment stability. In early mitosis, kinetochore-microtubule attachments are unstable and undergo rapid turnover as a consequence, thus enabling improper attachments to be “reset” until correct, amphitelic attachments are established (Figure 1.2 A). As mitosis progresses, the number of microtubules bound to each kinetochore increases, leading to stable attachments that can harness the forces generated by microtubule dynamics

to drive chromosome movement (Zhai et al., 1995; Salmon et al., 2005; Cimini et al., 2006; DeLuca et al., 2006; Bakhoun et al., 2009; Godek et al., 2015; Figure 1.2 B). This increase in microtubule occupancy at each kinetochore also serves to silence the spindle assembly checkpoint, which is a quality-assurance mechanism cells use to prevent anaphase onset until all kinetochores are properly attached to spindle microtubules (Etemad et al., 2015; Krenn and Musacchio, 2015). Aurora B kinase, the enzymatic component of the Chromosomal Passenger Complex (CPC) that localizes to centromeres and kinetochores of mitotic chromosomes, has been recognized as the “master regulator” of kinetochore-microtubule attachment stability for almost 20 years. A large body of work in multiple organismal systems has demonstrated that Aurora B kinase activity at kinetochores promotes turnover of kinetochore-attached microtubules, which in turn, prevents premature stabilization and accumulation of erroneous attachments during mitosis (Biggins et al., 1999; Kallio et al., 2002; Murata-Hori and Wang, 2002; Tanaka et al., 2002; Ditchfield et al., 2003; Hauf et al., 2003; Lampson et al., 2004; Figure 1.2). The Hec1 tail domain has since been identified as a key substrate of Aurora B kinase, and numerous studies from the last decade provide compelling evidence that phosphorylation of this domain serves as a major effector of Aurora B kinase’s regulation of kinetochore-microtubule attachment stability in metazoan cells (Cheeseman et al., 2006; DeLuca et al., 2006, 2011, 2018; Nousiainen et al., 2006; Kettenbach et al., 2011).

Initial evidence for Hec1 tail-mediated phospho-regulation of kinetochore-microtubule attachment stability came from a study in PtK1 cells (derived from female rat kangaroo

kidney epithelium), in which cells were microinjected with an antibody directed to the N-terminus of Hec1 (DeLuca et al., 2006). Injected cells formed hyper-stable kinetochore-microtubule attachments, as evidenced by (1) increased kinetochore-microtubule lifetimes and inter-kinetochore distances (stretched centromeres), (2) a high frequency of kinetochore-microtubule attachment errors which persisted into anaphase, and (3) dampened kinetochore oscillations. *In vitro* kinase assays and mass spectrometry analysis revealed that a recombinantly expressed Hec1<sup>1-230</sup> fragment was phosphorylated by Aurora B kinase on multiple sites in its far N-terminal domain. Mutagenesis of these target sites to prevent phosphorylation partially recapitulated the microinjection results, suggesting that the injection phenotypes were, at least in part, due to loss of Hec1 tail domain phospho-regulation (DeLuca et al., 2006). These results were corroborated by subsequent studies in rat kangaroo, human, chicken, and *Caenorhabditis elegans* cells, in which Aurora B kinase target residues in the Hec1 tail were mutated to prevent phosphorylation (by Ala substitution) or to mimic phosphorylation (by substitution with either aspartic acid or glutamic acid). In these studies, preventing phosphorylation of the Hec1 tail resulted in hyper-stabilization of kinetochore-microtubule attachments, while mimicking phosphorylation led to unstable attachments in cells (Guimaraes et al., 2008; Welburn et al., 2010; DeLuca et al., 2011; Sundin et al., 2011; Cheerambathur et al., 2013; Zaytsev et al., 2014). Coincident with in-cell studies, *in vitro* microtubule binding experiments using recombinantly expressed, purified NDC80 complexes provided insight into the mechanism for this phospho-regulation. In the first of these, Cheeseman et al. (2006) demonstrated that purified *C. elegans* NDC80 complexes phosphorylated by Ipl1 (the budding yeast

Aurora kinase) bound microtubules with significantly lower affinity than unphosphorylated complexes. Subsequent studies reported similar decreases in binding affinity for microtubules *in vitro* using purified human NDC80 complexes assembled with mutants of Hec1 containing phospho-mimetic substitutions at Aurora B kinase target sites (Alushin et al., 2012; Umbreit et al., 2012; Zaytsev et al., 2015). Together, these *in vitro* and cell-based studies substantiate a model in which phosphorylation of the Hec1 tail domain decreases the affinity of the NDC80 complex for microtubules, which consequentially decreases the attachment strength between kinetochores and spindle microtubules (Figure 1.2 B).

### **1.3 Temporal Regulation of Hec1 Tail Domain Phosphorylation**

If kinetochore-microtubule attachment strength is temporally regulated through Hec1 phosphorylation, it follows that Hec1 phosphorylation itself must be temporally regulated. In 2011, phospho-specific antibodies were generated against four Aurora B kinase target sites in the Hec1 tail (Ser 8, Ser 15, Ser 44, and Ser 55), and were used to monitor phosphorylation levels at kinetochores during mitosis. All four sites were found to be phosphorylated at high levels in early prometaphase, and at much lower levels as cells progressed through metaphase and anaphase (DeLuca et al., 2011). Later studies found that expression of Hec1 mutants with increasing numbers of phospho-mimetic substitutions in the tail domain caused a corresponding decrease in kinetochore-microtubule attachment stability in cells (Zaytsev et al., 2014; Yoo et al., 2018; Etemad et al., 2019; Kuhn and Dumont, 2019). These findings were corroborated by *in vitro* data revealing a direct correlation between increasing number of phospho-mimetic

substitutions in the Hec1 tail domain in purified human NDC80 complexes and decreasing microtubule binding affinity (Zaytsev et al., 2015). Together, these studies support a model in which phosphorylation of the Hec1 tail “tunes” kinetochore-microtubule attachment stability in cells by modulating the binding properties of NDC80 complexes for microtubules (Figure 1.2 B).

One exception to this trend is the Ser at position 69 (Ser 69) in the human Hec1 tail domain. A recent study from our lab demonstrated that, in contrast to all other Aurora kinase sites investigated to date, Ser 69 remains phosphorylated throughout mitosis (DeLuca et al., 2018). Interestingly, mutagenically blocking phosphorylation of this site accelerates chromosome alignment, dampens chromosome oscillations, and leads to defective chromosome segregation, implicating a role for this site in maintenance of proper attachment dynamics. Furthermore, and in contrast to the aforementioned phospho-sites, Ser 69 is primarily phosphorylated by Aurora A kinase (DeLuca et al., 2018). Thus, maintenance of phosphorylation at this residue seems to play a role in preventing hyper-stable attachment formation.

#### **1.4 The Hec1 Tail Domain and Microtubule Dynamics**

In addition to the array of studies implicating a direct role for Hec1 tail phosphorylation in reducing kinetochore-microtubule attachment stability, there is evidence that these phospho-modifications may also impact the dynamic behavior of microtubule polymers at the kinetochore. Umbreit et al. (2012) demonstrated that recombinant human NDC80 complexes, when linked to beads at relatively high density, were able to track dynamic

microtubule ends *in vitro*, even when an external force was applied by an optical trap. This group also noted that the bead-bound NDC80 complexes promoted microtubule rescue events, in which microtubule ends switch from a state of depolymerization to one of polymerization. Rescue events were not observed with similarly bead-bound phospho-mimetic NDC80 mutant complexes (9D-Hec1, in which all nine Aurora kinase target sites in the tail domain are mutated to aspartic acid) (Umbreit et al., 2012). This inability to promote rescue events was not due to the fact that 9D-Hec1-containing NDC80 complexes bound more weakly to microtubules, because complexes lacking the entire Hec1 tail, which bound to microtubules as poorly as those containing 9D-Hec1, were capable of promoting some degree of rescue (Umbreit et al., 2012). These results bring to light the interesting possibility that phosphorylation of the Hec1 tail may not only promote release of kinetochore-bound microtubules, but may also promote plus-end microtubule depolymerization. This idea is consistent with an earlier study demonstrating that syntelically attached sister kinetochore pairs initiate Aurora B kinase-mediated error correction with rapid poleward movement along depolymerizing microtubules (Lampson et al., 2004). A role for Hec1 tail phosphorylation in kinetochore-mediated regulation of microtubule dynamics could also help explain the well-documented phenotype of dampened kinetochore oscillations in cells expressing non-phosphorylatable 9A-Hec1 mutants (DeLuca et al., 2011; Zaytsev et al., 2014; Long et al., 2017). Reduced kinetochore oscillatory behavior is typically attributed to hyper-stable kinetochore-microtubule attachments, which lead to increased frictional forces that ultimately reduce kinetochore mobility (DeLuca et al., 2011; Zaytsev et al., 2014; Long et al., 2017). It is also plausible, however, that preventing phosphorylation of

the Hec1 tail domain leads to increased rescue frequency, and thus decreases dynamics of the kinetochore-bound microtubules, which could result in dampened oscillations. Determining if the dynamic behavior of microtubule ends can be “tuned” *in vitro* by the phosphorylation state of the Hec1 tail domain would shed light on this interesting question.

In-cell and *in vitro* assays have allowed investigation into how phosphorylation of the Hec1 tail affects the ability of NDC80 complexes to track with and transduce forces from polymerizing and depolymerizing microtubules. In a recent study, Long et al. (2017) used laser ablation in PtK1 cells to sever metaphase kinetochore fibers and differentially induce sister kinetochores to move either poleward, along mostly depolymerizing microtubules, or anti-poleward, along mostly polymerizing microtubules, in order to investigate how Hec1 tail phosphorylation affects the tracking behavior of kinetochores. By quantitating kinetochore movements after laser ablation, the authors found that preventing Hec1 tail phosphorylation significantly decreased the velocity of sister kinetochores moving anti-poleward, while the velocity of those moving poleward was unaffected (Long et al., 2017). This led the authors to conclude that phosphorylation of the Hec1 tail regulates the kinetochore’s affinity for polymerizing, but not depolymerizing microtubules. *In vitro*, NDC80 complexes bind more weakly to depolymerizing microtubule ends than to polymerizing ends, and this has been attributed to a lower affinity of the Hec1 CH domain for curved microtubule protofilaments (which are formed at microtubule ends during depolymerization; McIntosh et al., 2008) than for straight protofilaments (Alushin et al., 2010; Schmidt et

al., 2013). Thus, it is possible that in cells, the majority of kinetochore-bound NDC80 complexes unbind from depolymerizing ends, and attachments are maintained by other kinetochore-associated microtubule binding proteins. Unbinding of NDC80 complexes from microtubules may explain why Long et al. (2017) found that the phosphorylation state of the tail domain does not impact velocities of kinetochores moving poleward. Recent experiments from Yoo et al. (2018), however, may argue against this idea. In their study, the authors employed FRET sensors (in tubulin and the Nuf2 subunit of the NDC80 complex) to measure the fraction of microtubule-bound NDC80 complexes during metaphase chromosome oscillations in human cells. While the authors reported a statistically significant decrease of microtubule-bound NDC80 complexes on poleward moving kinetochores (containing mostly depolymerizing microtubules) in comparison to those on anti-poleward moving kinetochores (containing mostly polymerizing microtubules), this difference was small (~11% change in NDC80 complex FRET fraction), especially compared to the FRET change measured in early prometaphase with respect to late metaphase (~50% change in FRET fraction; Yoo et al., 2018). These observations suggest that NDC80 complexes remain closely associated with the microtubule lattice on both the poleward and anti-poleward moving kinetochores of a sister pair. Furthermore, a recent study by Huis in't Veld et al. (2019) investigated how the phosphorylation state of the Hec1 tail domain impacted the ability of human NDC80 complexes to maintain attachments to depolymerizing microtubules *in vitro*. The authors reported that while the phosphorylation state of the tail did not affect the ability of trimerized, bead-bound NDC80 complexes to track with depolymerizing microtubules in the absence of tension, when a resisting force was applied with an optical trap,

phosphorylated NDC80 complexes detached from depolymerizing microtubules with significantly higher frequency than non-phosphorylated complexes (Huis in't Veld et al., 2019). These results suggest that, at least *in vitro*, Hec1 tail phosphorylation affects the ability of human NDC80 complexes under tension to transduce forces from depolymerizing microtubules. Why the phosphorylation state of the tail domain affects kinetochore movement along anti-poleward moving, but not poleward-moving kinetochores in cells remains an important unanswered question.

### **1.5 Hec1 Tail Contribution to NDC80 Complex-Microtubule Binding *in vitro***

In addition to its role in regulating kinetochore-microtubule attachment stability, the Hec1 tail domain is also implicated in the ability of NDC80 complexes to directly bind to microtubules. Using a variety of *in vitro* approaches, multiple studies have demonstrated that recombinant NDC80 complexes and Hec1-Nuf2 dimers exhibit reduced binding affinity for microtubules in the absence of the Hec1 tail domain. Notably, this has been reported for NDC80 complexes (or complex components) from all species tested to date. For example, Wei et al. (2007) found a 7–10X reduction in microtubule binding affinity for the CH domains of the budding yeast NDC80 complex components Hec1/Ndc80 and Nuf2 when the N-terminal 116 amino acid tail domain was deleted. Ciferri et al. (2008) characterized the binding affinity of a tail deletion mutant of an engineered version of the human tetrameric NDC80 complex (lacking the majority of the internal coiled-coil region, termed NDC80<sup>Bonsai</sup>) and demonstrated that tail-less complexes exhibited decreased co-sedimentation with microtubules, with calculated binding affinities of ~100X lower than wild-type complexes. These results reported for

human NDC80<sup>Bonsai</sup> complexes were later corroborated by Umbreit et al. (2012) using a TIRF-based fluorescence assay to characterize recombinantly expressed, full-length, GFP-tagged human NDC80 complexes. In population studies, NDC80 complexes lacking the Hec1 tail domain bound microtubules with ~9X decreased affinity, and in single molecule studies, tail-less complexes exhibited an ~14X increase in their dissociation rate from microtubules (Umbreit et al., 2012). A similar role for the tail was found using recombinant *C. elegans* NDC80 complexes, in which mutants lacking the N-terminal 60 amino acid Hec1/Ndc80 tail domain exhibited severely reduced microtubule binding affinity (Cheerambathur et al., 2013). Thus, the role of the tail domain in affecting the microtubule binding activity of the NDC80 complex appears to be conserved across species.

A recent study using engineered scaffolds to multimerize human NDC80 complexes has provided insight into how the tail domain might influence NDC80 complex-microtubule binding (Huis in't Veld et al., 2019). The authors of this study found that bead-bound NDC80 complexes lacking the Hec1 tail exhibited almost wild-type microtubule residence times, in situations in which the tail-less NDC80 complexes were oligomerized on the bead surface (Huis in't Veld et al., 2019). However, unlike wild-type complexes, these oligomerized tail-less NDC80 complexes were unable to track depolymerizing microtubule plus-ends. This effect may be due to the previously mentioned phenomenon that the NDC80 complex binds more weakly to curved, depolymerizing microtubule ends compared to straight, polymerizing ends (Alushin et al., 2010; Schmidt et al., 2013). Thus, the decreased microtubule binding affinity

resulting from deletion of the Hec1 tail is likely compensated for by complex oligomerization on stabilized or polymerizing microtubules, but not on depolymerizing microtubules.

### **1.6 Hec1 Tail Contribution to Kinetochore-Microtubule Attachments in Cells**

Although it is well established that the Hec1 tail domain contributes to high affinity microtubule binding *in vitro*, its role in forming stable kinetochore-microtubule attachments in cells is less clear. Budding yeast cells expressing Hec1/Ndc80 tail domain deletion mutants are viable, undergo normal chromosome segregation, and generate normal kinetochore-microtubule attachments (Kemmler et al., 2009; Demirel et al., 2012; Lampert et al., 2013). However, findings from a recent study indicate that the tail domain plays at least some role at the kinetochore-microtubule interface in this organism (Suzuki et al., 2016). By inserting a FRET-based sensor between the loop and CH domains of Hec1/Ndc80, the authors found that expression of the tail-less mutant resulted in decreased tension at the kinetochore-microtubule interface (Suzuki et al., 2016). They also noted that cells expressing the tail-less mutant experienced a prometaphase-to-anaphase delay, which led to a ~10% increase in mitotic index. Thus, while the tail domain is not explicitly required for kinetochore-microtubule attachment in budding yeast, it has a role in force production at the attachment interface. Consistent with observations in budding yeast, the Hec1/Ndc80 tail is not required for normal mitotic progression in *C. elegans*. Specifically, Cheerambathur et al. (2013) found that the kinetics of spindle pole separation in the first division of *C. elegans* embryos were unchanged in cells expressing Hec1/Ndc80 tail deletion mutants

compared to wild-type embryos, which is indicative of normal kinetochore-microtubule attachments. Interestingly, the authors reported that the tail was required for interaction between the NDC80 complex and the RZZ complex component ROD-1. RZZ binding to the Hec1/Ndc80 tail was shown to negatively regulate kinetochore-microtubule attachments by inhibiting NDC80 complex-microtubule binding. The authors propose this mechanism is important in early mitosis to prevent premature stabilization of kinetochore-microtubule attachments. A similar inhibitory scheme involving Rod, Dynein, and NDC80 complexes has recently been reported in human cells, but whether this interaction requires the Hec1 tail domain is not clear (Amin et al., 2018). Collectively, studies from budding yeast and *C. elegans* suggest that although the tail domain plays some role at the kinetochore-microtubule interface, it is not strictly required for productive attachments in cells.

In mammalian cells, the role of the Hec1 tail in generating stable kinetochore-microtubule attachments is not entirely resolved. Two studies published in 2008 reported that PtK1 and HeLa cells expressing Hec1 tail deletion mutants exhibited defects in chromosome alignment and mitotic progression, and failed to accumulate stable kinetochore-microtubule attachments (Guimaraes et al., 2008; Miller et al., 2008). More recent studies corroborated these findings by showing that expression of tail deletion mutants in HeLa cells leads to mitotic arrest and decreased inter-kinetochore distances (Etemad et al., 2015; Janczyk et al., 2017). In light of its requirement for high affinity NDC80 complex-microtubule interactions *in vitro*, these data led to the emergent view that the Hec1 tail domain is required for kinetochore-microtubule attachments in

mammalian cells. Why this domain is uniquely required in human cells, but not in other organisms, is unclear.

### **1.7 Compensation for Hec1 Tail Function by Co-factors**

Given the conserved role of the Hec1 tail domain in high affinity binding of NDC80 complexes to microtubules *in vitro*, an obvious question is why this domain is not ubiquitously required in cells – if budding yeast and *C. elegans* NDC80 complex require the tail for high-affinity microtubule binding, why is the tail dispensable for attachments in cells? One likely explanation for this discrepancy is the presence of compensatory cellular factors that are missing from *in vitro* reconstitution experiments. In the case of budding yeast, this factor is likely the Dam1 complex. As noted previously, budding yeast cells expressing tail-less Hec1/Ndc80 mutants are viable; however, simultaneous expression of Hec1/Ndc80 tail deletion mutants and loss-of-function Dam1 mutants renders cells inviable (Demirel et al., 2012; Lampert et al., 2013). Consistently, Suzuki et al. (2016) demonstrated that budding yeast cells expressing tail-less Hec1/Ndc80 mutants and wild-type Dam1 exhibit decreased force generation at the kinetochore-microtubule interface; however, in spite of this, wild-type inter-kinetochore distances were maintained, indicating the presence of stable kinetochore-microtubule attachments. This led the authors to conclude that the Dam1 complex is able to compensate for loss of the Hec1/Ndc80 tail, and becomes the primary load-bearing complex at kinetochores in the absence of this domain (Suzuki et al., 2016). These findings are consistent with results from *in vitro* studies in which the microtubule binding

activity of tail-less budding yeast NDC80 complexes is enhanced by the addition of Dam1 complexes (Lampert et al., 2010, 2013).

In the case of *C. elegans* and human cells, where the Dam1 complex is absent, compensation for Hec1 tail deletion may occur through the Ska complex. It has been appreciated for several years that the Ska complex is able to increase NDC80 complex-microtubule binding affinity, and to enable end-tracking of NDC80 complexes on depolymerizing microtubules *in vitro* (Schmidt et al., 2013). Recent studies have suggested that, like the budding yeast Dam1 complex, Ska complexes can compensate for loss of the Hec1/Ndc80 tail domain in NDC80 complex-microtubule interaction assays. For instance, Helgeson et al. (2018) used optical trapping assays to show that Ska complexes can impart almost wild-type end-tracking activity to tail-less NDC80 complex-coated beads on depolymerizing microtubules, even under applied force. Similarly, Huis in't Veld et al. (2019) demonstrated that Ska complexes can restore end-tracking activity to oligomerized tail-less complexes in the absence or presence of applied force. These results raise the possibility that the Ska complex may be able to – in part or in whole – functionally compensate for the Hec1 tail domain in *C. elegans* and human cells.

## **1.8 Mechanistic Perspectives of Hec1 Tail-Mediated Attachment Stabilization and Regulation**

There is compelling evidence that the Hec1 tail domain plays a central role in the regulation of kinetochore-microtubule attachment stability and in the generation of force-

transducing attachments between NDC80 complexes and microtubules during mitosis. Below we discuss three models, which are not mutually exclusive, that may explain how the Hec1 tail domain contributes to these critical mitotic functions.

### **1.8a Models for Attachment Stabilization and Regulation by Direct Tail Domain-Microtubule Binding**

One mechanism by which the Hec1 tail domain may promote NDC80 complex binding to microtubules is one in which the tail directly contacts the microtubule lattice, termed the direct binding model. The Hec1 tail domain is enriched in positively charged amino acids (isoelectric point  $\sim 11$ ), while the microtubule surface is enriched in negatively charged residues, many of which are within the unstructured C-terminal acidic tail domains of alpha and beta tubulin, which extend outward from the microtubule surface (Ponstingl et al., 1979; Sackett, 1995; Nogales et al., 1998, 1999; Löwe et al., 2001; Roll-Mecak, 2015). As such, electrostatic interactions may promote Hec1 tail-microtubule binding to provide an additional microtubule contact point within the NDC80 complex. Consistent with this prediction, isolated tail domain fragments from human Hec1 directly bind microtubules *in vitro* (Miller et al., 2008; Alushin et al., 2012), and removal of the C-terminal tubulin tails (via limited protease digestion) leads to reduced affinity of NDC80 complexes for microtubules (Ciferri et al., 2008). Furthermore, Tooley et al. (2011) demonstrated that NDC80 complexes containing Hec1 tail domain mutants in which ten positively charged Lys/Arg residues were substituted with neutral Ala residues bound to microtubules with reduced affinity compared to wild-type complexes. Expression of these “neutral tail” Hec1 mutants also compromised kinetochore-

microtubule attachments in cells (Tooley et al., 2011). Although these experiments support the notion that the Hec1 tail directly contacts the microtubule lattice, it is important to note that this domain is not sufficient for high-affinity NDC80-microtubule, or kinetochore-microtubule interactions. Notably, single point mutations in the Hec1 CH domain (within the “toe” domain) significantly reduce NDC80 complex-microtubule binding *in vitro*, and prevent formation of kinetochore-microtubule attachments in cells (Ciferri et al., 2008; Sundin et al., 2011; Tooley et al., 2011; Cheerambathur et al., 2013; Lampert et al., 2013). These defects in cells cannot be rescued by additional mutation of the Hec1 tail domain in which all Aurora B kinase target sites are mutated to prevent phosphorylation, which on its own results in hyper-stabilization of kinetochore-microtubule attachments (Sundin et al., 2011). An important question is why the NDC80 complex would require a second microtubule-binding site within the tail? One possibility is that in cells, a second microtubule binding domain would ensure that kinetochores remain bound to microtubules under conditions that might otherwise favor detachment. One such scenario might be poleward-moving kinetochores, where attached microtubules are predominantly depolymerizing, a state that may be unfavorable for microtubule binding by the Hec1 toe domain (Alushin et al., 2010; Schmidt et al., 2013).

The direct binding model has also been useful for explaining how phosphorylation of the tail domain regulates kinetochore-microtubule attachment stability. In this model, addition of phosphate groups by Aurora kinases, or introduction of phospho-mimetic mutations in the Hec1 tail – both of which reduce the positive charge of the tail – are predicted to decrease NDC80 complex-microtubule binding affinity *in vitro* (Figure 1.3

A). This is indeed the case (Cheeseman et al., 2006; Umbreit et al., 2012; Zaytsev et al., 2015). In fact, as mentioned above, NDC80 complexes with incrementally increasing numbers of phospho-mimetic substitutions in the Hec1 tail bind to microtubules with a corresponding step-wise decrease in affinity (Zaytsev et al., 2015). While data from numerous studies support a model in which phosphorylation of the Hec1 tail domain directly affects its interaction with microtubules, they do not rule out alternative NDC80 complex-intrinsic (i.e., in the absence of other factors) modes of regulating NDC80 complex-microtubule binding. For example, it is possible that the tail domain interacts directly with the Hec1 CH domain to influence CH domain-mediated microtubule binding. Given its contour length of  $\sim 25$  nm, this is indeed feasible. In such a model, phosphorylation of the tail may weaken kinetochore-microtubule attachments by enhancing the interaction between the Hec1 tail and CH domains, thereby preventing the CH domain from interacting with the microtubule lattice (Ciferri et al., 2008; Umbreit et al., 2012).

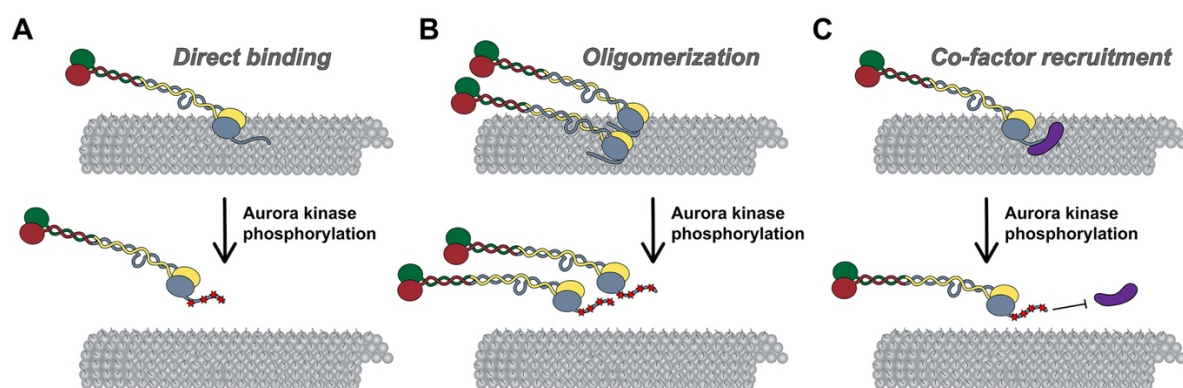


**Figure 1.3.** Models for Hec1 tail domain function. **(A)** Direct binding. In this model, the tail domain directly interacts with the microtubule lattice to increase CH-domain-mediated NDC80 complex-microtubule interactions. Phosphorylation of the Hec1 tail reduces the positive charge of the tail domain and as a result, reduces the affinity of NDC80 complexes for the negatively charged microtubule lattice. **(B)** Oligomerization.

In this model, a dephosphorylated tail domain functions to oligomerize adjacent NDC80 complexes, which promotes high affinity NDC80-complex-microtubule binding. Upon phosphorylation of the tail domain, complex oligomerization is no longer favored, possibly due to a decrease in affinity of a phosphorylated tail domain for a negatively charged region within the CH domain of Hec1. **(C) Co-factor recruitment.** In this model, a dephosphorylated Hec1 tail domain recruits kinetochore-associated microtubule binding proteins or protein complexes to promote high affinity NDC80 complex-microtubule binding. In contrast, a phosphorylated tail domain restricts co-factor recruitment. As discussed in the text, these models are not mutually exclusive.

## **1.8b Models for Attachment Stabilization and Regulation by NDC80 Complex**

### **Oligomerization**

Multiple studies have suggested that the Hec1 tail domain promotes NDC80 complex-microtubule binding by affecting oligomerization of NDC80 complexes (Figure 1.3 B; Alushin et al., 2010, 2012). It is well established that the NDC80 complex binds to microtubules in a cooperative manner (Ciferri et al., 2008; Alushin et al., 2010; Umbreit et al., 2012; Zaytsev et al., 2015; Helgeson et al., 2018), and that NDC80 complex oligomerization promotes high affinity interactions with microtubules (Powers et al., 2009; Volkov et al., 2018; Huis in't Veld et al., 2019). A structural study from Alushin et al. (2010) suggested that this propensity to self-associate may be mediated by the Hec1 tail domain. In this study, the authors employed cryo-EM to obtain high-resolution electron density maps of NDC80<sup>Bonsai</sup> complex-decorated microtubules that allowed for docking of the solved crystal structures of both tubulin and NDC80<sup>Bonsai</sup> lacking the Hec1 tail domain. Electron densities were observed between adjacent NDC80 complexes that were not present in the crystal structures, and therefore the authors attributed these densities to the Hec1 tail (Alushin et al., 2010). Additionally, they reported that NDC80 complexes bound to microtubules in clusters of ~6–8 complexes, and that deletion of the Hec1 tail reduced the number of complexes per cluster (Alushin

et al., 2010). In a subsequent study, the authors found that the tail domain contains two functionally distinct zones: zone one (amino acids 41–80), which contributes to both NDC80 complex oligomerization and microtubule binding; and zone two (amino acids 1–20), which contributes only to NDC80 complex oligomerization (Alushin et al., 2012). Hec1 tail phosphorylation has also been suggested to regulate NDC80 complex-microtubule binding affinity by modulating NDC80 complex oligomerization (Figure 1.3 B). Specifically, Alushin et al. (2012) found that the number of microtubule-bound NDC80 complexes per cluster decreased when the complexes contained phospho-mimetic substitutions in the Hec1 tail domain (Alushin et al., 2012). As a consequence, the authors proposed that NDC80 complex-NDC80 complex interactions – which promote high microtubule-binding affinity – are facilitated by tail dephosphorylation (Figure 1.3 B).

Although these studies support the notion that the Hec1 tail domain facilitates high affinity microtubule binding through phospho-regulated oligomerization of NDC80 complexes, several lines of evidence indicate that this may not be the case. For instance, multiple studies have reported that phospho-mimetic substitutions in the Hec1 tail decrease microtubule binding affinity of single NDC80 complexes independently of their oligomerization (Umbreit et al., 2012; Zaytsev et al., 2015). Furthermore, neither tail deletion nor phospho-mimetic mutants of Hec1 affect cooperative microtubule binding (Umbreit et al., 2012; Zaytsev et al., 2015), and tail-less human NDC80 complexes can still assemble into oligomers that bind microtubules with high affinity (Huis in't Veld et al., 2019). Thus, while it remains possible that the Hec1 tail domain –

and the phosphorylation state thereof – contributes to NDC80 complex oligomerization, it does not appear to be a critical effector for assembly or activity of NDC80 complex oligomers.

### **1.8c Models for Attachment Stabilization and Regulation by Co-factor**

#### **Recruitment**

In a third model, the Hec1 tail may regulate kinetochore-microtubule attachment stability in cells by recruiting additional microtubule-binding proteins to the kinetochore (Figure 1.3 C). During mitotic progression, several candidate factors localize to kinetochores coincident with Hec1 tail dephosphorylation and increased microtubule attachment stability. One of these is the Ska complex discussed above (Jeyaprasakash et al., 2012; Cheerambathur et al., 2017). In metazoan cells, the Ska complex loads to kinetochores in an NDC80 complex-dependent manner, where it contributes to the establishment of stable kinetochore-microtubule attachments and is required for silencing the spindle assembly checkpoint (Hanisch et al., 2006; Daum et al., 2009; Gaiatanos et al., 2009; Guimaraes and DeLuca, 2009; Raaijmakers et al., 2009; Theis et al., 2009; Auckland et al., 2017). In a recent EM study using recombinant human proteins, it was found that NDC80<sup>Bonsai</sup> complexes recruit “V”-shaped structures to the microtubules that were posited to be Ska complexes based on their size and shape (Jeyaprasakash et al., 2012; Janczyk et al., 2017). Mutagenesis of the C-terminal half of the Hec1 tail to reduce its positive charge reduced clustering of the microtubule-bound NDC80 complexes, and also the incidence of the “V”-shaped structures on microtubules (Janczyk et al., 2017). The authors correlated this finding with human cell

studies in which expression of this Hec1 mutant exhibited reduced kinetochore localization of the Ska complex. From this work, the authors concluded that the Hec1 tail plays a direct role in oligomerizing NDC80 complexes, and in recruiting the Ska complex to NDC80 complexes at the kinetochore-microtubule interface. These findings, however, contrast with a number of other studies that examined the Ska complex-NDC80 complex interaction. For example, several groups have reported that the tail domain of human Hec1 is dispensable for Ska complex-mediated enhancement of NDC80 complex-microtubule binding *in vitro* (Helgeson et al., 2018; Huis in't Veld et al., 2019) and for kinetochore recruitment of Ska complexes in *C. elegans* and human cells (Cheerambathur et al., 2017; Wimbish et al., 2020). Instead, evidence suggests that the Ska complex contacts the NDC80 complex within the extended coiled-coil domain. For instance, multiple studies have reported that NDC80<sup>Bonsai</sup> complexes, which are missing most of this internal coiled-coil, are unable to interact with Ska complexes (Zhang et al., 2017; Huis in't Veld et al., 2019; Wimbish et al., 2020), presumably because this region mediates the interaction, a notion supported by cross-linking/mass spectrometry data (Helgeson et al., 2018). Thus, although NDC80 complex oligomerization may be part of the mechanism by which Ska complexes enhance NDC80 complex-microtubule binding, this is likely a Hec1 tail-independent phenomenon.

The phosphorylation state of the Hec1 tail has also been implicated in regulating recruitment of the Ska complex to kinetochores (Figure 1.3 C). Expression of non-phosphorylatable Hec1/Ndc80 tail domain mutants in *C. elegans* embryos resulted in premature and enhanced recruitment of Ska complexes to kinetochores, as well as

hyper-stabilized kinetochore-microtubule attachments (Cheerambathur et al., 2017).

The authors found that these hyper-stable attachments could be rescued by depletion of Ska complexes, suggesting that dephosphorylation of the tail strengthens microtubule attachments in a Ska complex-dependent manner. Thus, there is evidence in *C. elegans* that phosphorylation of the Hec1/Ndc80 tail may modulate kinetochore-microtubule attachment stability through co-factor recruitment.

## **1.9 Thesis Rationale**

As discussed above, there is compelling evidence that the Hec1 N-terminal tail is a critical effector of kinetochore-microtubule attachment formation and regulation during mitosis. It remains unclear, however, how the tail contributes to these processes in human cells – namely, discrepancies regarding Hec1 tail function have been reported in different organisms. In this thesis, we set out to investigate the role of this small domain in attachment stability and force generation in human cells, and to understand how phosphorylation of this domain affects its kinetochore function.

In Chapter 2 of this thesis, we investigate how phosphorylation of the Hec1 tail regulates kinetochore-microtubule attachment strength. We provide evidence that the co-factor recruitment model proposed in section 1.8c is likely not conserved from *C. elegans* to human cells – rather, Hec1 tail phosphorylation and Ska complex recruitment both provide distinct pathways for regulating attachment strength. Furthermore, in this chapter we interrogate which domain(s) of the NDC80 complex are critical for Ska complex recruitment and force-transducing kinetochore-microtubule attachments. Our

findings here demonstrate that the Hec1 tail domain is a critical effector of force generation and attachment regulation at the kinetochore-microtubule interface, but that this domain is dispensable for attachment formation, similar to the case in budding yeast and *C. elegans*. This analysis provides a detailed description of how two key microtubule binding factors are temporally coordinated to strengthen kinetochore-microtubule attachments.

An interesting finding from Chapter 2 is that, contrary to previous reports, the Hec1 tail domain is not required for kinetochore-microtubule attachments in human cells. As discussed above, this contradicts previous reports in human cells; however, we highlight experimental discrepancies that may have led to previous conclusions regarding the necessity of the tail. In Chapter 3, we investigate the mechanism by which the Hec1 tail contributes to attachment formation and regulation. Using length-specific mutants of the Hec1 tail domain, we determine the requirements for rescuing the mitotic defects associated with Hec1 tail deletion. Furthermore, we detail the requirements within the tail domain for regulation and generation of high-force attachments. Finally, we perform *in vitro* microtubule binding experiments with recombinant NDC80 complexes that support our in-cell findings. In Chapter 4, I summarize our progress in understanding regulation of force-transducing kinetochore-microtubule attachments and outline future experiments that should be carried out to address outstanding questions that pertain to this work.

## CHAPTER 2: MULTI-DOMAIN REQUIREMENTS FOR FORCE GENERATION AND SKA RECRUITMENT TO KINETOCHORES BY THE NDC80 COMPLEX

2

### 2.1 Introduction

Successful chromosome segregation during mitosis depends on the formation of stable attachments between chromosomes and spindle microtubules. These attachments are generated at kinetochores, which are macromolecular structures built on centromeric heterochromatin of mitotic chromosomes. Once stable kinetochore–microtubule connections are formed, forces generated by plus-end microtubule dynamics are harnessed for the purpose of congressing chromosomes to the spindle equator and silencing the spindle assembly checkpoint, which prevents anaphase onset until all kinetochores are properly attached to spindle microtubules. The kinetochore-associated NDC80 complex, composed of the proteins Hec1 (also known as Ndc80), Nuf2, Spc24,

---

<sup>2</sup> The work in this chapter was published in July 2020 under the title, “The Hec1/Ndc80 tail domain is required for force generation at kinetochores, but is dispensable for kinetochore–microtubule attachment formation and Ska complex recruitment”

JGD and I co-wrote the manuscript with input from KFD and AAJ. JEM and IJS assisted with protein purification and cloning, and JH assisted with data analysis for the nocodazole Ska recruitment experiments. KFD conducted and analyzed the fluorescence co-localization experiments in Figure 2.13. I conducted all other experiments and data analysis.

Wimbish RT, DeLuca KF, Mick JE, Himes J, Jiménez-Sánchez I, Jeyaprakash AA, and DeLuca JG. 2020. The Hec1/Ndc80 tail domain is required for force generation at kinetochores, but is dispensable for kinetochore–microtubule attachment formation and Ska complex recruitment. *Mol Biol Cell*, 31: 1453-1473

and Spc25, serves as the core linkage between kinetochores and spindle microtubules (DeLuca and Musacchio, 2012).

A direct interaction has been mapped between the “toe” domain of Hec1, which resides in its well-ordered, N-terminal calponin homology (CH) domain, and the microtubule lattice (Ciferri *et al.*, 2008; Wilson-Kubalek *et al.*, 2008; Alushin *et al.*, 2010). This interaction is required for high-affinity NDC80 complex–microtubule interactions in vitro and for kinetochore–microtubule attachment formation in cells from all organisms tested to date (Ciferri *et al.*, 2008; Sundin *et al.*, 2011; Tooley *et al.*, 2011; Lampert *et al.*, 2013; Cheerambathur *et al.*, 2017). The Hec1 protein contains an N-terminal, unstructured “tail” domain that has also been implicated in forming kinetochore–microtubule attachments in cells, although the requirement for the tail domain in this process varies among eukaryotic species (Wimbish and DeLuca, 2020). The Hec1 tail domain in *Saccharomyces cerevisiae* and *Caenorhabditis elegans* is dispensable for formation of stable kinetochore–microtubule attachments (Kemmler *et al.*, 2009; Demirel *et al.*, 2012; Cheerambathur *et al.*, 2013; Lampert *et al.*, 2013). In contrast, expression of Hec1 mutants lacking the N-terminal tail domain in mammalian cells has been reported to inhibit the formation of stable attachments (Guimaraes *et al.*, 2008; Miller *et al.*, 2008). The tail domain of Hec1 from all species tested, however, is required for high-affinity binding of NDC80 complexes to microtubules in vitro (Wei *et al.*, 2007; Ciferri *et al.*, 2008; Miller *et al.*, 2008; Alushin *et al.*, 2012; Umbreit *et al.*, 2012; Cheerambathur *et al.*, 2013; Lampert *et al.*, 2013; Zaytsev *et al.*, 2015), suggesting that cellular factors likely compensate for Hec1 tail domain functions to various degrees in different organisms. Why the Hec1 tail

domain is required for attachments in mammalian cells, but not in other eukaryotic species, remains an unanswered question.

In addition to generating attachments to spindle microtubules, kinetochores regulate their stability. In early mitosis attachments are labile and undergo rapid turnover, whereas in late mitosis, attachments are stable and long-lived (Zhai *et al.*, 1995; Cimini *et al.*, 2006; DeLuca *et al.*, 2006; Bakhoun *et al.*, 2009). This scheme helps ensure that any erroneous attachments formed in early mitosis are released and corrected and that mature attachments on correctly bi-oriented chromosomes are stabilized. Temporal regulation of attachment strength is primarily achieved through phosphorylation of kinetochore substrates by the Aurora family of kinases (Biggins *et al.*, 1999; Tanaka *et al.*, 2002; Carmena *et al.*, 2012; Krenn and Musacchio, 2015), and the Hec1 N-terminal tail domain is a key component of this phosphoregulatory system (Cheeseman *et al.*, 2006; DeLuca *et al.*, 2006). Nine sites in the Hec1 tail domain have been identified as substrates of Aurora kinases A and B *in vitro*, and at least five are confirmed to be phosphorylated in cells (Nousiainen *et al.*, 2006; DeLuca *et al.*, 2011, 2018; Kettenbach *et al.*, 2011). *In vitro*, progressive mutation of these nine target sites to aspartic acid to mimic increasing phosphorylation results in a coordinate decrease in microtubule binding affinity of human NDC80 complexes (Zaytsev *et al.*, 2015). Increasing the number of phosphomimetic substitutions also results in a corresponding decrease in kinetochore–microtubule attachment stability, as evidenced by decreased interkinetochore distances and kinetochore–microtubule bundle densities in mammalian cells (Zaytsev *et al.*, 2014; Etemad *et al.*, 2019; Kuhn and Dumont, 2019). Conversely, expression of Hec1 mutants in which all mapped

Aurora kinase target sites are mutated to Ala to prevent phosphorylation results in hyperstabilization of kinetochore–microtubule attachments and defective attachment error correction in mammalian cells (DeLuca *et al.*, 2011; Sundin *et al.*, 2011; Zaytsev *et al.*, 2014; Tauchman *et al.*, 2015; Long *et al.*, 2017; Yoo *et al.*, 2018). A similar phenomenon is observed in embryonic *C. elegans* cells, where mutation of the four mapped Hec1 tail domain Aurora kinase target sites to Ala results in premature kinetochore–microtubule stabilization (Cheerambathur *et al.*, 2017). One model to explain these results proposes that increased phosphorylation of the Hec1 tail reduces the affinity of the NDC80 complex for microtubules, which in turn decreases kinetochore–microtubule attachment stability (Figure 1.3 A).

In addition to the NDC80 complex, the spindle and kinetochore-associated (Ska) complex, a trimer composed of Ska1, Ska2, and Ska3, contributes to the generation and stabilization of kinetochore–microtubule attachments. The Ska complex loads progressively onto kinetochores during mitosis and is required for efficient chromosome congression and for silencing the spindle assembly checkpoint (Hanisch *et al.*, 2006; Daum *et al.*, 2009; Gaitanos *et al.*, 2009; Guimaraes and DeLuca, 2009; Raaijmakers *et al.*, 2009; Theis *et al.*, 2009; Sivakumar *et al.*, 2014, 2016; Auckland *et al.*, 2017). The Ska complex binds both the NDC80 complex and microtubules and stabilizes NDC80 complex–mediated kinetochore–microtubule attachments, likely through its ability to remain bound to depolymerizing microtubule plus ends (Welburn *et al.*, 2009; Jeyaprakash *et al.*, 2012; Schmidt *et al.*, 2013; Abad *et al.*, 2014; Zhang *et al.*, 2017; Helgeson *et al.*, 2018). A major outstanding question is how the Ska complex is recruited to kinetochore-bound NDC80 complexes

to promote kinetochore–microtubule attachment stability. Previous studies have suggested that this recruitment is mediated through the Hec1 tail domain (Cheerambathur *et al.*, 2017; Janczyk *et al.*, 2017), the Hec1 loop domain (Zhang *et al.*, 2012, 2017), and the coiled-coil regions of the heterotetrameric complex (Helgeson *et al.*, 2018; Huis in't Veld *et al.*, 2019); thus the recruitment mechanism remains unresolved.

The Ska complex has also been implicated in regulating kinetochore–microtubule attachment stability. Expression of a nonphosphorylatable Hec1 tail domain mutant in *C. elegans* embryos resulted in increased kinetochore recruitment of the Ska complex, whereas expression of a phosphomimetic Hec1 tail domain mutant led to the opposite effect (Cheerambathur *et al.*, 2017). Importantly, the increased stability of kinetochore–microtubule attachments observed in cells expressing the nonphosphorylatable mutant version of Hec1 was dependent on the presence of the Ska complex. Thus, in some organisms, rather than directly regulating NDC80 complex–microtubule affinity, phosphorylation of the Hec1 tail likely controls recruitment of Ska complexes, which in turn regulates attachment stability. Whether this mechanism functions in human cells remains to be tested (Figure 1.3 C).

Here we investigate how the human Ska complex is recruited to the NDC80 complex in cells and in vitro and how Hec1 tail phosphorylation impacts Ska function. We report that the N-terminal Hec1 tail domain, while required for force generation and attachment regulation, is not explicitly required for either kinetochore–microtubule attachment formation or Ska complex recruitment to kinetochores in human cells. The tail domain is

also dispensable for Ska complex–mediated enhancement of NDC80 complex–microtubule binding *in vitro*. We demonstrate that phospho-regulation of kinetochore–microtubule attachments occurs in the absence of the Ska complex in human cells, providing support for a mechanism whereby Aurora kinase phosphorylation of the Hec1 tail directly modulates kinetochore–microtubule attachment strength. Finally, using two-color fluorescence localization microscopy, we map the location of the Ska complex to a region coincident with the central coiled-coil domain of the NDC80 complex, and consistent with this, we find that this domain of the NDC80 complex is required for the Ska complex to enhance NDC80-microtubule interactions *in vitro*.

## **2.2 Results**

### **Phosphorylation of the Hec1 tail affects Ska complex loading to kinetochores**

To determine how phosphorylation of the Hec1 tail impacts recruitment of Ska complexes to kinetochores, we expressed mutant versions of green fluorescent protein (GFP)-tagged Hec1 in human cells in which the nine mapped Aurora phosphorylation sites were mutated to either Ala (9A) to prevent phosphorylation or aspartic acid (9D) to mimic constitutive phosphorylation. Western blot analysis revealed that transgene expression levels were variable between Hec1-GFP mutants; thus, we analyzed only cells with similar protein levels based on kinetochore GFP intensity (Figure 2.1 A–C; see also Methods). We confirmed that expression of the exogenous constructs led to depletion of endogenous Hec1 protein from kinetochores to undetectable levels by staining cells with an antibody to phosphorylated Hec1 Ser-69 (pS69), which does not

recognize 9A- or 9D-Hec1 proteins and whose levels do not vary during mitotic progression (DeLuca *et al.*, 2018) (Figure 2.2 A and B). Similar to the situation described for *C. elegans* (Cheerambathur *et al.*, 2017), we found that kinetochores in cells expressing 9A-Hec1-GFP were enriched for the Ska complex, while kinetochores in cells expressing 9D-Hec1-GFP exhibited lower levels compared with kinetochores in cells expressing WT-Hec1-GFP (Figure 2.2 A and C). Similar results were observed in cells expressing Hec1-GFP constructs and depleted of endogenous Hec1 by small interfering RNA (siRNA), confirming that Hec1 transgene expression is sufficient to elicit a dominant phenotype without the additional need for siRNA treatment (Figure 2.1 D–F; Tauchman *et al.*, 2015).

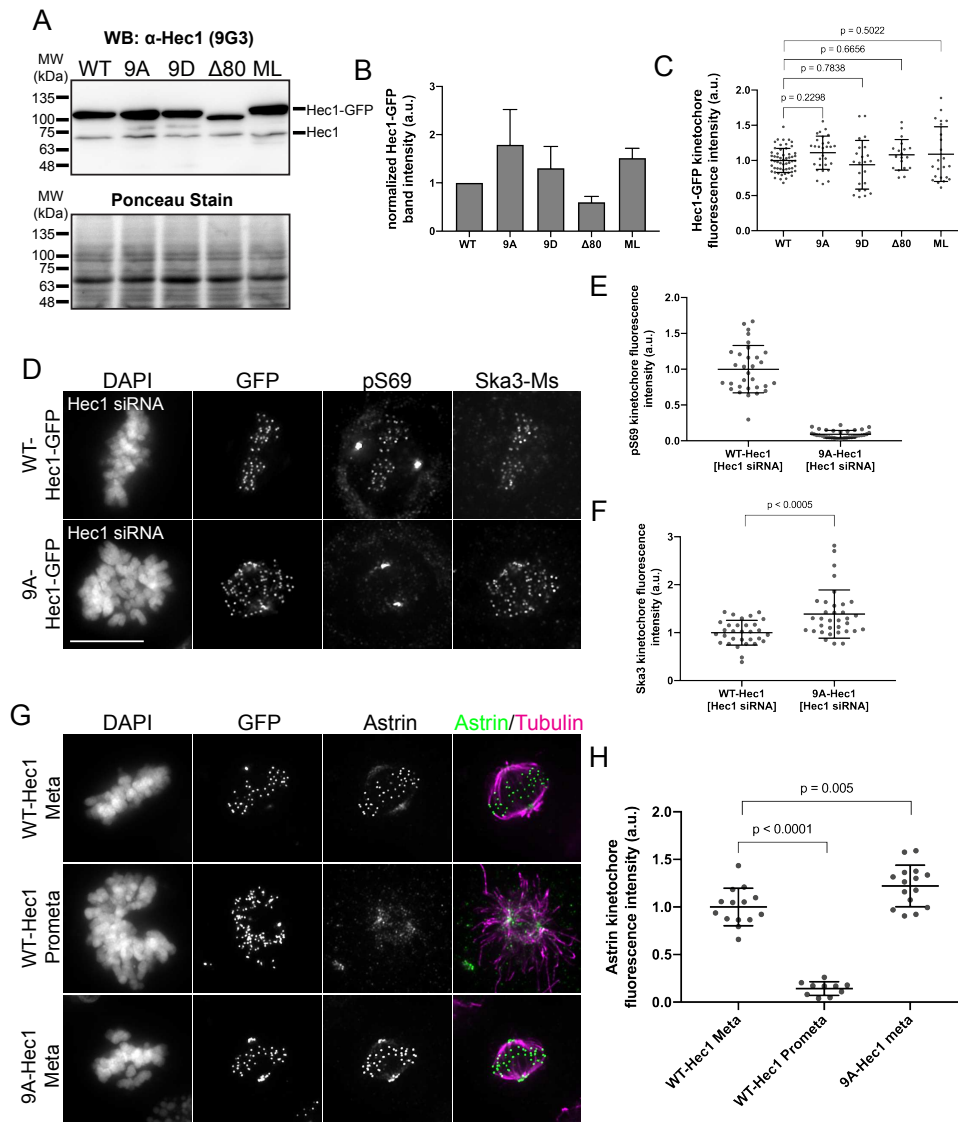


**Figure 2.1. Hec1-GFP transgene expression is sufficient to elicit a dominant phenotype and 9A-Hec1 hyper-recruits Astrin to kinetochores.** (A) Representative Western blot showing Hec1-GFP expression levels in HeLa Kyoto cells. Prominent bands correspond to endogenous Hec1 (72 kDa) and Hec1-GFP (97 kDa, or ~90 kDa for  $\Delta$ 80-Hec1). Ponceau stained blot is shown as a loading control. (B) Quantification of average Hec1-GFP expression levels from 3 independent Western blot experiments. Hec1-GFP band intensity was normalized to WT-Hec1 expression and corrected for protein loading by Ponceau stain (see Materials and Methods). (C) Hec1-GFP kinetochore fluorescence intensity levels measured from RO/NZ experiment (Figure 2D). For experiments in which kinetochore fluorescence intensity was not quantified, cells with similar GFP expression were analyzed qualitatively (see Materials and Methods). (D) Immunofluorescence images of WT- and 9A-Hec1 expressing cells

depleted of endogenous Hec1 with siRNA and stained with antibodies to Hec1-pS69 and Ska3 (generated in mouse). (E) Quantification of pS69 kinetochore fluorescence intensity from Hec1 siRNA-treated cells expressing WT- and 9A-Hec1-GFP. For each condition, at least 20 kinetochores per cell were measured from at least 9 cells per experiment from 3 separate experiments. (F) Quantification of Ska3 kinetochore fluorescence intensity from Hec1 siRNA-treated cells expressing WT- and 9A-Hec1-GFP. For each condition, at least 20 kinetochores per cell were measured from at least 9 cells per experiment from 3 separate experiments. A Student's t-test was carried out to determine statistical significance. (G) Immunofluorescence images of WT- and 9A-Hec1 expressing cells stained with antibodies to Astrin and tubulin. (H) Quantification of Astrin kinetochore fluorescence intensity from cells expressing WT- and 9A-Hec1. For each condition, at least 20 kinetochores per cell were analyzed from at least 5 cells per condition from 2 separate experiments. Statistical significance was determined by a one-way Anova analysis. On all dot plots (C, E, F, and H), each dot represents the average value for all kinetochores from a single cell. Scale bar: 10  $\mu$ m.

Although these results suggest that the phosphorylation state of the tail domain might directly regulate Ska complex recruitment to kinetochores, there is an important caveat to this experiment. Cells expressing 9A-Hec1 mutants generate hyperstable kinetochore–microtubule attachments, in which kinetochore–microtubule bundle densities are increased (Zaytsev *et al.*, 2014), the pulling forces between two sister kinetochores are higher (DeLuca *et al.*, 2011; Yoo *et al.*, 2018), and end-on kinetochore–microtubule attachments are formed earlier than in control cells (Figure 2.2 D and E). Conversely, cells expressing 9D-Hec1 mutants fail to form stable kinetochore–microtubule attachments during mitosis (DeLuca *et al.*, 2011; Zaytsev *et al.*, 2014). Because the Ska complex loads to kinetochores as microtubule attachments are progressively stabilized (Hanisch *et al.*, 2006; Auckland *et al.*, 2017) (Figure 2.2 F and G), results from the experiment described above (Figure 2.2 A–C) do not allow us to differentiate between the two following scenarios: 1) dephosphorylation of the Hec1 tail promotes Ska complex recruitment, and in turn, the Ska complex increases kinetochore–microtubule

attachment stability, or 2) dephosphorylation of the Hec1 tail generates stable kinetochore–microtubule attachments, and in turn, stable attachments promote recruitment of the Ska complex to kinetochores.

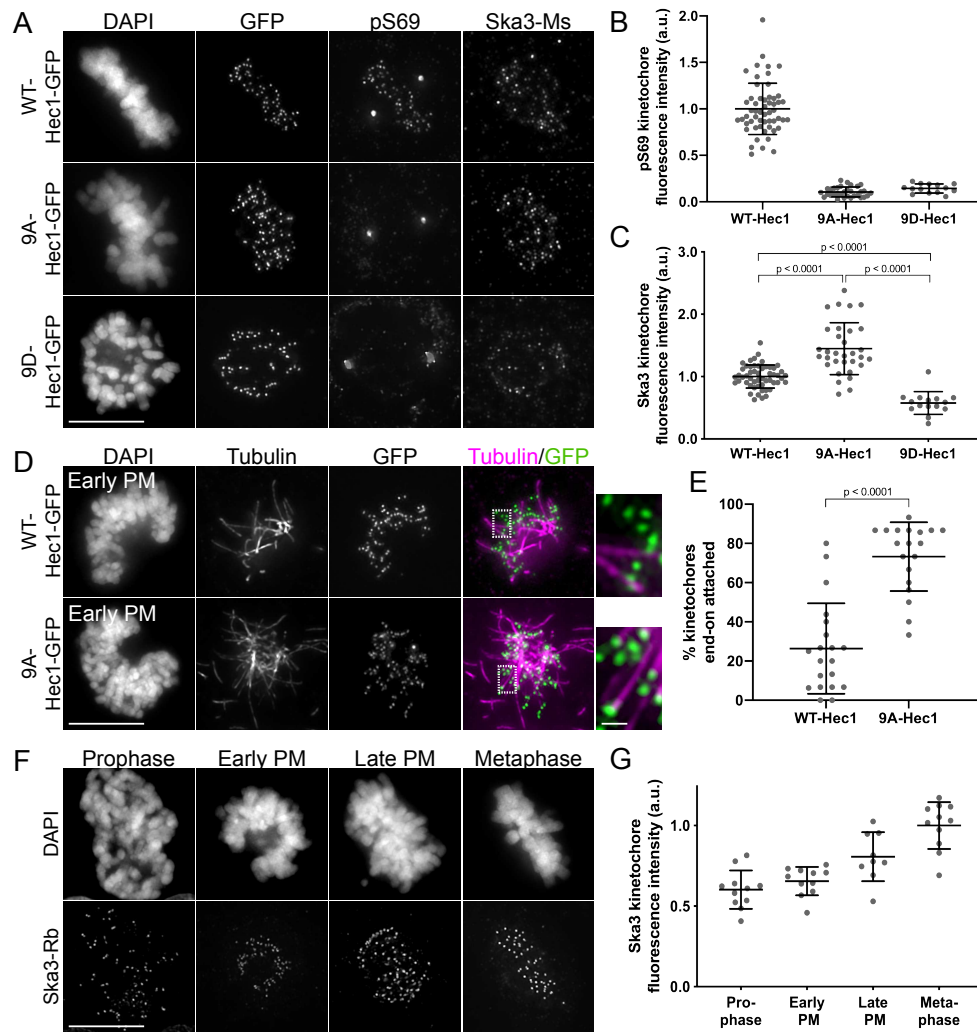


**Figure 2.2. Phosphorylation of the Hec1 tail domain affects kinetochore–microtubule attachment stability and Ska complex loading to kinetochores.** (A) Immunofluorescence images of cells expressing WT-, 9A-, and 9D-Hec1-GFP. Cells were fixed and stained using antibodies to Hec1 pS69 and Ska3 (mouse). (B) Quantification of pS69 kinetochore fluorescence intensity from cells expressing WT-,

9A-, and 9D-Hec1-GFP. For each condition, at least 20 kinetochores per cell were measured from at least five cells per experiment from three separate experiments. (C) Quantification of Ska3 kinetochore fluorescence intensity from cells expressing WT-, 9A-, and 9D-Hec1-GFP. For each condition, at least 20 kinetochores per cell were measured from at least five cells per experiment from three separate experiments. Statistical significance was determined by a one-way analysis of variance (ANOVA). (D) Immunofluorescence images of cold-treated cells expressing WT- and 9A-Hec1-GFP. Cells were incubated in ice-cold DMEM for 12 min before fixation, permeabilized, fixed, and stained using antibodies to tubulin. Insets are enlargements of the region indicated by the dashed box. (E) Quantification of end-on attachment in cold-treated cells expressing WT- and 9A-Hec1-GFP. For each condition, at least 15 kinetochores per cell were measured from at least nine cells per experiment from two separate experiments. A Student's *t* test was carried out to determine statistical significance. (F) Immunofluorescence images of untreated, control cells in different stages of mitosis fixed and stained with antibodies to Ska3 (rabbit). (G) Quantification of Ska3 kinetochore fluorescence intensity in control cells in progressive stages of mitosis. For each mitotic phase, at least 20 kinetochores were measured from at least four cells per experiment from two separate experiments. On all graphs, each dot represents the average value for all kinetochores from a single cell. Scale bars: 10 and 1  $\mu\text{m}$  for panels and insets, respectively.

### **Phosphorylation of the Hec1 tail does not affect microtubule-independent Ska complex loading to kinetochores**

To differentiate between the two possibilities, we measured Ska complex loading to kinetochores in cells expressing WT, 9A-, and 9D-Hec1-GFP in the absence of microtubules. This allowed us to test how mutations in Hec1 affect Ska recruitment without the confounding effects of their impact on kinetochore–microtubule attachment stability. Previous reports have demonstrated that while Ska complexes are maximally loaded onto kinetochores after microtubule attachment, a population of Ska complex localizes to kinetochores in a Hec1-dependent, microtubule-independent manner (Chan *et al.*, 2012; Zhang *et al.*, 2017). Cells transfected with either WT-, 9A-, or 9D-Hec1-GFP were synchronized and arrested in G2 with RO-3306 and then washed out into nocodazole before entry into mitosis. We confirmed that microtubule-independent

Ska complex recruitment to kinetochores required the NDC80 complex (Figure 2.3 A and B) and found that kinetochores in cells expressing WT-, 9D- or 9A-Hec1-GFP all loaded similar levels of the Ska complex (Figure 2.3 C and D). These results suggest that in the absence of microtubules, the phosphorylation state of the human Hec1 tail domain does not influence Ska complex recruitment to kinetochores. In this experiment, all cells subjected to analysis entered mitosis in the presence of nocodazole, and therefore kinetochores had no contact with microtubules before fixation. Interestingly, when we carried out a similar experiment in an asynchronous population, where nocodazole was added to cells in various stages of mitosis, we found that kinetochores in cells expressing 9A-Hec1-GFP exhibited somewhat higher levels of Ska3 compared with those in cells expressing WT-Hec1-GFP (Supplemental Figure 2.4 A and B). We speculate that a population of kinetochores in asynchronous cells expressing 9A-Hec1-GFP had previously established kinetochore–microtubule attachments and loaded high levels of the Ska complex to kinetochores before exposure to nocodazole. These results suggest that once Ska complexes are loaded onto kinetochores by microtubule attachment, a subpopulation of the complex remains bound even after microtubule depolymerization.

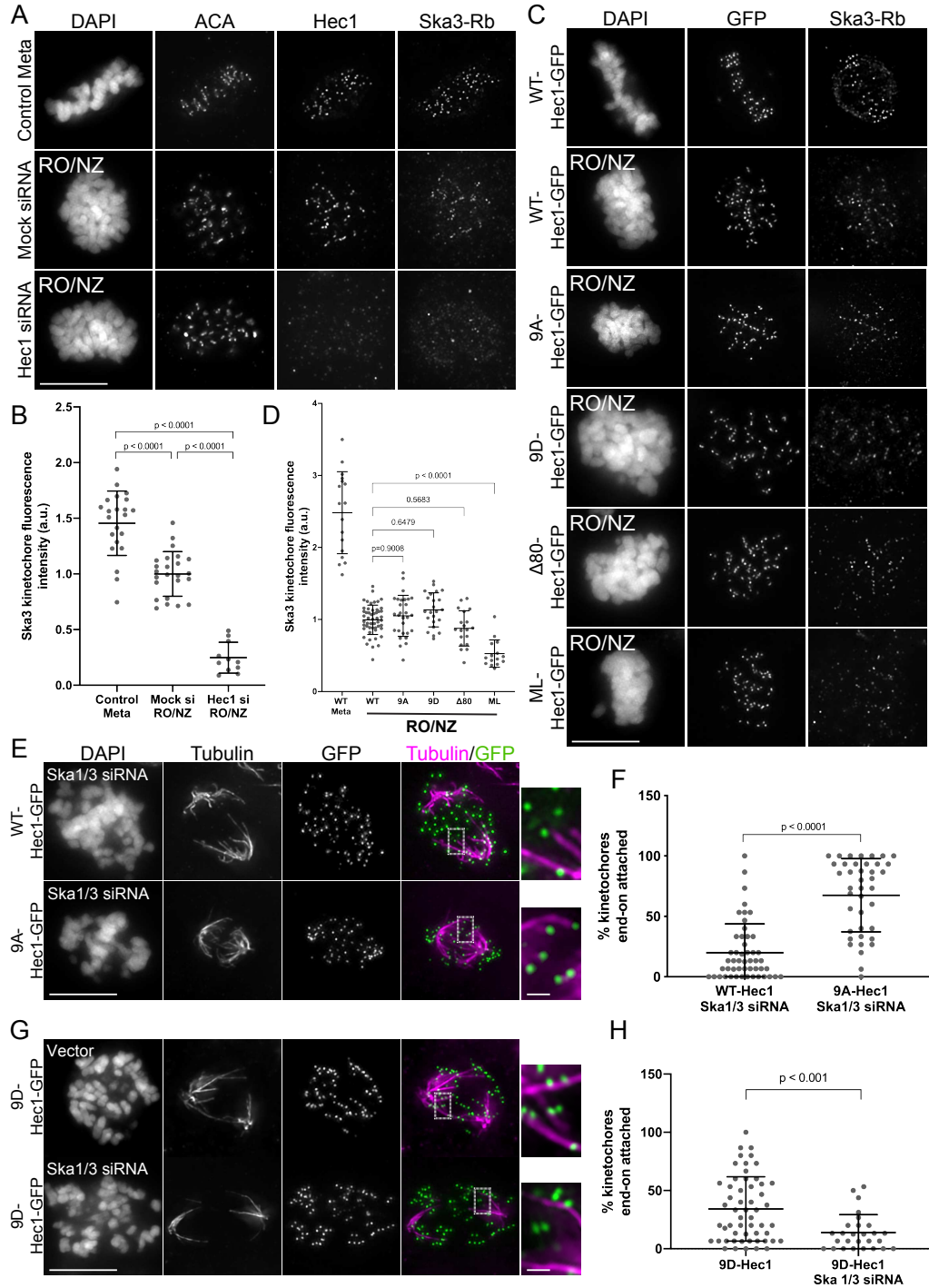


**Figure 2.3: Hec1 tail dephosphorylation does not affect microtubule-independent Ska complex kinetochore loading and stabilizes attachments in the absence of the Ska complex.** (A) Immunofluorescence images of untreated cells (top row) or RO3306-synchronized cells released into mitosis in the presence of 10  $\mu$ M nocodazole (bottom two rows). Cells were stained with ACA (anti-centromere) antibodies and antibodies to Hec1 and Ska3 (rabbit). (B) Quantification of Ska3 kinetochore

fluorescence intensity from cells described in panel A. For each condition, at least 20 kinetochores per cell were measured from at least five cells per experiment from two separate experiments. Ska3 intensity was measured only for Hec1 siRNA-treated cells with <20% of endogenous kinetochore-associated Hec1 as determined by staining with an antibody to the CH domain of Hec1 (9G3). A Student's *t* test was carried out to determine statistical significance. (C) Immunofluorescence images of cells expressing the indicated Hec1-GFP fusion protein in the absence (top row) or presence of RO3306 synchronization and release into 10  $\mu$ M nocodazole (remaining rows). Cells were stained with antibodies to Ska3 (rabbit). (D) Quantification of Ska3 kinetochore fluorescence intensity from cold-treated cells described in panel C. For each condition, at least 20 kinetochores per cell were measured from at least five cells per experiment from three separate experiments. Statistical significance was determined by a one-way ANOVA between RO3306-synchronized WT-Hec1-GFP expressing cells and cells expressing the indicated Hec1 fusion proteins. (E) Immunofluorescence images of cold-treated cells expressing WT- and 9A-Hec1-GFP and treated with Ska1 and Ska3 siRNA. Cells were incubated in ice-cold DMEM for 12 min, permeabilized, fixed, and stained using antibodies to tubulin. Insets are enlargements of the regions indicated by the dashed boxes. (F) Quantification of end-on attachment in cells expressing WT- and 9A-Hec1-GFP and treated with Ska1 and Ska3 siRNA. For each condition, at least 15 kinetochores were measured from at least 10 cells from three separate experiments. A Student's *t* test was carried out to determine statistical significance. (G) Immunofluorescence images of cells expressing 9D-Hec1-GFP and treated with (bottom panel) or without (top panel) Ska1 and Ska3 siRNA. Cells were incubated in ice-cold DMEM for 12 min, permeabilized, fixed, and stained using antibodies to tubulin. Insets are enlargements of the regions indicated by the dashed boxes. (H) Quantification of end-on attachments in cold-treated cells expressing 9D-Hec1-GFP and treated with or without Ska1 and Ska3 siRNA. For each condition, at least 15 kinetochores were measured per cell from at least nine cells per experiment from at least three separate experiments. A Student's *t* test was carried out to determine statistical significance. On all graphs, each dot represents the average value for all kinetochores from a single cell. Scale bars: 10 and 1  $\mu$ m for panels and insets, respectively.

### **Hec1 tail phosphorylation contributes to kinetochore–microtubule attachment stability independently of the Ska complex**

To investigate the functional dependencies between Hec1 tail dephosphorylation, Ska complex loading, and kinetochore–microtubule attachment stability, we tested whether the stable attachments formed in human cells expressing 9A-Hec1-GFP were

dependent on the Ska complex. For these experiments, we depleted the Ska complex from HeLa cells using siRNAs targeting the Ska complex subunits Ska1 and Ska3, which has previously been shown to disrupt kinetochore–microtubule attachments and chromosome alignment (Gaitanos *et al.*, 2009). Immunofluorescence analysis revealed an ~80% reduction in Ska3 signal at kinetochores of Ska1/Ska3 siRNA-treated cells compared with control cells in metaphase (Figure 2.4 C and D), and most Ska-depleted cells exhibited unaligned chromosomes and defective cold-stable kinetochore–microtubule attachment formation (Figure 2.4 E and F).

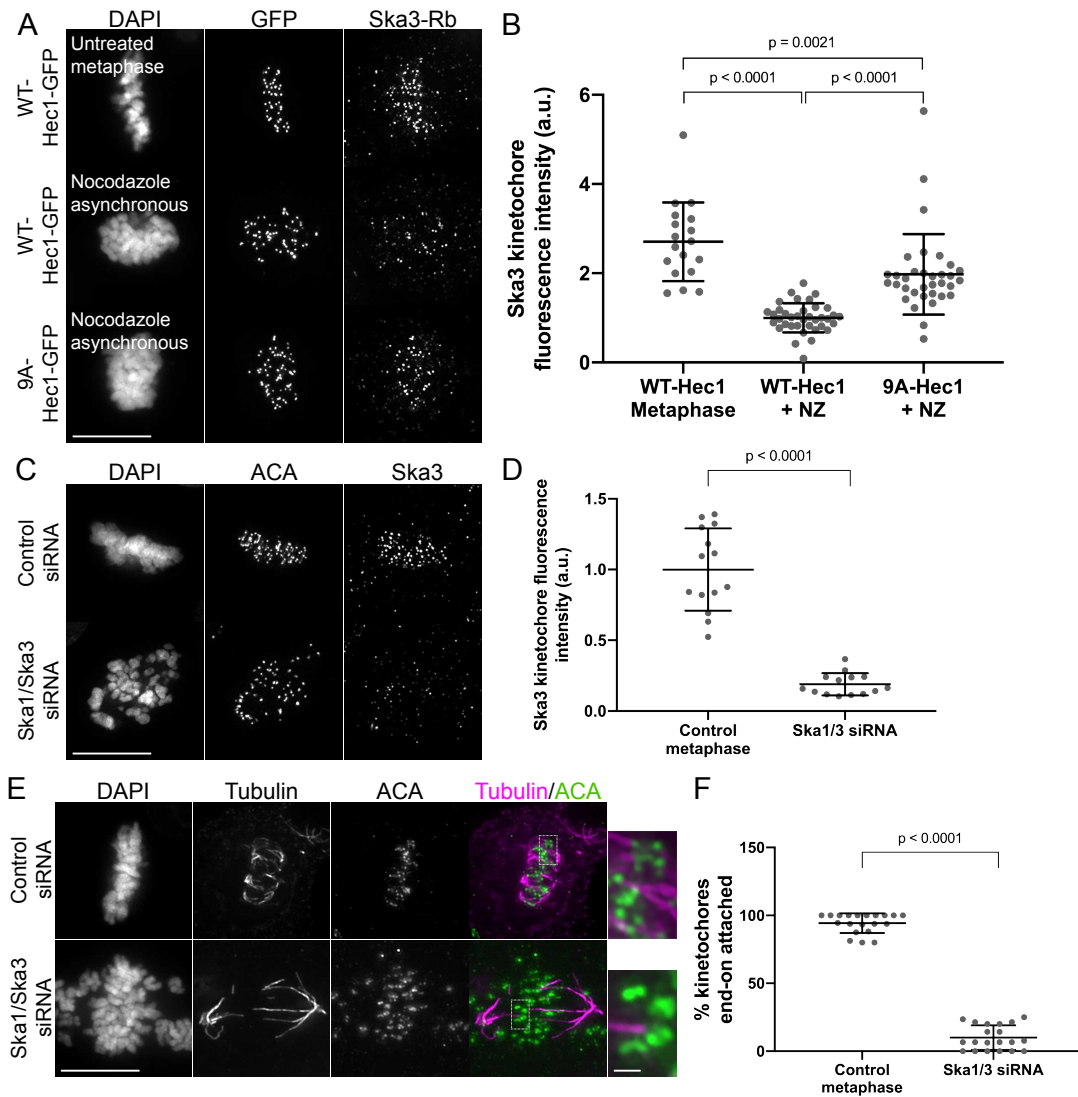


**Figure 2.4. 9A-Hec1 expression causes hyper-recruitment of Ska3 in nocodazole, and Ska depletion disrupts end-on attachment formation in cells. (A)**

Immunofluorescence images of asynchronous cells expressing WT- and 9A-Hec1-GFP treated with or without 10  $\mu\text{m}$  nocodazole for 1h prior to fixation. Cells were fixed and stained with antibodies to Ska3 (rabbit). (B) Quantification of Ska3 kinetochore fluorescence intensity from cells expressing WT- and 9A-Hec1-GFP treated with or without nocodazole. For each condition, at least 20 kinetochores per cell were measured from at least 5 cells per experiment from 4 separate experiments. Statistical significance was determined by a one-way Anova analysis. (C) Immunofluorescence images of control cells or cells treated with Ska1 and Ska3 siRNA. Cells were fixed and stained with anti-centromere antibodies (ACA) or antibodies to Ska3 (mouse). (D) Quantification of Ska3 kinetochore fluorescence intensity from control cells or cells treated with Ska1 and Ska3 siRNA. For each condition, at least 20 kinetochores per cell were analyzed from at least 7 cells per experiment from 2 independent experiments.

Statistical significance was determined by a Student's t-test. (E) Immunofluorescence panels of control cells or cells treated with Ska1 and Ska3 siRNA. Cells were incubated in ice-cold DMEM for 12 minutes prior to fixation, permeabilized, fixed, and stained with antibodies to tubulin and an anti-centromere antibody (ACA). Insets are enlargements of the region indicated by the dashed box. (F) Quantification of end-on attachment in control cells and cells treated with Ska1 and Ska3 siRNA. For each condition, at least 15 kinetochores per cell were measured from 10 cells per experiment from 2 separate experiments. Statistical significance was determined using a Student's t-test. On all graphs, each dot represents the average value for all kinetochores from a single cell. Scale bars: 10  $\mu\text{m}$  and 1  $\mu\text{m}$  for panels and insets, respectively.

To determine how the Ska and NDC80 complexes coordinate to form kinetochore–microtubule attachments, we expressed WT- and 9A-Hec1-GFP constructs in Ska-depleted cells, treated the cells with ice-cold media before fixation, stained them with antibodies to tubulin, and scored them for cold-resistant end-on kinetochore–microtubule attachments. Similar to what we observed for Ska-depleted cells alone, cells expressing WT-Hec1-GFP and depleted of Ska1/Ska3 exhibited defects in chromosome alignment and formation of end-on kinetochore–microtubule attachments (Figure 2.3 E and F). However, in Ska1/Ska3-depleted cells expressing 9A-Hec1-GFP, we observed robust formation of end-on attachments despite cells exhibiting similar defects in chromosome alignment (Figure 2.3 E and F). These results suggest that Hec1 tail phosphorylation and Ska complex recruitment contribute to regulation of kinetochore–microtubule attachments independently of each other. We reasoned that if this were the case, then the destabilizing effects of expressing a phospho-mimetic Hec1 tail mutant in Ska1/Ska3-depleted cells should be more severe than the effects of expressing a phospho-mimetic Hec1 tail mutant in non–Ska1/Ska3-depleted cells. We found that cells expressing 9D-Hec1-GFP exhibited defects in forming stable, end-on

kinetochore–microtubule attachments (average of ~34% of kinetochores attached per cell), which is consistent with previous studies (Figure 2.3 G and H; Guimaraes *et al.*, 2008; Zaytsev *et al.*, 2014). In cells depleted of Ska1 and Ska3, expression of 9D-Hec1-GFP indeed resulted in a more penetrant kinetochore–microtubule attachment defect (average of ~14% of kinetochores attached per cell) (Figure 2.3 G and H), providing further evidence that in human cells, phosphorylation of the Hec1 tail contributes to kinetochore–microtubule attachment stability independently of the Ska complex. Collectively, these results suggest that the increased loading of Ska complexes to kinetochores in cells expressing 9A-Hec1 is a consequence of increased kinetochore–microtubule attachment stability, rather than a direct effect of blocking Hec1 tail phosphorylation. Similarly, we found that expression of 9A-Hec1-GFP also resulted in higher kinetochore recruitment of Astrin, a subunit of the Astrin-SKAP complex, which has been reported to specifically localize to end-on attached kinetochores (Figure 2.1 G and H; Schmidt *et al.*, 2010; Conti *et al.*, 2019).

### **Phosphorylation of Hec1 Ser-69 prevents excess Ska loading to kinetochores**

In contrast to most Aurora target sites on the Hec1 tail, Ser-69 remains phosphorylated at high levels throughout mitosis, and this modification is important for maintaining proper kinetochore–microtubule attachment dynamics (DeLuca *et al.*, 2018). We next tested whether phosphorylation of this site imparted differences in Ska recruitment compared with a completely dephosphorylated tail. To this end, we expressed 8A-Hec1-GFP in cells, in which eight of the nine mapped Aurora kinase target sites are mutated

to Ala and Ser-69 is kept in its wild-type state (DeLuca *et al.*, 2018). In contrast to what we observed for 9A-Hec1, cells expressing 8A-Hec1 recruited normal, wild-type levels of Ska3 in metaphase (Figure 2.5 A and B). In line with the need for high levels of Hec1 tail phosphorylation in early mitosis (Zaytsev *et al.*, 2014), 8A-Hec1 expression resulted in premature stabilization of kinetochore–microtubule attachments (Figure 2.5 C and D). Additionally, and in a manner similar to 9A-Hec1, expression of 8A-Hec1 constructs led to robust kinetochore–microtubule attachment formation in the absence of the Ska complex (Figure 2.5 E and F). These results provide further support for the notion that Hec1 tail dephosphorylation strengthens attachments independently of the Ska complex and suggest that maintenance of wild-type Hec1 tail phosphorylation levels allow normal Ska loading to kinetochores.

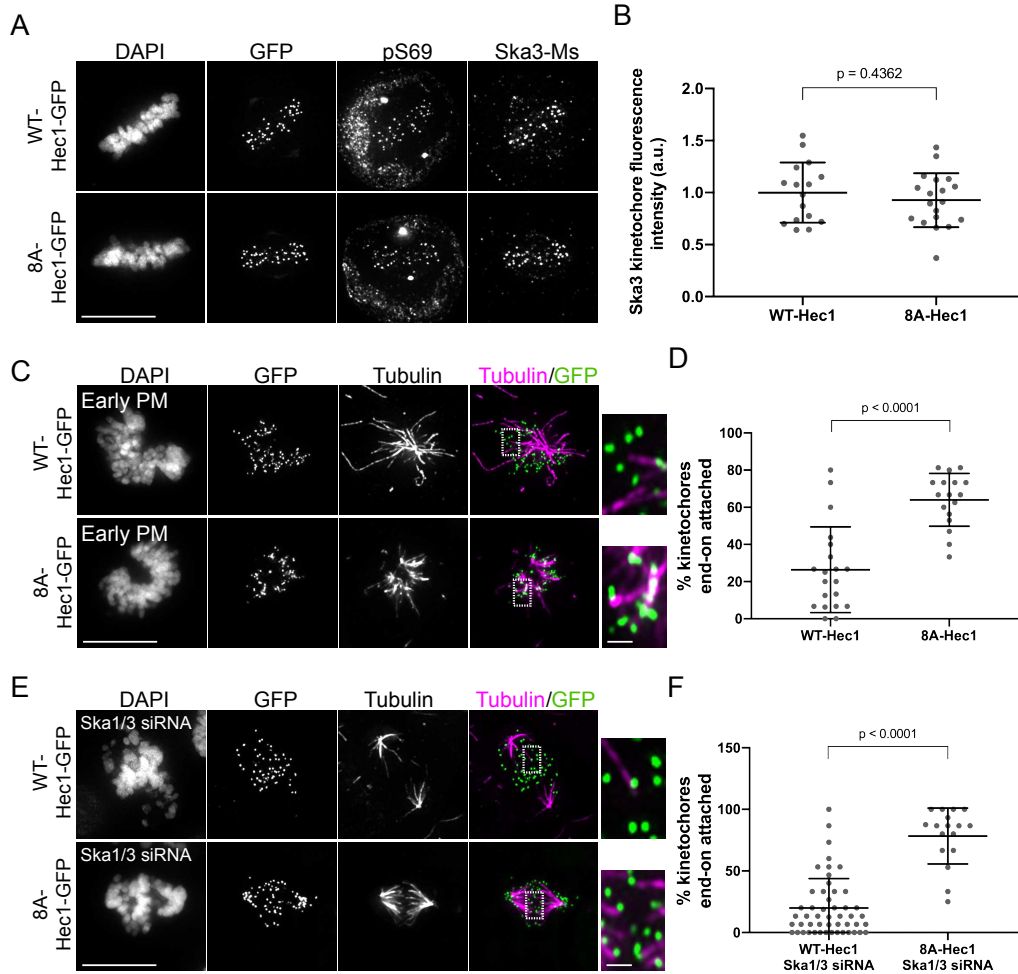


**Figure 2.5. 8A-Hec1 expression phenocopies 9A-Hec1 in kinetochore-microtubule attachment formation and WT-Hec1 in Ska recruitment.** (A) Immunofluorescence images of cells expressing WT- and 8A-Hec1-GFP. Cells were fixed and stained with antibodies to Hec1-pS69 and Ska3 (mouse). (B) Quantification of Ska3 kinetochore fluorescence intensity from metaphase cells expressing WT- and 8A-Hec1-GFP. For each condition, at least 20 kinetochores per cell were quantified for at least 7 cells per experiment from 2 independent experiments. (C) Immunofluorescence images of early prometaphase cells expressing WT- and 8A-Hec1-GFP. Cells were incubated in ice-cold DMEM for 12 minutes prior to fixation, permeabilized, fixed and stained using antibodies to tubulin. Insets are enlargements of the region indicated by the dashed box. (D) Quantification of end-on attachments in early prometaphase cells expressing WT- and 8A-Hec1-GFP. For each condition, at least 15 kinetochores per cell were measured from at least 8 cells per experiment from 2 independent experiments. Data for WT-Hec1 are from Figure 2.2 D. (E) Immunofluorescence images of cold-treated cells expressing WT- and 8A-Hec1-GFP and treated with Ska1 and Ska3 siRNA. Cells were incubated in ice-cold DMEM for 12 minutes prior to fixation, permeabilized, fixed and stained using antibodies to tubulin. Insets are enlargements of the region indicated

by the dashed box. (F) Quantification of end-on attachments in cells expressing WT- and 8A-Hec1-GFP and treated with Ska1 and Ska3 siRNA. For each condition, at least 15 kinetochores per cell were measured from at least 8 cells per experiment from at least two independent experiments. Data for WT-Hec1 are from Figure 2.4 F. For all quantifications, statistical significance was determined using a Student's t-test. On all graphs, each dot represents the average value for all kinetochores from a single cell. Scale bars: 10  $\mu\text{m}$  and 1  $\mu\text{m}$  for panels and insets, respectively

### **The Hec1 tail domain is not required for Ska complex–mediated enhancement of NDC80 complex–microtubule binding**

Independent of its phosphorylation state, the tail domain of Hec1 has been implicated in recruiting the Ska complex to the NDC80 complex–microtubule interface in vitro and to kinetochores in human cells (Janczyk *et al.*, 2017). In contrast, other studies have reported that the Hec1 tail is dispensable for the NDC80-Ska complex interaction (Helgeson *et al.*, 2018; Huis in't Veld *et al.*, 2019). To further investigate these discrepancies, we first asked whether the tail domain is required in vitro for Ska complexes to enhance NDC80 complex–microtubule affinity. Previous studies have shown that purified, recombinant Ska complexes increase the affinity of NDC80 complexes for microtubules in vitro (Schmidt *et al.*, 2012; Helgeson *et al.*, 2018). We therefore measured the microtubule binding affinity of GFP-tagged, recombinantly expressed, purified NDC80 complexes containing WT-Hec1 and Hec1 deleted of its N-terminal 80-amino-acid tail domain ( $\Delta 80$ -Hec1) using a total internal reflection fluorescence (TIRF) microscopy-based assay. For these experiments, we generated NDC80 complexes in which Nuf2 is fused to Spc24 and Hec1 is fused to Spc25-GFP (Figure 2.6 A), termed NDC80<sup>Bronsai</sup>. These complexes are missing the tetramerization

domains from all four subunits but contain the majority of the central coiled-coil region of the complex (Ciferri *et al.*, 2005, 2008), as well as the “loop” domain of Hec1, which is a 40-amino-acid region that briefly disrupts the coiled-coil region (Maiolica *et al.*, 2007). The name represents a hybrid between “NDC80<sup>Bonsai</sup>,” which is an engineered, truncated version of the NDC80 complex composed of a Nuf2-Spc24 fusion and a Hec1-Spc25-GFP fusion missing the central coiled-coil and tetramerization domains (Ciferri *et al.*, 2008) and “NDC80<sup>Broccoli</sup>,” which is a dimer of nearly full-length Nuf2 and Hec1 containing the coiled-coil and loop domains (Schmidt *et al.*, 2012). For the binding assays, we incubated increasing concentrations of GFP-labeled NDC80<sup>Bonsai</sup> complexes with Alexa<sup>647</sup>-labeled microtubules in the presence or absence of 10 nM recombinantly expressed human Ska complex and measured the average fluorescence intensity along microtubules. WT-NDC80<sup>Bonsai</sup> complexes robustly bound microtubules, and binding affinity was increased approximately two-fold upon the addition of Ska complexes (Figure 2.6 A and B). The  $\Delta$ 80-NDC80<sup>Bonsai</sup> complexes bound to microtubules with significantly lower affinity than the WT complexes (Figure 2.6 C and D), which is consistent with previously published studies (Ciferri *et al.*, 2008; Miller *et al.*, 2008; Umbreit *et al.*, 2012; Zaytsev *et al.*, 2015). However, addition of purified Ska complex increased the affinity of  $\Delta$ 80-NDC80<sup>Bonsai</sup> complexes for microtubules by nearly two-fold, similar to the case for WT-NDC80<sup>Bonsai</sup> (Figure 2.6 D). These results confirm that the Hec1 tail domain is not required for Ska complex-mediated enhancement of microtubule binding by NDC80 complexes *in vitro* and that Ska complexes are able to compensate for the decreased microtubule binding observed with NDC80 complexes lacking the N-terminal tail domain (Helgeson *et al.*, 2018; Huis

in't Veld *et al.*, 2019). These results also demonstrate that the tetramerization domain of the NDC80 complex is not required for Ska complex binding.

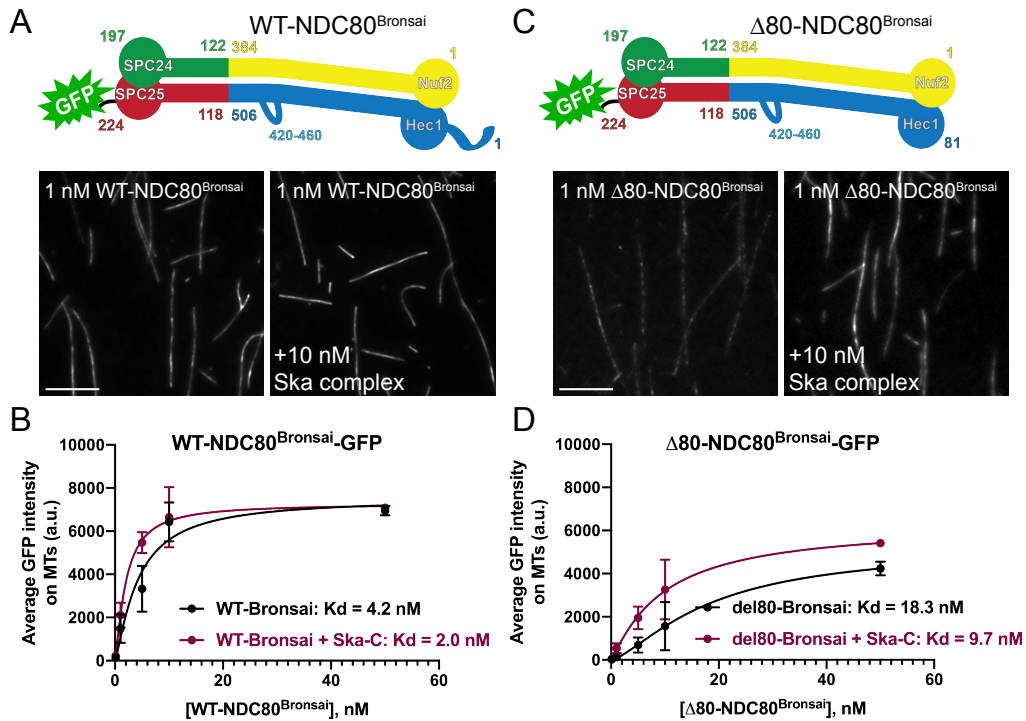


**Figure 2.6. The Hec1 tail domain is not required for Ska complex-mediated enhancement of NDC80 complex–microtubule binding.** (A and C) Top: schematics of NDC80<sup>Bronasai</sup> complexes used in the TIRF-based microtubule binding experiments. Bottom: GFP fluorescence images of NDC80 complexes decorating microtubules in the presence and absence of Ska complex. All images show a single concentration of the NDC80 complex from the experiment (1 nM) with and without added Ska complex (10 nM). (B and D) Binding curves from the microtubule binding assays. Datapoints and curve fits shown in black are from experiments without added Ska complex. Those shown in burgundy are from experiments with added Ska complex. Each point on the curve represents the average fluorescence intensity from three separate experiments. At each concentration, GFP-NDC80 complex fluorescence intensity was measured from at least 40 individual microtubules from at least 10 different TIRF fields per experiment. Scale bars: 10  $\mu$ m.

We note that one difference between the TIRF-based microtubule binding assays described here and those described in our previous study (Zaytsev *et al.*, 2015) is the choice of assay buffer. When we used standard microtubule binding assay buffers BRB80 (80 mM PIPES, 1 mM MgCl<sub>2</sub>, 1 mM EGTA, pH 6.8) or BRB20 (20 mM PIPES, 1 mM MgCl<sub>2</sub>, 1 mM EGTA, pH 6.8), purified Ska complexes aggregated in the presence of microtubules (Figure 2.7 A). In addition, Ska complexes induced aggregation of NDC80 complexes on microtubules in the presence of BRB80 (Figure 2.7 B), which precluded quantitative analysis of fluorescence intensities along microtubules. We therefore developed “SN” buffer (for “Ska-NDC80”) for our assays (20 mM Tris, 50 mM NaCl, pH 7.0), which did not induce aggregation of either Ska or NDC80 complexes (Figure 2.7 A).

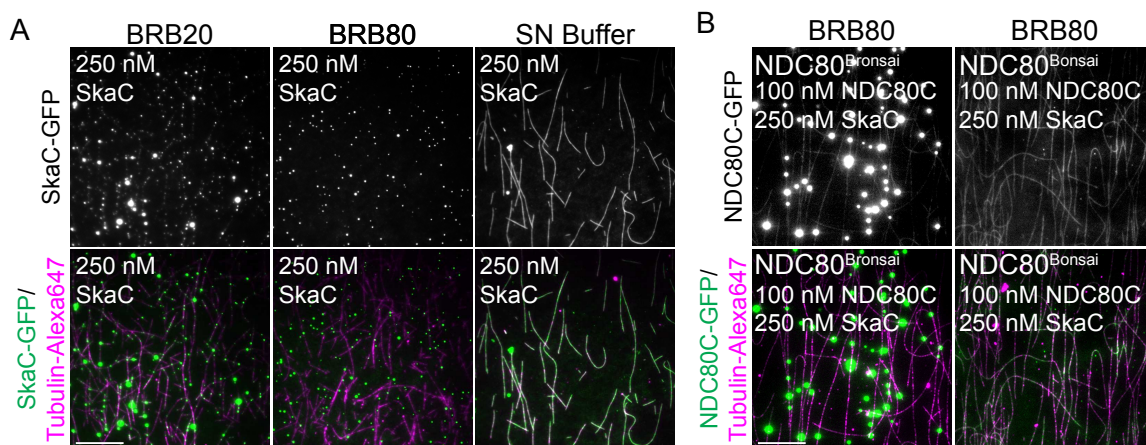


**Figure 2.7. Oligomerization of Ska and NDC80 complexes in vitro is buffer dependent.** (A) GFP fluorescence (top row) and overlay with Alexa647-tubulin (bottom row) images of GFP-tagged Ska complex (SkaC-GFP) diluted to the noted concentrations in buffers indicated above each column. SkaC-GFP microtubule binding reactions were carried out in the same manner as experiments from Figure 2.6 (see Materials and Methods). (B) GFP fluorescence (top row) and overlay with Alexa647-tubulin (bottom row) images of indicated NDC80C-GFP constructs incubated with unlabeled Ska complex (SkaC) in BRB80 buffer. Scale bars: 20 μm.

## **The Hec1 tail domain is not required for Ska complex recruitment to kinetochores or for kinetochore–MT attachment in human cells**

In light of our *in vitro* results, we next wanted to ask whether the Hec1 tail domain is required for Ska complex recruitment to kinetochores in human cells. For these experiments, we expressed exogenous  $\Delta 80$ -Hec1-GFP in HeLa cells and analyzed only cells with undetectable levels of Hec1-pSer69 at kinetochores. Previous studies in mammalian cells demonstrated that Hec1 tail deletion impacts kinetochore–microtubule attachment stability as evidenced by reductions in interkinetochore distances, decreased cold-resistant microtubule attachments, failure to align chromosomes, and significant mitotic delays (Guimaraes *et al.*, 2008; Miller *et al.*, 2008; Etemad *et al.*, 2015; Janczyk *et al.*, 2017). In line with this, we found that cells expressing  $\Delta 80$ -Hec1-GFP exhibited significant chromosome alignment defects and decreased interkinetochore distances and were unable to silence the spindle assembly checkpoint (Figure 2.8 A and B, and Figure 2.9 A–C). However, contrary to previous studies, we found that cells expressing  $\Delta 80$ -Hec1-GFP were competent to form cold-resistant kinetochore–microtubule attachments (Figure 2.8 C). This is in contrast to cells expressing 9D-Hec1, which are able neither to properly align chromosomes nor to form stable, cold-resistant kinetochore–microtubule attachments (Figure 2.8 A–C; DeLuca *et al.*, 2011). Analysis of spindle morphology in  $\Delta 80$ -Hec1 expressing cells revealed that the majority of cells with unaligned chromosomes contained multipolar spindles (Figure 2.8 D). Identical defects in alignment and spindle bipolarity were

observed in cells expressing  $\Delta 80$ -Hec1-GFP and depleted of endogenous Hec1 by siRNA (Figure 2.9 D–F).

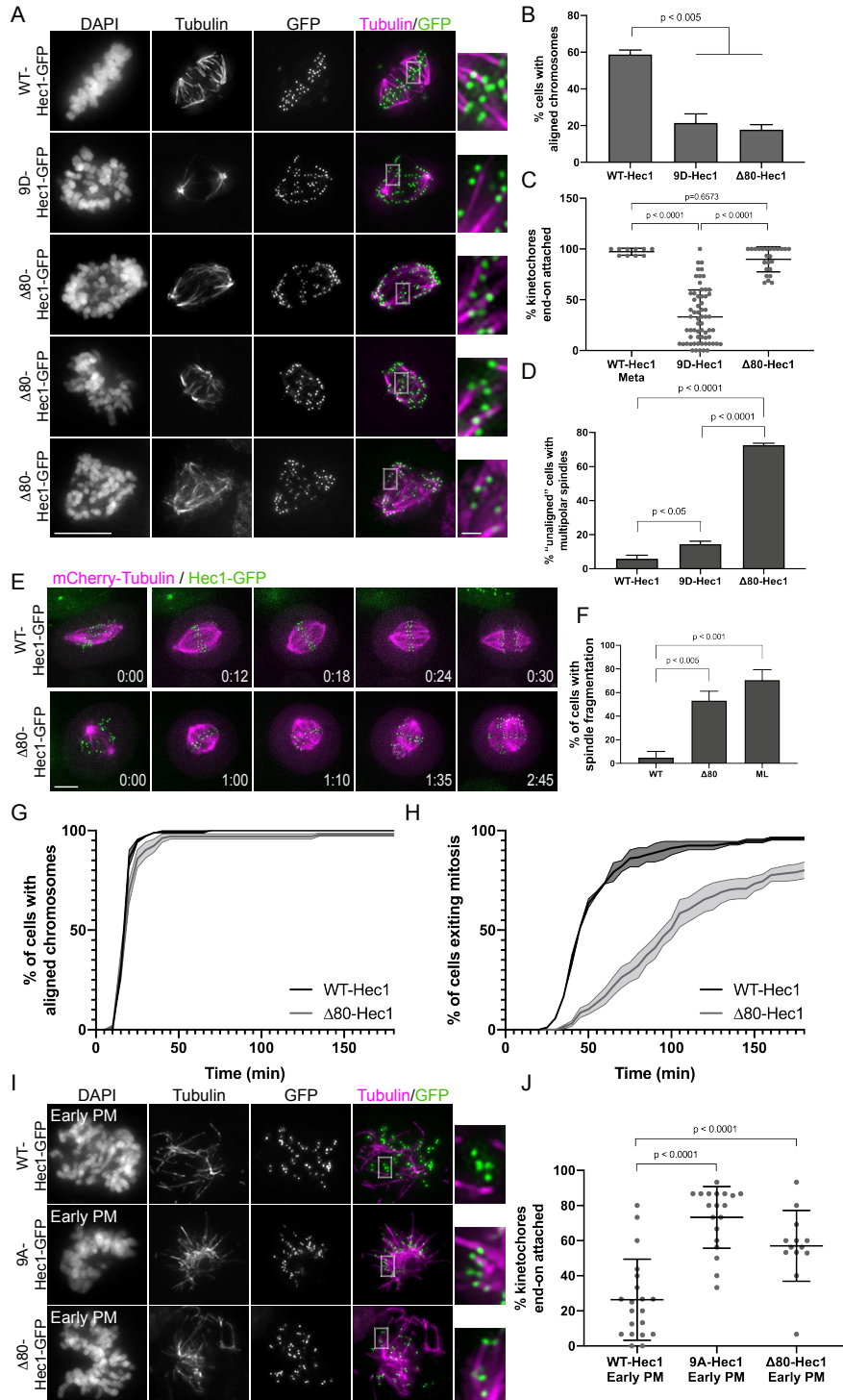


**Figure 2.8. The Hec1 tail domain is not required for the formation of stable end-on kinetochore–microtubule attachments in cells.** (A) Immunofluorescence images of cold-treated cells expressing WT-, 9D-, and  $\Delta$ 80-Hec1-GFP. Cells were incubated in ice-cold DMEM for 12 min, permeabilized, fixed, and stained using antibodies to tubulin. Insets are enlargements of the regions indicated by the dashed boxes. Three examples of cells expressing  $\Delta$ 80-Hec1-GFP are shown. (B) Quantification of chromosome alignment in cells expressing WT-, 9D-, and  $\Delta$ 80-Hec1-GFP. For each condition, chromosome alignment was assessed in at least 100 cells per experiment from two separate experiments. Cells were scored as “aligned” if they had a metaphase plate with <5 chromosomes off the plate. Statistical significance was determined by a one-way ANOVA. (C) Quantification of end-on attachment in cells expressing WT-, 9D-, and  $\Delta$ 80-Hec1-GFP and cold-treated prior to fixation. For each condition, at least 15 kinetochores per cell were measured from at least 10 cells per experiment from two separate experiments. Statistical significance was determined by a one-way ANOVA. (D) Quantification of multipolarity observed in cells expressing WT-, 9D- and  $\Delta$ 80-Hec1-GFP. Cells with unaligned chromosomes were scored for containing bi- vs multipolar spindles, and the percent of cells with multipolar spindles is shown. For each condition, at least 100 cells per experiment were analyzed from two separate experiments. Statistical significance was determined by a one-way ANOVA. (E) Still images from time-lapse experiments of cells expressing Hec1-GFP and mCherry-tubulin. Time from nuclear envelope breakdown (NEBD) is denoted on bottom right corner of each image (hours:minutes). (F) Quantification of spindle pole fragmentation frequency quantified from time-lapse imaging experiments. Cells were scored as undergoing fragmentation events if loss of spindle bipolarity was observed during time-lapse imaging as determined from the mCherry-tubulin signal. Quantifications shown are averages from two (WT-, ML-) or four ( $\Delta$ 80-Hec1) independent experiments. Statistical significance was determined by a one-way ANOVA. (G) Quantification of chromosome alignment efficiency in cells from the experiment shown in panel E. Cell fate was tracked after mitotic entry (as determined by NEBD) for 3 h, and cells were scored as “aligned” upon metaphase plate formation (as determined by Hec1-GFP fluorescence). Data for WT- and  $\Delta$ 80-Hec1 are from 175 cells from two independent experiments and 165 cells from four independent experiments, respectively. (H) Quantification of mitotic exit timing in cells from the experiment shown in panel E. Cell fate was tracked after mitotic entry (as determined by NEBD) for 3 h, and cells were scored as “exiting mitosis” upon anaphase entry. Data for WT- and  $\Delta$ 80-Hec1 are from 175 cells from two independent experiments and 165 cells from four independent experiments, respectively. (I) Immunofluorescence images of cold-treated, early prometaphase cells expressing WT-, 9A-, and  $\Delta$ 80-Hec1-GFP. Cells were incubated in ice-cold DMEM for 12 min, permeabilized, fixed, and stained with antibodies to tubulin. Insets are enlargements of the regions indicated by the dashed boxes. (J) Quantification of end-on attachment in early prometaphase cells expressing WT-, 9A-, and  $\Delta$ 80- Hec1-GFP. The WT- and 9A-Hec1 data shown are from the experiment presented in Figure 2.3. For each condition, at least 15 kinetochores per cell were measured from at least six cells per experiment from at least two separate experiments. Statistical significance was determined by a one-way ANOVA. On all dot plots, each dot represents the average value for all

kinetochores from a single cell. Scale bars: 10 and 1  $\mu\text{m}$  for panels and insets, respectively.

To further investigate the origin of the multipolar spindle phenotype, we carried out time-lapse imaging of mCherry-tubulin and Hec1-GFP expressing cells. In the case of WT-Hec1-GFP expressing cells, we found that almost all cells formed bipolar spindles and entered anaphase without errors, with only  $\sim 5\%$  of cells undergoing spindle fragmentation before anaphase. Strikingly, while most  $\Delta 80$ -Hec1-GFP expressing cells aligned their chromosomes in a timely manner, cells experienced a metaphase arrest followed by spindle pole fragmentation and subsequent loss of chromosome alignment, resulting in prolonged mitotic delays (Figure 2.8 E–H). Several non-centrosomal processes, including cohesin fatigue and defective kinetochore force generation, have been suggested to contribute to loss of spindle bipolarity (Daum *et al.*, 2011; Maiato and Logarinho, 2014). Interestingly, live cell imaging revealed that  $\Delta 80$ -Hec1 expressing cells undergo spindle fragmentation with a frequency similar to that of cells expressing a scrambled loop mutant of Hec1 (ML-Hec1; Figure 2.8 F; see also Figure 2.12 later in this chapter), which are unable to form stable kinetochore–microtubule attachments and experience dramatic delays in mitotic exit (Varma *et al.*, 2012; Zhang *et al.*, 2012; see Figure 2.12 H–K, later in this chapter). Taken with the observation that kinetochores in cells expressing  $\Delta 80$ -Hec1 retain end-on attachments that are under significantly lower tension than kinetochores in cells expressing WT-Hec1 (Figure 2.8 D and Figure 2.9 A and B), these results suggest that the Hec1 tail is dispensable for attachments, but is required for sustaining force at the kinetochore–microtubule interface and timely

transit through mitosis.

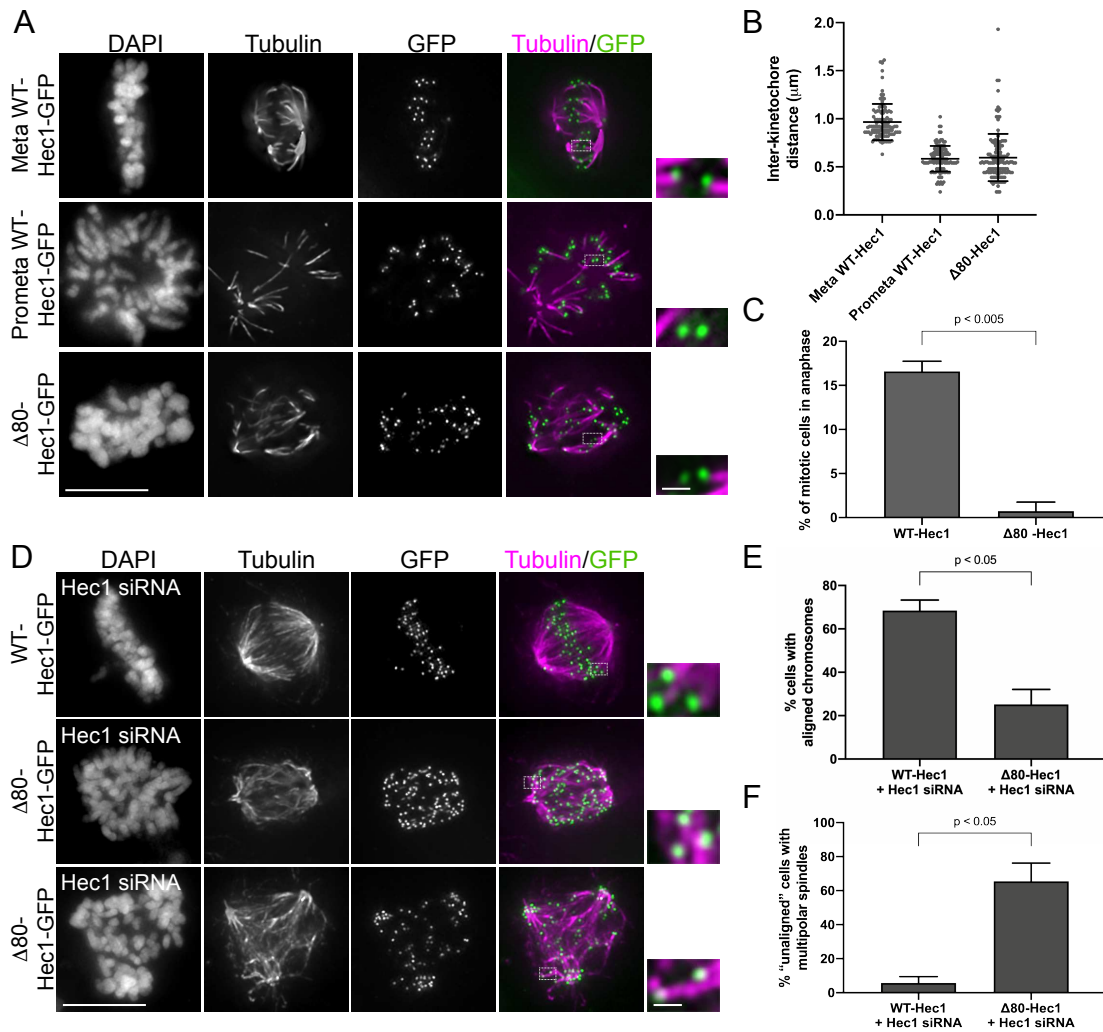


**Figure 2.9. Hec1 tail deletion impacts tension generation at kinetochores.** (A) Immunofluorescence images of HeLa cells expressing WT- and  $\Delta 80$ -Hec1-GFP. Cells were incubated in ice-cold DMEM for 12 minutes prior to fixation, permeabilized, fixed, and stained with antibodies to tubulin. Insets are enlargements of the region indicated by the dashed box. (B) Quantification of inter-kinetochore distances in metaphase and prometaphase cells expressing WT-Hec1-GFP, and cells expressing  $\Delta 80$ -Hec1-GFP. For each condition, inter-kinetochore distances were measured from at least 10 kinetochores per cell in at least 10 cells per experiment from at least 3 independent experiments. Each dot represents the distance measured for a single kinetochore pair. (C) Quantification of anaphase index in cells expressing WT- or  $\Delta 80$ -Hec1-GFP. For each condition, anaphase index was assessed for at least 100 mitotic cells per experiment in 2 separate experiments. (D) Immunofluorescence images of HeLa cells expressing WT- and  $\Delta 80$ -Hec1-GFP and depleted of endogenous Hec1 stained with antibodies to tubulin. Insets are enlargements of the region indicated by the dashed

box. (E) Quantification of chromosome alignment in cells expressing WT- and  $\Delta 80$ -Hec1-GFP. For each condition, chromosome alignment was assessed in at least 100 cells per experiment in 2 separate experiments. Cells were scored as “aligned” if they had a metaphase plate with < 5 chromosomes off the plate. (F) Quantification of multipolarity observed in cells expressing WT- and  $\Delta 80$ -Hec1-GFP. Cells with unaligned chromosomes were scored for containing multi-polar spindles, and the percent of cells with multipolar spindles is shown. For each condition, at least 100 cells per experiment from two separate experiments were assessed. On all bar graphs (C, E, F), statistical significance was determined using a Student’s t-test. Scale bars: 10  $\mu\text{m}$  and 1  $\mu\text{m}$  for panels and insets, respectively.

Given that cells expressing  $\Delta 80$ -Hec1 form cold-stable attachments, we hypothesized that these attachments are mediated through the Hec1 CH domain and have lost their ability to be negatively regulated through Aurora kinase phosphorylation. To test this hypothesis, we analyzed cold-resistant end-on attachments in early prometaphase cells shortly after nuclear envelope breakdown. Similar to 9A-Hec1-GFP expressing cells, and in contrast to WT-Hec1-GFP expressing cells, early prometaphase cells expressing  $\Delta 80$ -Hec1-GFP formed end-on kinetochore–microtubule attachments that resisted cold depolymerization (Figure 2.8 I and J), suggesting that the Hec1 tail domain is required for temporal regulation of attachments. Collectively, these data support a role for the Hec1 tail in force generation and attachment regulation at the kinetochore, but suggest that it is not required for kinetochore–microtubule attachment formation.

We were somewhat surprised at the ability of cells expressing  $\Delta 80$ -Hec1-GFP to retain end-on attachments after cold treatment, since it was previously observed that the tail domain contributes to the formation and/or maintenance of kinetochore–microtubule attachments in both human and marsupial cells (Guimaraes *et al.*, 2008; Miller *et al.*, 2008; Etemad *et al.*, 2015; Janczyk *et al.*, 2017). To confirm that this was not a cell

type-specific phenomenon, we expressed WT- and  $\Delta 80$ -Hec1-GFP constructs in human RPE1 cells and found that, similar to what was observed in HeLa cells, RPE1 cells expressing  $\Delta 80$ -Hec1-GFP were competent to form cold-resistant end-on kinetochore-microtubule attachments (Figure 2.10 A). Interestingly, we found that location of the GFP had a major impact on the ability of  $\Delta 80$ -Hec1 expressing cells to form kinetochore-microtubule attachments. HeLa cells expressing either C- or N-terminally GFP-tagged WT-Hec1 constructs formed stable, end-on attachments, as previously reported (Guimaraes *et al.*, 2008; Miller *et al.*, 2008; DeLuca *et al.*, 2011; Mattiuzzo *et al.*, 2011; Etemad *et al.*, 2015; Janczyk *et al.*, 2017). In contrast, HeLa cells expressing C-terminally GFP-tagged  $\Delta 80$ -Hec1 formed end-on kinetochore-microtubule attachments, while those expressing N-terminally GFP-tagged  $\Delta 80$ -Hec1 did not (Figure 2.10 B). Similar results were found in RPE1 cells (Figure 2.10 D). We quantified cold-resistant attachment stability in HeLa cells expressing either C- or N-terminally GFP-tagged  $\Delta 80$ -Hec1 and confirmed that while cells expressing C-terminally tagged  $\Delta 80$ -Hec1 were able to form cold-stable, end-on attachments, cells expressing N-terminally tagged  $\Delta 80$ -Hec1 were not (Figure 2.10 C and D).

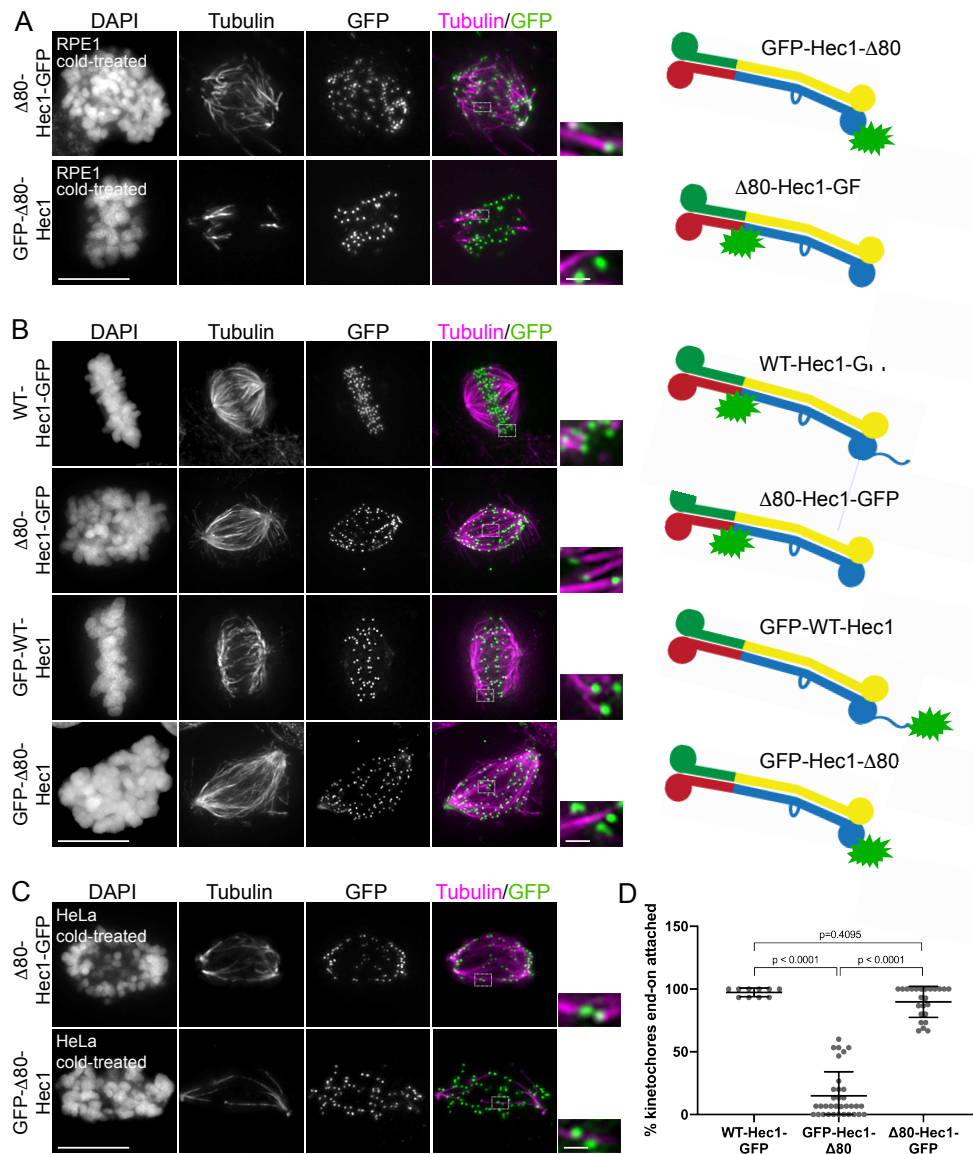


**Figure 2.10. Location of the GFP tag differentially affects end-on attachment formation.** (A) Immunofluorescence images of cold-treated RPE1 cells expressing N- and C-terminally GFP-tagged  $\Delta 80$ -Hec1 constructs. Cells were incubated in ice-cold DMEM for 15 minutes prior to fixation, permeabilized, fixed, and stained with antibodies to tubulin. Insets are enlargements of the region indicated by the dashed box. Schematics of the constructs used are indicated on the right. (B) Immunofluorescence images of HeLa cells expressing N- and C-terminally GFP-tagged WT- and  $\Delta 80$ -Hec1 constructs. Insets are enlargements of the region indicated by the dashed box. Schematics of the constructs used are indicated on the right. (C) Immunofluorescence images of cold-treated HeLa cells expressing N- and C-terminally tagged  $\Delta 80$ -Hec1 constructs. Cells were incubated in ice-cold DMEM for 12 minutes prior to fixation,

permeabilized, fixed, and stained with antibodies to tubulin. Insets are enlargements of the region indicated by the dashed box. (D) Quantification of end-on kinetochore-microtubule attachment in cold-treated HeLa cells expressing WT-Hec1-GFP, and N- and C-terminally tagged  $\Delta 80$ -Hec1 constructs. For N- and C-terminally tagged  $\Delta 80$ -Hec1 constructs, at least 15 kinetochores per cell were quantified from at least 8 cells from 3 independent experiments. For the WT-Hec1-GFP metaphase data, 15 kinetochores per cell were quantified from 5 cells per experiment from 2 independent experiments. The data for C-terminally tagged  $\Delta 80$ -Hec1- GFP and WT-Hec1-GFP are from Figure 2.8 C. Statistical significance was determined using a Student's t-test. Scale bars: 10  $\mu\text{m}$  and 1  $\mu\text{m}$  for panels and insets, respectively

After characterizing the phenotype of cells expressing  $\Delta 80$ -Hec1-GFP, we returned to our original question of whether the Hec1 tail is required for Ska complex recruitment to kinetochores. Immunofluorescence analysis revealed no significant difference in Ska3 levels at kinetochores in metaphase cells expressing WT- versus  $\Delta 80$ -Hec1-GFP (Figure 2.11 A and B). Similarly, microtubule-independent Ska3 recruitment to kinetochores also remained high in cells expressing  $\Delta 80$ -Hec1-GFP (Figure 2.3 C and D), suggesting that the tail domain is dispensable for both microtubule-dependent and -independent Ska complex recruitment. Because purified Ska complexes compensated for the weak binding affinity of  $\Delta 80$ -NDC80 complexes in vitro (Figure 2.6), we asked whether formation of kinetochore-microtubule attachments in cells expressing  $\Delta 80$ -Hec1-GFP required the presence of an intact Ska complex. We depleted Ska1 and Ska3 from HeLa cells, expressed either WT- or  $\Delta 80$ -Hec1-GFP, incubated the cells in cold media, and measured the abundance of end-on kinetochore-microtubule attachments. Kinetochore-microtubule attachments failed to form in Ska1/Ska3-depleted cells expressing either WT- or  $\Delta 80$ -Hec1-GFP (Figure 2.11 C and D), which is in contrast to cells expressing 8A- and 9A-Hec1-GFP (Figure 2.3 E and F; Figure 2.5 E

and F). Thus, tail-less NDC80 complexes, similar to WT complexes, require the Ska complex to form attachments to microtubules. Collectively, our results suggest that the tail domain of Hec1 is not explicitly required for either Ska complex recruitment to kinetochores or formation of stable kinetochore–microtubule attachments, but it likely plays a role in force generation at the attachment interface in human cells.

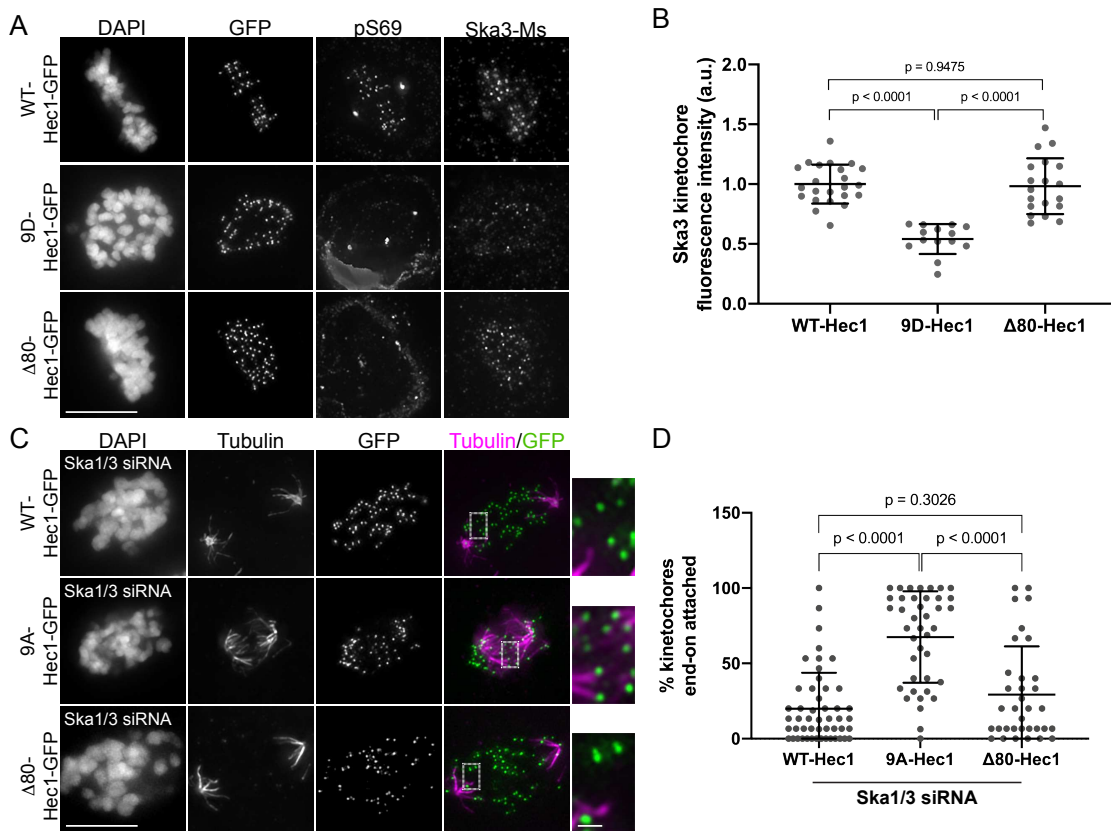


**Fig 2.11. The Hec1 tail domain is dispensable for Ska complex recruitment to kinetochores and is required for kinetochore–microtubule attachments in the absence of the Ska complex.** (A) Immunofluorescence images of cells expressing WT-, 9D-, and Δ80-Hec1-GFP. Cells were fixed and stained using antibodies to Hec1-pS69 and Ska3 (mouse). (B) Quantification of Ska3 kinetochore fluorescence intensity from cells expressing WT-, 9D-, and Δ80-Hec1-GFP. For each condition, at least 20 kinetochores per cell were measured from at least five cells per experiment from three separate experiments. Statistical significance was determined by a one-way ANOVA. (C) Immunofluorescence images of cold-treated cells expressing WT-, 9A-, and Δ80-Hec1-GFP and treated with Ska1 and Ska3 siRNA. Cells were incubated in ice-cold

DMEM for 12 min, permeabilized, fixed, and stained with antibodies to tubulin. Insets are enlargements of the regions indicated by the dashed boxes. (D) Quantification of end-on attachment in cells expressing WT-, 9A-, and  $\Delta$ 80-Hec1-GFP and treated with Ska1 and Ska3 siRNA. The WT- and 9A-Hec1 data shown are from the experiment presented in Figure 2.3. For each condition, at least 15 kinetochores per cell were measured from at least 10 cells per experiment from three separate experiments. Statistical significance was determined by a one-way ANOVA. On all dot plots, each dot represents the average value for all kinetochores from a single cell. Scale bars: 10 and 1  $\mu$ m for panels and insets, respectively.

### **The Ska complex is recruited to the internal coiled-coil domain region of the NDC80 complex to enhance NDC80-MT binding**

To home in on the Ska complex recruitment domain within the NDC80 complex, we carried out two-color fluorescence localization mapping of Ska complex components at metaphase kinetochores (Wan *et al.*, 2009). Since the C-terminal half of Ska3 contains the putative NDC80 binding site, we first mapped the distance between a Ska3 antibody that recognizes amino acids 226–253 (Figure 2.13 A; “Ska3-M,” for “middle”) and both CENP-C (inner kinetochore) and the N-terminus of Hec1 (outer kinetochore). These measurements revealed that amino acids 226–253 of Ska3 reside ~47 nm outside of CENP-C and ~29 nm inside of the N-terminus of Hec1 (Figure 2.13, A–D), suggesting that a region encompassed by the NDC80 complex–binding domain is localized near the internal, coiled-coil region of the NDC80 complex. Reconstituted, purified human Ska complexes have been shown to exist as either monomers or dimers of the Ska1, Ska2, and Ska3 trimer, which are formed through oligomerization of the N-termini of each protein to form a three-helix bundle (Jeyaprakash *et al.*, 2012; Helgeson *et al.*, 2018). Ska1’s C-terminus contains a winged-helix domain that has microtubule binding activity, and Ska3 contains a predominantly unstructured C-terminal region that is

responsible for interaction with the NDC80 complex (Jeyaprakash *et al.*, 2012; Abad *et al.*, 2014, 2016).

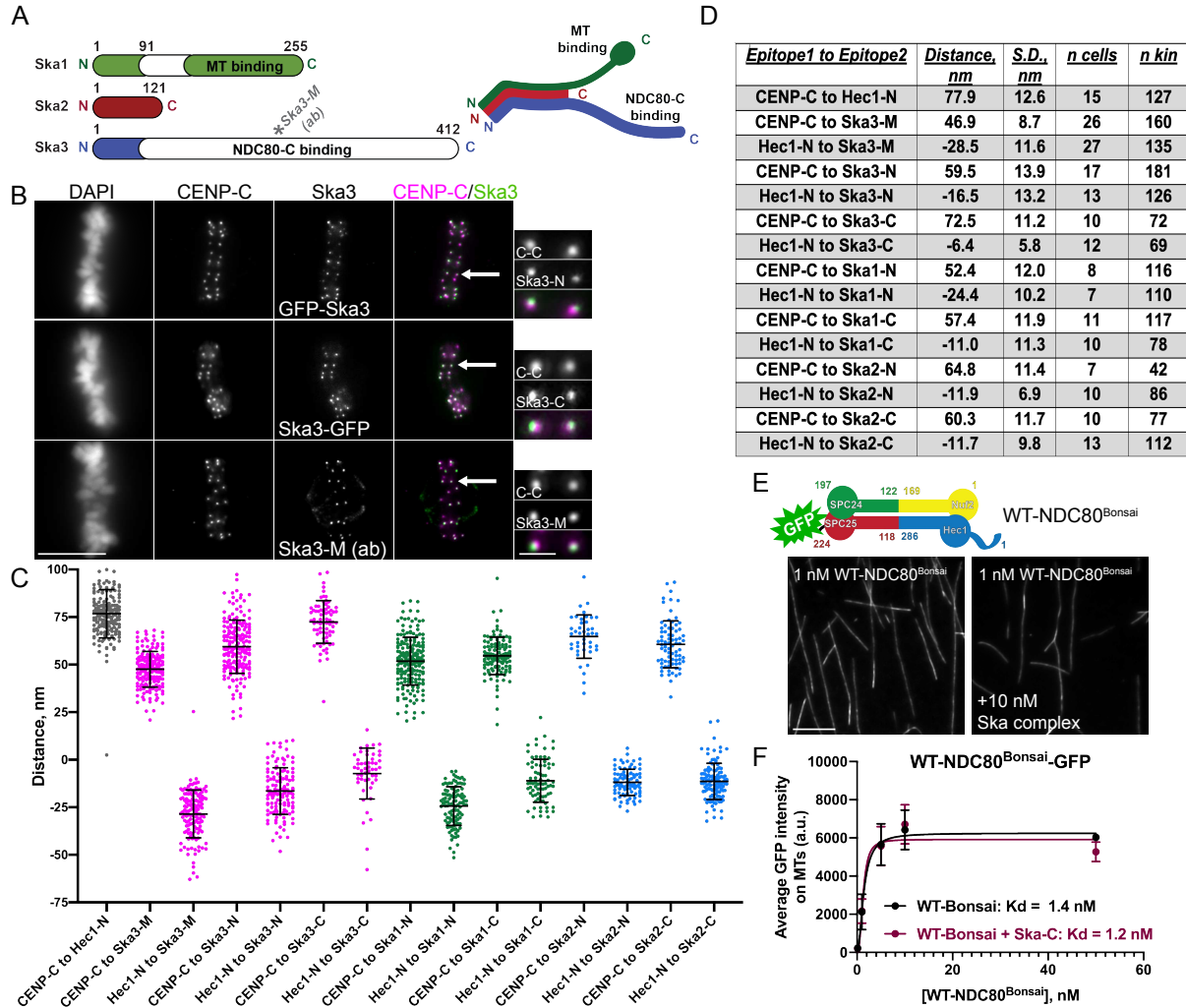


**Fig 2.13. The Ska complex localizes to kinetochores at the central coiled-coil domain of the NDC80 complex.** (A) Left: schematic showing the domain architecture of the Ska complex components. White regions indicate predicted disordered domains (Jeyaprakash *et al.*, 2012). The Ska3 antibody directed to amino acids 226–253 is indicated on the schematic and represents the “Ska3-Middle Domain” (“Ska3-M”). Right: schematic of a single Ska complex (one copy of each subunit), showing the trimerization domains located in the N-termini of Ska1, Ska2, and Ska3, the microtubule binding domain of Ska1 (green), and the proposed NDC80 complex–binding region in Ska3 (blue). (B) Immunofluorescence images of metaphase cells expressing N- and C-terminally GFP-tagged Ska3 and stained with antibodies to inner kinetochore protein

CENP-C (top two rows) and immunofluorescence images of a metaphase cell stained with antibodies to Ska3-M (rabbit) and CENP-C (bottom row). Arrows point to the kinetochore pairs shown in the insets. (C) Plots of the mean distance between the indicated kinetochore proteins/protein domains. Measurements with “Hec1-N” were carried out with an antibody to the CH domain in the N-terminus of Hec1 (9G3). “N” and “C” epitopes for each of the Ska complex components are N- and C-terminal GFP moieties, respectively. Each point on the graph represents a distance measurement for a pair of sister kinetochores. (D) Summary of data presented in panel C. Positive values indicate that epitope 1 was mapped inside epitope 2. Negative values indicate that epitope 1 was mapped outside of epitope 2. The numbers of cells ( $n$  cells) and kinetochore pairs ( $n$  kin) are indicated. (E) Top: schematic of the NDC80<sup>Bonsai</sup> complex. Bottom: GFP fluorescence images of the NDC80<sup>Bonsai</sup> complex decorating microtubules in the presence and absence of Ska complex. Images show a single concentration of the NDC80<sup>Bonsai</sup> complex from the experiment (1 nM) with and without added Ska complex (10 nM). (F) Binding curves from the microtubule binding assays. Datapoints and curve fits shown in black are from experiments without added Ska complex. Those shown in burgundy are from experiments with added Ska complex. Each point on the curve represents the average fluorescence intensity at that concentration from three separate experiments. For each concentration, fluorescence intensities of GFP-NDC80 complexes were measured on at least 40 individual microtubules from at least 10 different TIRF fields per experiment. Scale bars: 10 and 1  $\mu$ m for panels and insets, respectively.

To better understand how the Ska complex components are organized at the kinetochore–microtubule interface, we carried out further paired fluorescence localization mapping using N- and C-terminal GFP tags on the Ska complex components. The N-terminal GFP tags on Ska1, Ska2, and Ska3 all mapped to a similar domain within the kinetochore, which was 52–65 nm outside of CENP-C and 12–24 nm inside the CH domain of Hec1 (Figure 2.13 C and D). This is not surprising, since the N-termini of Ska1, 2, and 3 form a well-folded, relatively compact oligomerization domain (Jeyaprakash *et al.*, 2012). Furthermore, we found that all C-terminal domains of Ska1, Ska2, and Ska3 also mapped to a region inside the Hec1 CH domain. However, we note that the C-terminal GFP tag on Ska3 was localized very close to this region, with a

mapped distance of ~73 nm outside of CENP-C and ~6 nm inside the Hec1 CH domain (Figure 2.13 B–D). This suggests that the unstructured domain of Ska3 may extend substantially along the length of the coiled-coil domain of the NDC80 complex. These experiments were carried out using a 2D analysis of kinetochore domain localization (Wan *et al.*, 2009), and we note that our reported average distance between CENP-C and the CH domain of Hec1 is consistent with previously reported 2D and 3D measurements (Figure 2.13 C and D; Wan *et al.*, 2009; Suzuki *et al.*, 2018; Roscioli *et al.*, 2019).

The mapping experiments suggested that the Ska complex is recruited to the central coiled-coil region of the NDC80 complex. To further investigate a role for this region in Ska complex binding, we carried out microtubule binding experiments in the presence and absence of purified Ska complexes using NDC80<sup>Bonsai</sup>, a truncated NDC80 complex missing most of the central coiled-coil region and the loop domain (Ciferri *et al.*, 2008). Indeed, we found that while the NDC80<sup>Bonsai</sup> complexes bound robustly to microtubules, the affinity of NDC80<sup>Bonsai</sup> complexes for microtubules was not increased with the addition of Ska complexes (Figure 2.13 E and F). These findings are consistent with recent results from the Liu and Musacchio labs, which demonstrate that NDC80<sup>Bonsai</sup> complexes are unable to bind to purified Ska complexes (Zhang *et al.*, 2017; Huis in't Veld *et al.*, 2019). Additionally, we found that in BRB80 buffer, addition of the Ska complex did not induce clustering of NDC80<sup>Bonsai</sup> complexes on microtubules, in contrast to NDC80<sup>Bronsai</sup> complexes (Figure 2.7 B), further supporting the idea that the central coiled-coil region of the NDC80 complex is required for Ska complex association.

## **The Hec1 loop domain impacts kinetochore-microtubule attachments by Ska complex-dependent and -independent mechanisms**

We next generated a version of NDC80<sup>Bronsai</sup> in which the amino acids that make up the “loop” region of Hec1 (amino acids 420–460; Maiolica *et al.*, 2007) were substituted with alternative amino acids predicted to form a flexible motif (Varma *et al.*, 2012) (ML-NDC80<sup>Bronsai</sup>, Figure 2.13 A). We then tested whether the microtubule binding affinity of this mutant version of the complex was increased by addition of purified Ska complexes. We found that while ML-NDC80<sup>Bronsai</sup> bound to microtubules with an affinity similar to that of WT-NDC80<sup>Bronsai</sup>, the addition of purified Ska complex had no significant effect on its microtubule binding affinity (Figure 2.13 B and C). These results suggest that mutation of the loop domain either prevents the Ska complex from directly interacting with the NDC80 complex or precludes a conformation that promotes formation of a NDC80/Ska/microtubule complex.

We then asked whether the loop domain was required for Ska complex recruitment to kinetochores in cells. For this purpose, we expressed the Hec1 loop mutant (ML-Hec1-GFP) in HeLa cells and found that Ska3 levels were significantly reduced at kinetochores compared with kinetochores from cells expressing WT-Hec1-GFP (Figure 2.13 D and E). We also found, consistent with previously published results, that end-on kinetochore–microtubule attachments failed to form and chromosome alignment was abolished in cells expressing ML-Hec1-GFP (Figure 2.13 F–H) (Varma *et al.*, 2012; Zhang *et al.*, 2012). Live cell imaging revealed that cells expressing ML-Hec1 failed to align chromosomes and exit mitosis and that these cells exhibited high levels of

spindle fragmentation (Figures 2.13 I–K, and 2.8 F). Given that Ska complexes maximally load to kinetochores with end-on attachments, again we could not distinguish between two possibilities: 1) the Hec1 loop domain promotes Ska complex recruitment, and in turn, the Ska complex is required for end-on attachment formation; or 2) the Hec1 loop domain is required for generation of stable kinetochore–microtubule attachments, and in turn, stable attachments promote Ska complex loading. We therefore measured Ska complex loading to kinetochores in the absence of microtubules and found that cells expressing ML-Hec1-GFP exhibited reduced levels of Ska3 at kinetochores (Figure 2.3 C and D), suggesting that an intact loop domain is required for efficient Ska complex recruitment to kinetochores.

**A** Wild-type loop (WT): 420 RKLKLIIPKGAENSKGYDFEIKFNPEAGANCLVKYRAQVYVP 460  
 Mutant loop (ML) : 420 ASQGQGQGAQGGASSSGQQQGSASASAASAGQSASASAGGQQ 460

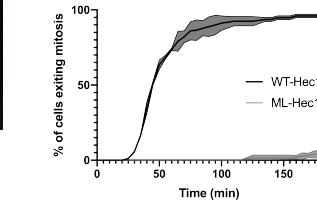
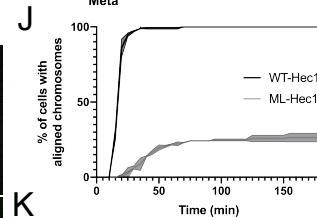
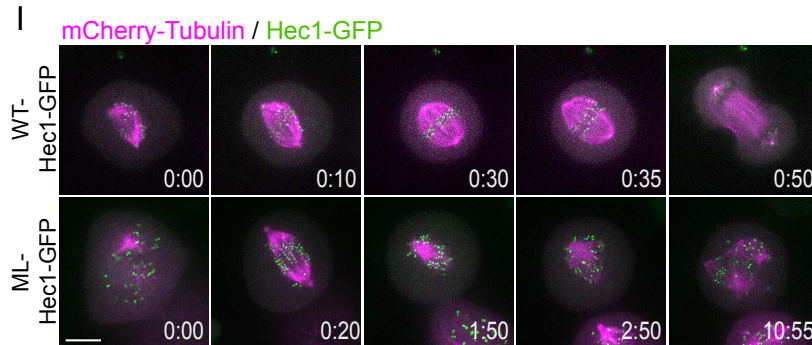
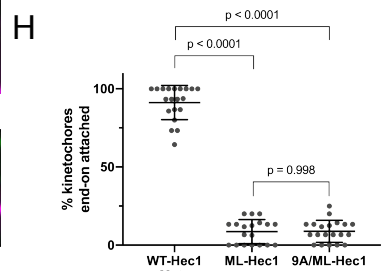
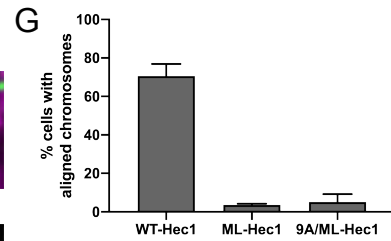
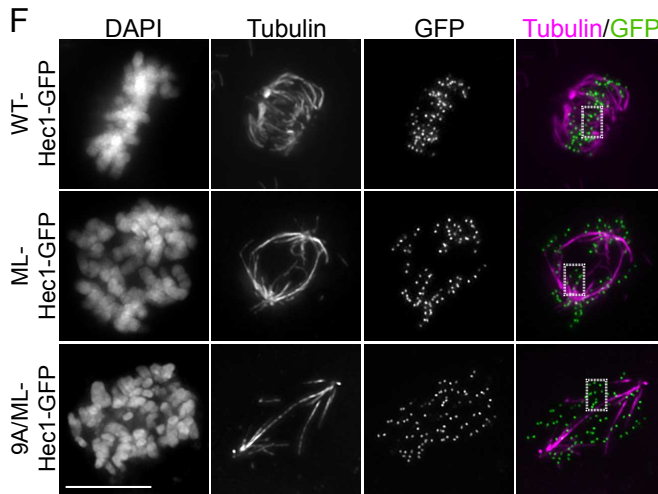
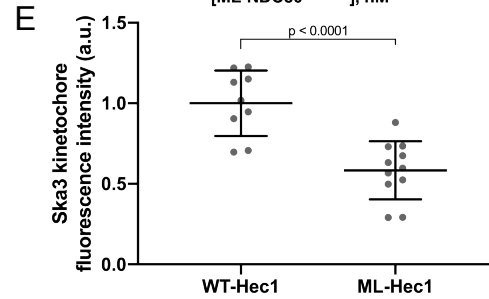
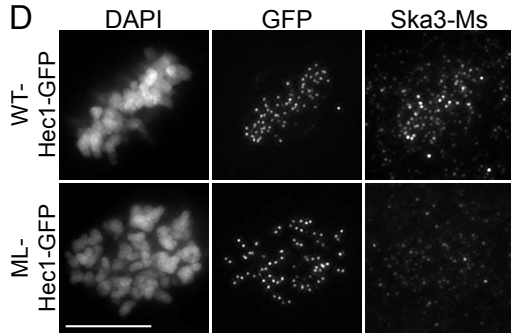
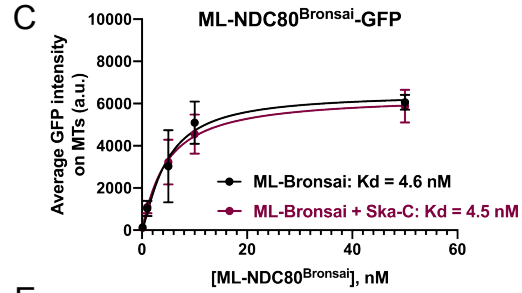
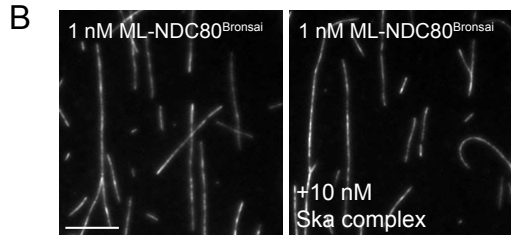


**Fig 2.13. The Hec1 loop domain contributes to Ska complex recruitment to kinetochores and generation of kinetochore–microtubule attachments.** (A) Sequence of the wild-type (WT) and mutated (ML) loop region in Hec1. (B) GFP fluorescence images of the ML-NDC80<sup>Bronsai</sup> complex decorating microtubules in the presence and absence of the Ska complex. Images show a single concentration of the ML-NDC80<sup>Bronsai</sup> complex from the experiment (1 nM) with and without added Ska complex (10 nM). (C) Binding curves from the microtubule binding assays. Datapoints and curve fits shown in black are from experiments without added Ska complex. Those shown in burgundy are from experiments with added Ska complex. Each point on the curve represents the average fluorescence intensity at that concentration from three separate experiments. For each concentration, fluorescence intensities of GFP-NDC80 complexes were measured on at least 40 individual microtubules from at least 10 different TIRF fields per experiment. (D) Immunofluorescence images of cells expressing WT- and ML-Hec1-GFP. Cells were fixed and stained using antibodies to Ska3 (mouse). (E) Quantification of Ska3 kinetochore fluorescence intensity from cells expressing WT- and ML-Hec1-GFP. For each condition, at least 20 kinetochores per cell were measured from at least four cells per experiment from two separate experiments. (F) Immunofluorescence images of cold-treated cells expressing WT-, ML-, and 9A/ML-Hec1-GFP. Cells were incubated in ice-cold DMEM for 12 min, permeabilized, fixed, and stained with antibodies to tubulin. Insets are enlargements of the regions indicated by the dashed boxes. (G) Quantification of chromosome alignment in cells expressing WT-, ML-, and 9A/ML-Hec1-GFP. For each condition, chromosome alignment was assessed in at least 100 cells per experiments from two separate experiments. Cells were scored as “aligned” if they contained a metaphase plate with <5 chromosomes off the plate. (H) Quantification of end-on attachment in cells expressing WT-, ML-, and 9A/ML-Hec1-GFP. Statistical significance was determined using a one-way ANOVA. For each condition, at least 15 kinetochores per cell were measured from at least nine cells per experiment from two separate experiments. (I) Still images from time-lapse experiments of cells expressing Hec1-GFP and mCherry-tubulin. Time from nuclear envelope breakdown (NEBD) denoted at bottom right corner of each image (hours:minutes). (J) Quantification of chromosome alignment efficiency in cells from the experiment shown in Figure I. Cell fate was tracked after mitotic entry (as determined by NEBD) for 3 h, and cells were scored as “aligned” upon metaphase plate formation (as determined by Hec1-GFP fluorescence). Data for WT- and ML-Hec1 are from 175 cells from two independent experiments and 165 cells from two independent experiments, respectively. (K) Quantification of mitotic exit timing in cells from the experiment shown in Figure I. Cell fate was tracked after mitotic entry (as determined by NEBD) for 3 h, and cells were scored as “exiting mitosis” upon anaphase entry. Data for WT- and ML-Hec1 are from 175 cells from two independent experiments and 165 cells from two independent experiments, respectively. Scale bars: 10 and 1  $\mu$ m for panels and insets, respectively.

Both chromosome alignment and kinetochore–microtubule attachment formation were severely impaired in cells expressing ML-Hec1-GFP. We therefore tested whether these defects were exclusively due to loss of Ska complex recruitment to kinetochores. Experiments in Figure 2.3 demonstrated that cells expressing 9A-Hec1-GFP formed hyperstable kinetochore–microtubule attachments, and this phenotype was independent of the Ska complex (Figure 2.3 E and F). These results indicate that attachment defects arising from Ska1/Ska3 depletion can be compensated for by the strong attachments generated in cells expressing 9A-Hec1-GFP. We therefore reasoned that if a mutated loop domain results in attachment defects solely due to loss of Ska complex recruitment, then preventing phosphorylation of the tail domain should rescue this defect. Thus, we generated a hybrid mutant containing a 9A tail domain and the mutant loop sequence (9A/ML-Hec1-GFP). We found that in cells expressing 9A/ML-Hec1-GFP, stable kinetochore–microtubule attachments failed to form and chromosome alignment was severely defective, similar to what we observed in cells expressing ML-Hec1-GFP (Figure 2.13 F–H). These results suggest that although the loop domain may participate in recruiting the Ska complex to kinetochores, it likely plays an additional, non-Ska complex–dependent role in generating kinetochore–microtubule attachments, perhaps through recruitment of other kinetochore proteins. It is also possible that mutation of the loop domain results in changes in NDC80 complex architecture at kinetochores that preclude formation of end-on, stable kinetochore–microtubule attachments.

A variety of loop mutations (including mutants with the loop sequence scrambled, reversed, or deleted altogether) have been reported to result in severe defects in

chromosome alignment and end-on attachment formation when expressed in human cells (Varma *et al.*, 2012; Zhang *et al.*, 2012; Figure 2.13). To narrow down the region of the loop required for wild-type function, we generated systematic Ala substitutions of short stretches of 5–6 amino acids within the Hec1 loop (Figure 2.14 A) and expressed these mutants in cells. Expression of several, but not all, of these mutants mimicked the phenotype observed in cells expressing the ML-Hec1-GFP mutant and led to severe chromosome alignment defects (Figure 2.14 A and B). We noted that mutating regions within the loop that resulted in substantial changes in local net charge produced the strongest chromosome misalignment phenotypes, while mutating regions with low net charge density resulted in no observable defects (Figure 2.14 A–C). This suggests that the distributed charge of the loop region is likely critical for formation of kinetochore–microtubule attachments, potentially through forming interactions with the Ska complex and/or other kinetochore-associated proteins such as Cdt1 (Varma *et al.*, 2012).

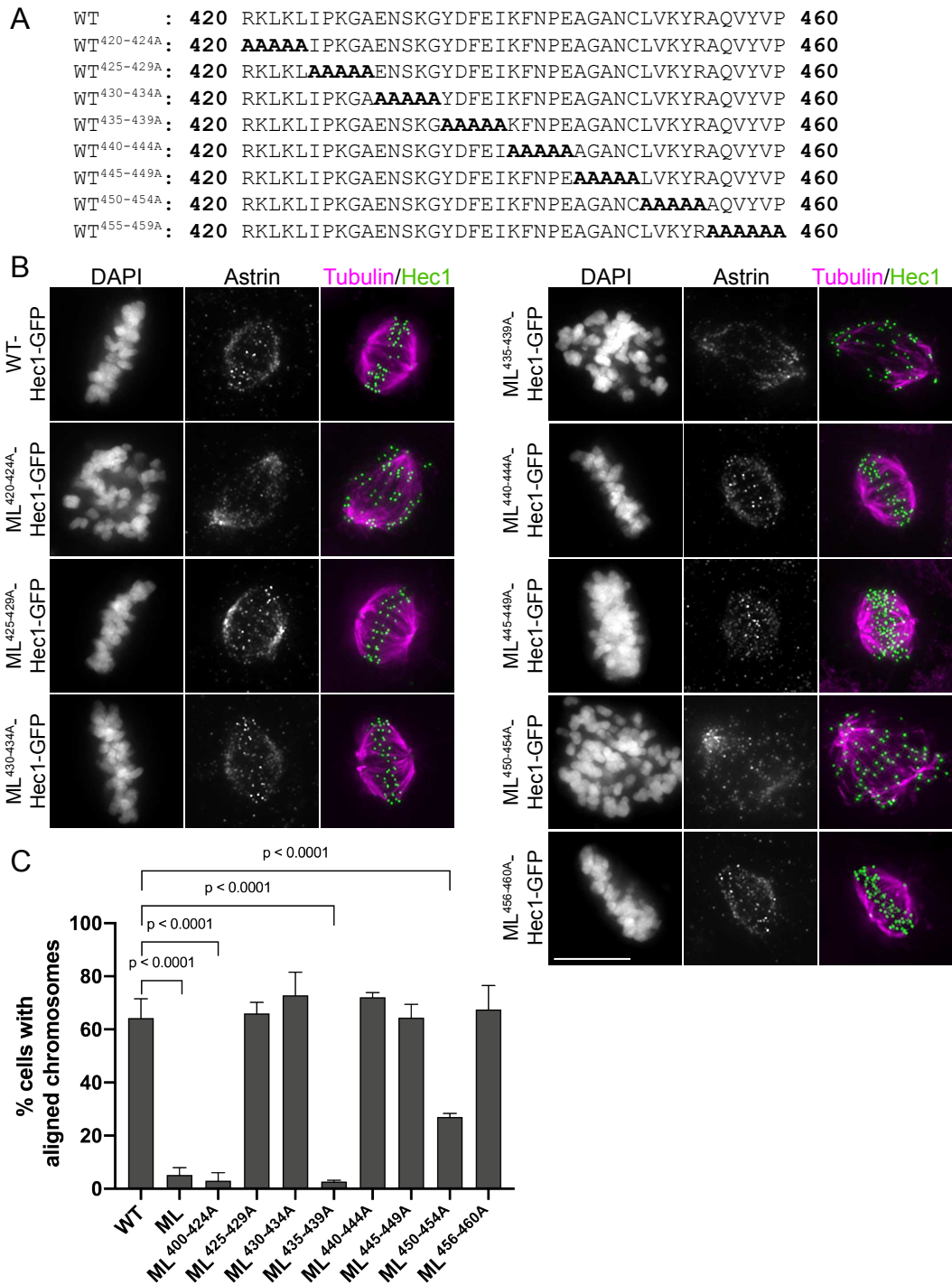


**Fig 2.14. Specific regions of the Hec1 loop are required for chromosome alignment in cells.** (A) List of loop mutants used. (B) Immunofluorescence images of cells expressing WT- or ML-Hec1-GFP constructs and stained with Astrin and tubulin antibodies. (C) Quantification of chromosome alignment in cells expressing WT- or ML-Hec1-GFP constructs. For each condition, at least 120 cells were analyzed from at least

2 separate experiments. Cells were scored as “aligned” if they had a metaphase plate with < 5 chromosomes off the plate. Statistical significance was determined using a one-way Anova analysis. Scale bar: 10  $\mu$ m.

## **2.3 Discussion**

### **Hec1 tail phosphorylation affects kinetochore–microtubule attachments independently of the Ska complex**

The positively charged, N-terminal tail domain of Ndc80/Hec1 is a target of Aurora kinases, and it has been suggested that phosphorylation of the tail directly reduces the affinity of NDC80 complexes for the negatively charged microtubule lattice, which in turn reduces kinetochore–microtubule attachment strength. It is also possible that phosphorylation of the Hec1 tail domain indirectly affects kinetochore–microtubule attachment strength by regulating the recruitment of additional kinetochore-associated microtubule-binding proteins. One possible candidate for imparting this regulation is the Ska complex, which loads to kinetochores progressively during mitosis and contributes to the stabilization of kinetochore–microtubule attachments. We found here that cells expressing a nonphosphorylatable Hec1 mutant (9A-Hec1) recruited increased levels of Ska complex components to kinetochores in human cells, similar to what has been reported in *C. elegans* (Cheerambathur *et al.*, 2017). However, we found that stable kinetochore–microtubule attachments were not dependent on the Ska complex in cells expressing 9A-Hec1, in which tail phosphorylation is completely blocked, or in cells expressing 8A-Hec1, where Ser-69 is left intact and remains phosphorylated throughout mitosis (DeLuca *et al.*, 2018). Furthermore, we demonstrated that the phosphorylation

state of the tail domain did not affect the levels of Ska complexes recruited to kinetochores in the absence of microtubules. Finally, we showed that kinetochore–microtubule attachments were additively destabilized in cells expressing a mutant version of Hec1 containing a phospho-mimetic tail (9D-Hec1) and depleted of the Ska complex. Collectively, these results suggest that, despite coincidental timing, Hec1 tail dephosphorylation and Ska complex recruitment to kinetochores likely contribute to kinetochore-microtubule attachment stabilization independently.

It is noteworthy to mention that the metaphase recruitment of Ska3 to kinetochores differed between 9A-Hec1 and 8A-Hec1 expressing cells. Previous studies have demonstrated that complete dephosphorylation of the Hec1 tail results in hyperstable kinetochore–microtubule attachment formation as evidenced by increases in interkinetochore distance and kinetochore-fiber intensity, lagging chromosomes in anaphase, and dampened metaphase chromosome oscillations (Guimaraes *et al.*, 2008; DeLuca *et al.*, 2011, 2018; Zaytsev *et al.*, 2014; Long *et al.*, 2017). Strikingly, leaving Ser-69 unperturbed while blocking phosphorylation at all other Aurora sites (8A-Hec1) was sufficient to restore chromosome oscillation kinetics to wild-type levels (DeLuca *et al.*, 2018). Similarly, we showed here that cells expressing 8A-Hec1 recruited wild-type levels of Ska3 to kinetochores, while cells expressing 9A-Hec1 recruited significantly higher levels. Despite this, and similar to the case for 9A-Hec1, cells expressing 8A-Hec1 formed cold-stable attachments prematurely and retained robust attachments in the absence of the Ska complex, supporting the model that Hec1 tail dephosphorylation modulates kinetochore–microtubule attachment strength in a Ska complex–independent manner.

Also of note are the somewhat divergent mechanisms for Ska complex recruitment and NDC80 complex–mediated kinetochore–microtubule attachment regulation described in this study compared with those described in *C. elegans*. In *C. elegans*, but not in human cells, depletion of the Ska complex rescued hyperstable kinetochore–microtubule attachment formation caused by expression of a nonphosphorylatable Hec1 tail domain mutant (Cheerambathur *et al.*, 2017). Furthermore, while a pool of attachment-independent Ska complex localizes to kinetochores in human cells, *C. elegans* Ska complex localizes to kinetochores at detectable levels only upon chromosome alignment. These results suggest that in *C. elegans*, dephosphorylation of the Hec1 tail domain promotes Ska complex association to kinetochores, which in turn promotes stabilization of kinetochore–microtubule attachments. As such, the mechanism for Ska complex recruitment to kinetochores is likely not completely conserved from *C. elegans* to humans.

### **The Hec1 tail is dispensable for kinetochore–microtubule attachments in cells**

Consistent with our findings here, chromosome alignment errors and decreased interkinetochore distances have been previously observed in mammalian cells expressing tail-less,  $\Delta 80$ -Hec1 mutants (Guimaraes *et al.*, 2008; Miller *et al.*, 2008; Etemad *et al.*, 2015; Janczyk *et al.*, 2017). These phenotypes have been widely attributed to loss of stable kinetochore–microtubule attachments (Guimaraes *et al.*, 2008; Miller *et al.*, 2008). Contrary to this, we found that  $\Delta 80$ -Hec1 expression did not prevent formation of cold-resistant, stable kinetochore–microtubule attachments in either HeLa or RPE1 cells. Instead, we report that cells lacking the tail domain formed

kinetochore–microtubule attachments prematurely, presumably due to a lack of Aurora kinase–mediated regulation. In such a scenario, cells expressing tail-less Hec1 are unable to negatively regulate the initial formation of end-on kinetochore–microtubule attachments, and the NDC80 complex is able to bind spindle microtubule plus ends through strong Hec1 CH domain–mediated interactions, which would otherwise be kept labile by a highly phosphorylated Hec1 tail domain. Despite this early accumulation of attachments, however, we found that cells expressing  $\Delta 80$ -Hec1-GFP exhibited decreased interkinetochore distances, suggesting that attachments are unable to produce sufficient forces to generate wild-type tension across sister kinetochore pairs.

Maintenance of a bipolar mitotic spindle requires a balance of forces within the spindle, some of which are derived from chromosomes and their attachments to spindle microtubules (Manning and Compton, 2007; Maiato and Logarinho, 2014).

Fragmentation of spindles leading to multipolarity can be caused by alterations in forces generated at the kinetochore–microtubule interface and by loss of sister chromatid cohesion (Daum *et al.*, 2011; Stevens *et al.*, 2011; Maiato and Logarinho, 2014). In the case of cells expressing tail-less Hec1, we observed a high incidence of multipolarity, similar to what we observed in cells expressing the Hec1 loop mutation, in which kinetochore-microtubule attachments failed to form altogether. Cells expressing  $\Delta 80$ -Hec1 were able to form cold-stable end-on attachments, but these attachments did not generate wild-type force and were not sufficient to allow cells to exit mitosis with normal timing. Thus, defective force generation and/or cohesin fatigue may contribute to the high incidence of multipolarity observed in  $\Delta 80$ -Hec1 expressing cells. Alternatively, the Hec1 tail may have an uncharacterized role at the centrosome, perhaps involving the

Hec1-Hice1 interaction, which is required for maintenance of spindle bipolarity (Wu *et al.*, 2009). Future studies will be required to fully characterize the causes of multipolarity in  $\Delta 80$ -Hec1 expressing cells.

It is noteworthy to mention that a recent *in vitro* study has also implicated the Hec1 tail domain in force generation at the kinetochore–microtubule interface: Huis in't Veld *et al.* (2019) artificially trimerized NDC80 complexes on the surface of beads and measured the ability of NDC80 complex trimers to resist force from an optical trap. NDC80 complex trimers lacking the Hec1 tail—despite binding to microtubules with high affinity—detached from depolymerizing microtubules in both the presence and absence of applied force, whereas wild-type NDC80 trimers remained bound under these conditions (Huis in't Veld *et al.*, 2019). These results led the authors to conclude that the Hec1 tail is critical for force coupling at the kinetochore–microtubule interface.

An important distinction between our study and several previously published studies is the requirement for the Hec1 tail in formation of kinetochore–microtubule attachments. Notable experimental differences may explain the conflicting results. For example, in one previous study, N-terminally tagged Hec1 constructs were used (Etemad *et al.*, 2015). In our current study, when we tagged WT-Hec1 with GFP on either the C- or N-terminus, we found that both constructs were competent to support formation of kinetochore–microtubule attachments. However, while cells expressing C-terminally tagged  $\Delta 80$ -Hec1-GFP were able to form attachments, those expressing N-terminally tagged GFP- $\Delta 80$ -Hec1 were not. Thus, replacing the N-terminal tail of Hec1 with a GFP moiety results in a failure to form kinetochore–microtubule attachments. In other

published studies, researchers used  $\Delta 80$ -Hec1 mutants lacking a GFP tag to rescue depletion of endogenous Hec1 and reported failure to form kinetochore–microtubule attachments (Miller *et al.*, 2008; Janczyk *et al.*, 2017). In our study, we found that transfection of equal amounts of Hec1 transgenic DNA led to significant differences in protein expression, with  $\Delta 80$ -Hec1 being expressed at ~50% lower levels than WT-Hec1 (Figure 2.1 A and B). In the case of siRNA silence-rescue experiments, this difference in expression would likely result in an incomplete rescue and defects in kinetochore–microtubule attachments. In most of our experiments, we did not treat cells with Hec1 siRNA, but rather measured endogenous Hec1 depletion from kinetochores using an antibody to the constitutively phosphorylated residue Ser-69 on the Hec1 tail. In this experimental scheme, we analyzed only cells with similar kinetochore GFP levels (Figure 2.1 C; see also *Materials and Methods*), thus avoiding any discrepancies associated with incomplete rescue. Finally, a previous study from our lab expressed C-terminally tagged  $\Delta 80$ -Hec1 mutants in PtK1 cells and reported defective kinetochore–microtubule attachment (Guimaraes *et al.*, 2008). This study was done using PtK1 cells stably expressing photo-activatable (PA)-GFP-tubulin, and it is possible that the expression levels of this tubulin construct specifically compromised the kinetochore–microtubule interface in a manner that sensitized cells to Hec1 tail loss. Alternatively, it is possible that PtK1 cells have a requirement for this domain of Hec1 different from that of human cells. Expressing  $\Delta 80$ -Hec1 in otherwise unperturbed PtK1 cells will be important to address this question.

Our results describing the formation of end-on attachments in human cells expressing tail-less Hec1 are consistent with results from both budding yeast and *C.*

*elegans*, where the Ndc80 tail domain is not strictly required for kinetochore–microtubule attachment (Kemmler *et al.*, 2009; Demirel *et al.*, 2012; Cheerambathur *et al.*, 2013; Lampert *et al.*, 2013). However, similar to the scenario in human cells, the tail domain does play some role at the kinetochore–microtubule interface in these organisms. For example, in budding yeast the tail domain becomes required for cell survival upon perturbation of the Dam1 complex, a kinetochore-associated complex found in yeasts but not higher eukaryotes, which contributes to generating stable kinetochore–microtubule attachments (Demirel *et al.*, 2012; Lampert *et al.*, 2013). In addition, a study using a tension sensor inserted near the N-terminus of budding yeast Hec1 demonstrated that while the tail domain is not required for kinetochore–microtubule attachment formation per se in cells, its deletion results in reduced tension at the NDC80 complex–microtubule interface (Suzuki *et al.*, 2016). Taken with the result that the Hec1 tail is required for load-bearing attachments of NDC80 complexes to microtubules (Huis in't Veld *et al.*, 2019), the available data suggest that this function of the Hec1 tail domain is generally conserved from budding yeast to humans.

### **The Ska complex compensates for Hec1 tail domain function**

Studies using NDC80 complexes purified from various organisms have demonstrated that the Hec1 tail domain is required for high-affinity NDC80 complex–microtubule binding in vitro (Cheeseman *et al.*, 2006; Wei *et al.*, 2007; Alushin *et al.*, 2012; Umbreit *et al.*, 2012; Cheerambathur *et al.*, 2013; Lampert *et al.*, 2013; Zaytsev *et al.*, 2015). In the case of human NDC80 complexes, addition of the

Ska complex compensates for deletion of the Hec1 tail in a number of in vitro NDC80 complex–microtubule interaction assays. Helgeson *et al.* (2018) carried out optical trapping experiments using NDC80 complex–coated beads to demonstrate that while NDC80 complexes lacking the Hec1 tail generated weak attachments to microtubules that could be disrupted under low rupture forces, addition of soluble Ska complexes significantly strengthened these attachments. Consistent with these findings, Huis in't Veld *et al.* (2019) found that addition of the Ska complex to trimerized NDC80 complexes lacking the Hec1 tail enabled these complexes to track depolymerizing microtubules, a property not observed in the absence of the Ska complex. The notion that the Ska complex can functionally compensate for Hec1 tail deletion is reminiscent of studies carried out in budding yeast with the Dam1 complex, which has been suggested to be a functional orthologue of the Ska complex (Welburn *et al.*, 2009). Analogous to the experiments described above for human Ska and NDC80 complexes, Dam1 is able to enhance the affinity of tail-less budding yeast NDC80 complexes for microtubules in vitro (Lampert *et al.*, 2010; Tien *et al.*, 2010; Lampert *et al.*, 2013). Consistently, deletion of the Ndc80/Hec1 tail is not lethal in budding yeast (Kemmler *et al.*, 2009; Demirel *et al.*, 2012; Lampert *et al.*, 2013), but deletion or mutation of Dam1 sensitizes cells to loss of the Ndc80/Hec1 tail, resulting in cell death due to cell division defects (Demirel *et al.*, 2012; Lampert *et al.*, 2013; Suzuki *et al.*, 2016). In line with these results, we found that cells expressing  $\Delta 80$ -Hec1-GFP were able to form cold-stable kinetochore–microtubule attachments, but this required the presence of the Ska complex. Collectively, our in vitro and cell-based results suggest

that the Ska complex can compensate for the Hec1 tail's role in forming stable kinetochore–microtubule attachments in human cells.

### **The Ska complex is recruited to the internal coiled-coil domain of the NDC80 complex rather than the Hec1 tail domain**

Ska complex loading to kinetochores requires the NDC80 complex (Gaitanos *et al.*, 2009; Welburn *et al.*, 2009; Chan *et al.*, 2012; Zhang *et al.*, 2012), and the two complexes directly interact (Zhang *et al.*, 2017; Helgeson *et al.*, 2018; Huis in't Veld *et al.*, 2019). Although Ska3 is known to mediate the interaction, its binding site on the NDC80 complex remains unresolved (Zhang *et al.*, 2018). Our results demonstrate that the Hec1 tail is not required for Ska complex–mediated enhancement of NDC80–microtubule interactions or for Ska complex localization to kinetochores in cells. We note that these results are inconsistent with a previous report from Janczyk *et al.* (2017), where it was shown that mutations in the Hec1 tail abolish Ska recruitment to the NDC80 complex–microtubule interface in vitro and to kinetochores in cells. It is unclear why our results differ from theirs, although a potential explanation is that the tail mutations made in the Janczyk *et al.* study impacted overall kinetochore architecture in a manner that precluded Ska recruitment independently of the Hec1 tail. To map the Ska complex kinetochore recruitment domain, we used two-color colocalization imaging and found that the Ska complex colocalized with the coiled-coil region of the NDC80 complex, inside the Hec1 CH domain. Interestingly, most of the N- and C-termini of all Ska complex components also mapped near this region, suggesting that the bulk of the complex is not significantly extended along the NDC80

complex axis. The one exception is the C-terminus of Ska3, which mapped closely to, but still inside, the CH domain of Hec1, suggesting that the unstructured region of Ska3 may be somewhat elongated along the length of the NDC80 complex. These results are consistent with a recent study from Helgeson *et al.* (2018), in which the authors found a large number of contact points between Ska3 and the coiled-coil region of the NDC80 complex using cross-linking mass spectrometry.

### **The Hec1 loop domain has Ska complex–dependent and –independent functions in chromosome alignment**

We report that mutation of the Hec1 loop domain prevents enhancement of NDC80 complex–microtubule binding by the Ska complex. This is possibly at odds with a recent study from Huis in't Veld *et al.* (2019), which reported that removal of the loop domain from Hec1 did not affect the interaction between soluble NDC80 and Ska complexes. This difference could possibly reflect a requirement for the loop domain in the interaction of NDC80 and Ska complexes specifically on microtubules. Alternatively, since Ska3 phosphorylation by CDK1 increases the affinity of soluble Ska and NDC80 complexes for each other (Zhang *et al.*, 2017; Huis in't Veld *et al.*, 2019), the phosphorylation state of Ska3 might impact the requirement of the Hec1 loop domain for the two complexes to associate. In such a scenario, dephosphorylated Ska complexes bind more weakly to NDC80 complexes in the presence of microtubules, and the loop domain is required for high-affinity interactions, specifically under these suboptimal binding conditions. Given our result that the loop domain is required in cells for

microtubule-independent Ska complex loading to kinetochores, we do not favor the latter hypothesis.

Both chromosome alignment and kinetochore–microtubule attachments were severely perturbed in cells expressing Hec1 constructs containing a mutated loop domain—more so than in cells expressing 9D-Hec1 mutants or in cells depleted of Ska1 and Ska3. This was observed in previous studies (Zhang *et al.*, 2012; Varma *et al.*, 2012) and led us to ask whether the defects observed were entirely due to loss of Ska complex recruitment. To test this, we modified the loop mutant to include a nonphosphorylatable N-terminal tail domain, since we demonstrated that expression of the 9A-Hec1 mutant abrogated the need for Ska1 and Ska3 to form stable kinetochore–microtubule attachments. Cells expressing the 9A/ML-Hec1 mutant showed no improvement in either chromosome alignment or formation of stable kinetochore–microtubule attachments compared with those expressing ML-Hec1. Thus, we conclude that in addition to contributing to efficient Ska complex recruitment to kinetochores, the Hec1 loop has an additional, non-Ska complex–dependent role in forming stable attachments. We found that mutating short stretches of the loop sequence that contain at least two charged residues phenocopied expression of the full ML-Hec1 construct. Thus it is possible that the loop domain recruits additional factors, such as Cdt1, that are required for generation of stable, end-on kinetochore–microtubule attachments (Varma *et al.*, 2012). Alternatively, the loop region could be critical for adoption of a conformation of NDC80 that is required for maintaining proper, end-on attachments to microtubules.

Overall, our results support a model in which the Hec1 tail domain, while not explicitly required for forming end-on kinetochore–microtubule attachments, is important in regulating the force-generating attachments between kinetochores and microtubule plus ends. They also suggest that the Ska complex is loaded to the central coiled-coil region of the NDC80 complex during mitosis to ensure proper force coupling at the kinetochore–microtubule interface, which may be particularly important at kinetochores containing NDC80 complexes with lower microtubule binding capacity (e.g., with highly phosphorylated tail domains). How tail domain phosphorylation and dephosphorylation are coordinated with Ska complex loading to kinetochores to ensure proper regulation of kinetochore–microtubule attachments is an important issue that requires future investigation.

## **2.4 Methods**

### **Cell culture**

HeLa Kyoto cells were cultured in DMEM supplemented with 10% fetal bovine serum (FBS) and 1% antibiotic/antimycotic solution. RPE1 (American Type Culture Collection) cells were cultured in 1:1 Ham's F12:DMEM supplemented with 10% FBS and 1% antibiotic/antimycotic solution. All cell lines were maintained at 37°C in 5% CO<sub>2</sub>.

### **Cell treatments and transfections**

For all fixed cell experiments, cells were grown on sterile, acid-washed coverslips in six-well plates. All nucleic acid transfections were done in Optimem (Life Technologies). siRNA duplexes were transfected as follows: Ska3 (5'-AGACAAACAUGAACAUUAA-3';

Gaitanos *et al.*, 2009) at 80 nM, Ska1 (5'-CCCGCTTAACCTATAATCAAA-3'; Hanisch *et al.*, 2006) at 80 nM, and Hec1 (5'-CCCUGGGUCGUGUCAGGAA-3'; DeLuca *et al.*, 2011) at 160 nM. All siRNA duplexes were transfected into HeLa cells using Oligofectamine (Thermo Fisher Scientific) according to the manufacturer's protocol. For all siRNA transfections, cells were processed for immunofluorescence 48 h after addition of siRNA. Plasmids encoding Hec1-GFP and mCherry-tubulin were transfected into HeLa Kyoto cells with Lipofectamine 2000 (Thermo Fisher Scientific) according to the manufacturer's protocol. RPE1 cells were transfected using a nucleofector (Lonza) and using Lonza Kit L according to the manufacturer's protocol with program X-001. Cells were processed for immunofluorescence 24 h following DNA transfection. For silence-rescue experiments of Hec1 and expression of Hec1 mutants in Ska-depleted cells, cells were transfected with siRNA using Oligofectamine and 24 h later were transfected with DNA using Lipofectamine 2000. At 24 h after DNA transfection (48 h post-siRNA addition), cells were processed for immunofluorescence. For end-on attachment experiments, transfection media was replaced with ice-cold DMEM 24 h post-DNA transfection and cells were incubated on ice for 12 min prior to fixation. For attachment-independent analysis of Ska3 localization, Hec1-GFP-transfected cells were arrested at the G2/M transition by inhibiting CDK1/Cyclin-B with 9  $\mu$ M RO-3306 (Sigma-Aldrich) for 16 h and then extensively washed out with warm DMEM and placed into DMEM supplemented with 10  $\mu$ M nocodazole (Tocris Bioscience), where they were incubated at 37°C for 1 h before being processed for immunofluorescence. For analysis of asynchronous, attachment-independent Ska3 levels (Figure 2.4), cycling HeLa cell populations were treated with 10  $\mu$ M nocodazole for 1 h without any synchronization and then were processed for

immunofluorescence. For live cell experiments, cells were synchronized with thymidine the day after being seeded into glass-bottom live cell dishes (35 mm), washed out of the first thymidine treatment 16 h later, and subsequently transfected with plasmids encoding Hec1-GFP and mCherry-tubulin. At eight hours post-transfection, cells were subjected to a second thymidine treatment. The following day (16 h after the second thymidine treatment), cells were washed out into warm DMEM and incubated for nine hours prior to live cell imaging.

### **Western blotting**

Hec1-GFP transfected cells were harvested 24 h post-transfection and stored at  $-20^{\circ}\text{C}$  until use, at which time they were thawed on ice and resuspended in lysis buffer (4 mM dithiothreitol [DTT] in phosphate-buffered saline with protease inhibitors). Cells were lysed by sonication and subjected to Western blot analysis. Hec1 expression was detected using mouse anti-Hec1 9G3 (Novus Biologicals) at 1:500 and donkey anti-mouse horseradish peroxidase (Jackson ImmunoResearch) at 1:10,000. Hec1-GFP band intensity was quantified using MetaMorph software with ponceau-stained blots as a loading control. All mutant Hec1-GFP band intensities were normalized to WT-Hec1-GFP.

### **Immunofluorescence microscopy**

Cells were rinsed in PHEM buffer (60 mM PIPES, 25 mM HEPES, 10 mM EGTA, 4 mM  $\text{MgCl}_2$ , pH 7.0) and permeabilized in lysis buffer (PHEM + 1.0% Triton X-100) for 5 min at  $37^{\circ}\text{C}$ . Post-lysis, cells were quickly washed in PHEM and subsequently fixed in freshly made fixative solution (4% paraformaldehyde in PHEM) for 20 min at  $37^{\circ}\text{C}$ . After fixation, cells were subjected to three 5-min washes in PHEM-T (PHEM + 0.1% Triton X-100), quickly rinsed in PHEM, and blocked in 10% boiled donkey serum (BDS) in PHEM for 1

h at room temperature. Following blocking, primary antibodies diluted in 5% BDS in PHEM were added to cells and incubated for 1 h at room temperature followed by 16 h at 4°C. Primary antibodies were used as follows: human anti-centromere antibody (ACA) at 1:300 (Antibodies, Inc.), mouse anti-tubulin (DM1 $\alpha$ ) at 1:600 (Sigma-Aldrich), mouse anti-Hec1 (9G3) at 1:3000 (Novus Biologicals), rabbit anti-phosphorylated Hec1-pSer69 (pS69) at 1:3000 (DeLuca *et al.*, 2018), mouse anti-Ska3 at 1:500 (Santa Cruz Biotechnology), rabbit anti-Ska3 at 1:300 (GeneTex), and rabbit anti-Astrin at 1:1000 (Sigma-Aldrich). After primary antibody incubation, unbound antibody was washed off using three 5-min PHEM-T rinses, followed by a quick wash in PHEM. Secondary antibodies (conjugated to Alexa 488, Cy3 dye, or Alexa 647; Jackson ImmunoResearch) were diluted 1:1000 in 5% BDS except mouse Ska3 and rabbit Ska3, for which secondary antibodies were diluted 1:500 and 1:300, respectively. Cells were incubated in secondary antibody for 45 min at room temperature, and unbound antibody was washed off with 3  $\times$  5 min PHEM-T washes followed by a quick rinse in PHEM. Cells were then incubated in a 2 ng/ml 4',6-diamidino-2-phenylindole (DAPI) solution (diluted in PHEM) for 30 s, subjected to two 5-min PHEM-T washes, quickly rinsed in PHEM, and mounted onto glass slides using an antifade solution (90% glycerol + 0.5% *N*-propyl gallate). Following mounting, coverslip edges were sealed with nail polish and slides were stored at 4°C.

### **Fixed cell imaging**

All fixed cell images were acquired using a DeltaVision Personal DV Imaging system (GE Healthcare) on an IX71 inverted microscope (Olympus) using SoftWoRx software (GE Healthcare). All fixed cell experiments were imaged using a 60  $\times$  1.42 NA differential interference contrast Plan Achromat oil immersion lens (Olympus). Images were acquired

using a CoolSNAP HQ2 camera (Photometrics/Roper Technologies) for a final magnification of 107 nm/pixel. For two-color distance measurements, a 1.6 magnification lens was inserted in the light path, providing a final magnification of 67 nm/pixel at the camera sensor.

### **Live cell imaging**

For live cell imaging experiments, cells were seeded into custom-built glass-bottom 35 mm dishes and imaged in Leibovitz's L-15 medium (Invitrogen) supplemented with 10% FBS, 7 mM HEPES, and 4.5 g/l glucose, pH 7.0. HeLa Kyoto cells were double thymidine synchronized and transfected with plasmids encoding Hec1-GFP and mCherry-tubulin as described above. After incubation for 9 h after the second thymidine washout, cells were imaged at 37°C on a Nikon Ti-E microscope equipped with a Piezo Z-control (Physik Instrumente), stage top incubation system (Okolab), and spinning disk confocal scanner unit (CSUX1; Yokogawa), using a 0.6 NA 40X objective and an iXon DU888 EM-CCD camera (Andor). Z-stacks were acquired taking seven planes at 1 µm steps using 488 and 594 nm lasers to excite GFP and mCherry, respectively. For each experiment, 20 fields were imaged at 5-min intervals for 12 h.

### **Protein expression and purification**

Glutathione-S-transferase (GST)-NDC80Bonsai (Ciferri *et al.*, 2008) was a generous gift from Andrea Musacchio (Max Planck Institute of Molecular Physiology, Dortmund, Germany). GST-NDC80Bonsai constructs were generated from GST-NDC80Bonsai (parent vector backbone = pGEX6P1-2RBS). Specifically, Nuf21-348/Spc24122-197, Hec11-506/Spc25118-224 fragments were obtained by PCR from parent vectors of each protein while creating 20-base pair overhangs for Gibson reaction for cloning back into

*Bam*H1/*Age*1-digested GST-Bonsai plasmid. Cloning of  $\Delta$ 80-NDC80Bonsai was carried out using the same fragments, except the Hec1 PCR used a forward primer with amino acid 81 immediately following the start codon. ML-NDC80Bonsai was generated by producing a PCR fragment of Hec11-461 with the mutant loop sequence from the cell expression vector used in this study and annealing it into the NDC80Bonsai vector digested with *Sac*1/*Aff*2. NDC80Bonsai and NDC80Bonsai constructs were expressed and purified using the following scheme: BL21-DE3 cells were transformed with NDC80 constructs, and cultures were grown to the appropriate OD600 before induction overnight (16 h) at 18°C with 400  $\mu$ M isopropyl  $\beta$ -d-1-thiogalactopyranoside. All steps after induction were carried out at 4°C. The next morning, cells were pelleted by centrifugation and resuspended in lysis buffer (25 mM Tris, pH 7.6, 300 mM NaCl, 1 mM EDTA) supplemented with protease inhibitors (Pierce Protease Inhibitor tablets; Thermo Scientific) and 1 mM DTT (Gold Bio). Resuspended cells were lysed using a microfluidic chamber at 80 psi. The resulting lysed mixture was cleared of cell debris by centrifugation at 40,000 rpm for 45 min in a Beckman L8-70M ultracentrifuge using a TY70-TI rotor. Supernatant was applied to glutathione-agarose resin (Pierce resin; Thermo Scientific) (pre-equilibrated in lysis buffer), and the mixture was rocked gently for 1 h. Following binding, unbound protein was washed from the resin with lysis buffer, and resin-bound protein was eluted by GST-tag cleavage overnight with human rhinovirus 3C protease (HRV3C protease, expressed and purified in-house). Elutions were pooled, concentrated, and run on a GE Superdex 200 HiLoad 16/60 sizing column in lysis buffer supplemented with 5% glycerol and 1 mM DTT. Protein fractions were pooled and concentrated, and glycerol was added to 20% final volume before small aliquots were snap-frozen in liquid

nitrogen and stored at  $-80^{\circ}\text{C}$ .

Purification of recombinant human Ska complex (SkaC) was carried out as described previously (Abad *et al.*, 2016). Briefly, BL21-Gold *Escherichia coli* cells were cotransformed with equal amounts of the individual Ska1, GST-Ska2, and Ska3 plasmids. Cells were grown to the appropriate OD600 before induction overnight (16 h) at  $18^{\circ}\text{C}$  with  $400\ \mu\text{M}$  isopropyl  $\beta$ -D-1-thiogalactopyranoside. All steps after induction were carried out at  $4^{\circ}\text{C}$ . The next morning, cells were pelleted by centrifugation and resuspended in SkaC lysis buffer (20 mM Tris, pH 8.0, 500 mM NaCl) supplemented with protease inhibitors and 5 mM DTT. Resuspended cells were lysed by microfluidics as specified in NDC80 complex purifications. The resulting lysed mixture was cleared of cell debris by centrifugation at 40,000 rpm for 45 min as noted for NDC80 complex purifications. The supernatant from lysed cells was applied to glutathione-agarose resin (preequilibrated in SkaC lysis buffer) and rocked gently for 3 h. Following binding, unbound protein was washed away with lysis buffer, and resin was further washed with chaperone buffer (20 mM Tris, pH 8.0, 1 M NaCl, 50 mM KCl, 10 mM  $\text{MgCl}_2$ , 2 mM ATP, 5 mM DTT) to remove associated protein chaperones. Resin-bound protein was then eluted using three sequential elutions for 1 h each in elution buffer (20 mM Tris, pH 8.0, 100 mM NaCl, 50 mM glutathione, 5 mM DTT). Elutions were pooled and dialyzed overnight into column buffer (20 mM Tris, pH 8.0, 100 mM NaCl, 5 mM DTT), and tags were simultaneously cleaved with tobacco etch virus (TEV) protease overnight while rocking. Cleaved SkaC was further purified by gel filtration on a Superose 6 Increase 10/300 in column buffer. Protein-containing fractions were collected and concentrated, and the protein was snap-frozen in liquid nitrogen and stored at  $-80^{\circ}\text{C}$ .

## **TIRF microscopy**

Immediately prior to the microtubule binding assays, the protein was flash-thawed and centrifuged at  $90,000 \times g$  to remove large aggregates. Supernatant was collected and concentration measured by Bradford assay. TIRF microscopy (TIRFM) binding assays were performed as described previously (Ecklund *et al.*, 2017). Briefly, flow chambers were constructed by adhering plasma cleaned, silanized coverslips ( $22 \times 30$  mm) to glass slides with double-sided tape. Silanized coverslips were incubated with a rat anti-tubulin antibody ( $8 \mu\text{g/ml}$ , YL1/2; Accurate Chemical & Scientific Corporation) for 5 min, and then blocked with 1% Pluronic F-127 solution (Fisher Scientific) for 5 min. Taxol-stabilized, Alexa647-labeled microtubules (made by mixing fluorescently labeled and unlabeled porcine tubulin at a 1:12.5 ratio) diluted in BRB80 (80 mM PIPES, 1 mM EGTA, 1 mM  $\text{MgCl}_2$ ) supplemented with  $20 \mu\text{M}$  taxol were flowed into the chamber and incubated for 5–10 min, and then unbound microtubules were washed out with one chamber volume of SN (“Ska-NDC80”) buffer (20 mM Tris, pH 7.0, 50 mM NaCl, 6 mg/ml bovine serum albumin [BSA], 4 mM DTT,  $20 \mu\text{M}$  taxol). GFP-NDC80 complex (either alone or supplemented with 10 nM unlabeled Ska complex) diluted to the appropriate concentration in SN buffer was introduced to the chamber, and the binding reaction was incubated for 2 min. Two more additions of NDC80 complex (or NDC80 complex + Ska complex) were subsequently perfused into the chamber to allow the binding reaction to reach equilibrium. Two minutes after the third addition (after binding reaction had reached equilibrium as determined by time-lapse imaging), TIRF images were collected from 10 individual fields. For analysis in BRB80 and BRB20 (Figure 2.7), all steps were performed as above, except protein (either GFP-NDC80 alone or supplemented with SkaC, or SkaC-GFP) was

diluted into either BRB80 or BRB20 supplemented with 6 mg/ml BSA, 4 mM DTT, and 20  $\mu$ M taxol. All TIRFM images were collected at room temperature using a 1.49 NA 100 X Plan Apo TIRF oil immersion lens on a Nikon Ti-E inverted microscope equipped with an iXon3 DU897 EM-CCD camera (Andor) for a final pixel size of 160 nm/pixel.

### **Data analysis**

For all mutant expression studies, cells were initially scored for kinetochore GFP fluorescence intensity as “low,” “intermediate,” or “high.” Cells scored as having low Hec1-GFP fluorescence were discarded from analysis. Subsequently, cells were scored for Hec1-pS69 staining, and only cells with undetectable Hec1-pS69 were analyzed where appropriate (for mutants lacking intact Ser-69). For experiments in which kinetochore fluorescence intensity was quantitatively measured, only cells within a defined range of Hec1-GFP kinetochore fluorescence intensity were analyzed to ensure that expression levels were equal for all mutants (see Figure 2.1 C). Measurement of kinetochore fluorescence intensity in fixed cells was measured from non-deconvolved, non-compressed images using a custom program in MatLab (Mathworks) courtesy of X. Wan (University of North Carolina at Chapel Hill; Wan *et al.*, 2009). For analysis of Ska3 levels at attached kinetochores (Figure 2.2 A–C, Figure 2.8 G and H, and Figure 2.3), cells from mutants lacking Hec1 Ser-69 with greater than 25% Hec1-pS69 levels measured in WT-Hec1-GFP cells were discarded from analysis to reduce effects of endogenous, non-mutant kinetochore Hec1. Measurements of end-on attachment and interkinetochore distances in cold-treated cells were performed in SoftWoRx Explorer software. End-on attachment was analyzed by selecting random kinetochores in the kinetochore channel and then subsequently overlaying the tubulin channel and scoring whether spindle

microtubules terminated at the preselected kinetochores (lateral attachments were not quantified). For analysis of end-on attachment in Ska-depleted cells, only kinetochores between the spindle poles were analyzed, as polar chromosomes remained unattached in all conditions (Figure 2.3). Inter-kinetochore distances were analyzed by measuring the distance between Hec1-GFP signals from two kinetochores in a sister pair in the same z-plane. For chromosome alignment analysis, bipolar Hec1-GFP expressing cells post-nuclear envelope breakdown were scored as either aligned (metaphase plate with <5 chromosomes off the plate) or unaligned (no metaphase plate, or metaphase plate with five or more chromosomes off the plate). For analysis of multipolarity, Hec1-GFP expressing cells were stained with anti-tubulin antibodies and assessed for the number of spindle poles. For two-color distance measurements, analyses were performed on kinetochore pairs in which their maximum fluorescence intensity centroids were not separated by more than one focal plane of 0.2  $\mu\text{m}$ . Centroids of each test antibody signal were calculated using SpeckleTracker in MatLab. Distances were also calculated in the SpeckleTracker program. A detailed description of the protocol can be found in Wan *et al.* (2009).

For analysis of TIRFM microtubule binding assays, GFP-NDC80 complex-microtubule binding was quantitated using ImageJ software (National Institutes of Health). The NDC80 fluorescent signal was measured along the microtubule axis (as determined from the Alexa647-tubulin signal), and the “background” signal was measured using the same mask (created along the microtubule’s length) in a region immediately adjacent to the microtubule. Corrected signal intensity was measured by subtracting the background signal from the GFP signal on the microtubule. Raw GFP-NDC80 fluores-

cence intensity at each concentration (averaged across all three replicates) was plotted, and curves were fitted using a Specific binding model with a Hill fit in Prism (GraphPad). All statistical analyses were carried out using Prism (GraphPad).

## CHAPTER 3: REQUIREMENTS FOR ATTACHMENT REGULATION AND TENSION GENERATION BY THE HEC1 TAIL DOMAIN

3

### 3.1 Introduction

Successful cell division is marked by the equal segregation of chromosomes into two new daughter cells. Precise regulation of the attachments between the mitotic spindle and chromosomes is critical to ensure that genetic material is not mis-segregated during cell division, an event that can result in aneuploidy and is linked to a number of developmental disorders and tumorigenesis (Bakhoun and Compton, 2012a, 2012b; Santaguida and Amon, 2015). The direct linkage between spindle microtubules and chromosomes is the kinetochore, a protein-rich machine built on each sister chromatid. Kinetochores bind directly to spindle microtubules and harness the forces from their dynamic instability to drive chromosome movement (DeLuca and Musacchio, 2012). Additionally, kinetochores regulate the strength with which they are bound to microtubules throughout mitosis: early on, when incorrect kinetochore-microtubule attachments form, kinetochores ensure that these attachments are labile so that they can be released and eventually corrected. Conversely, as chromosomes align to the cell equator, kinetochores bind more tightly to spindle microtubules such that they can

---

<sup>3</sup> The experiments in this chapter are unpublished and are intended for use in a future publication. JEM assisted with cloning and purification of NDC80<sup>Bonsai</sup> constructs, JGD and I designed the experiments, and I performed all experiments and analyzed all data. I wrote the manuscript with input from JGD. A suggested citation is given below.

Wimbish RT, Mick JE, and DeLuca JG. (2020). Requirements for regulation of kinetochore-microtubule attachments and tension generation by the Hec1 tail domain. *Manuscript in preparation.*

harness the forces generated by their dynamic instability, ultimately powering chromosome movement.

The key microtubule binding site within the kinetochore is the conserved NDC80 complex, a dumbbell-shaped heterotetrameric protein extending roughly 60 nm in length. Comprised of the subunits Spc24, Spc25, Nuf2 and Hec1, the NDC80 complex directly binds to spindle microtubules through the globular calponin homology (CH) domain of its Hec1 subunit (Ciferri et al., 2008; Wilson-Kubalek et al., 2008; Alushin et al., 2010). Hec1 also contains a highly basic, intrinsically disordered “tail” domain at its far N-terminus, which plays a role in force generation at the kinetochore-microtubule interface (Wimbish and DeLuca, 2020). Notably, it has been demonstrated that recombinant NDC80 complexes lacking the Hec1 tail domain are less resistant to pulling forces in an optical trapping assay (Helgeson et al., 2018; Huis in't Veld et al., 2019), and that this domain is required for NDC80 complexes to track with depolymerizing microtubules (Huis in't Veld et al., 2019). Furthermore, as shown in Chapter 2, cells expressing a tail-less Hec1 are defective in force generation at the kinetochore, leading to loss of spindle bipolarity and chromosome alignment.

In addition to its role in generating force, the Hec1 tail domain actively regulates kinetochore-microtubule attachment strength. Within the tail are 9 consensus sites for phosphorylation by the Aurora family of kinases, which are widely recognized as key regulators of mitosis (Biggins et al., 1999; Lampson et al., 2004; DeLuca et al., 2006; Cheeseman et al., 2006; DeLuca et al., 2011; Wimbish and DeLuca, 2020). Studies with

phospho-specific antibodies have shown that most sites in the tail are highly phosphorylated in early mitosis, coincident with weak kinetochore-microtubule attachments, and are predominantly dephosphorylated in metaphase when attachments are more robust (DeLuca et al., 2011). The exception is Ser 69, which remains phosphorylated throughout mitosis and which is important for maintaining normal kinetochore-microtubule attachment dynamics (DeLuca et al., 2018). Importantly, mimicking phosphorylation of Aurora kinase sites within the Hec1 tail (by Ser/Thr to Asp/Glu mutation) weakens kinetochore-microtubule attachments as evidenced by reductions in kinetochore-fiber intensity, inter-kinetochore distances, and chromosome alignment efficiency (Guimaraes et al., 2008; DeLuca et al., 2011; Zaytsev et al., 2014; Yoo et al., 2018; Kuhn and Dumont, 2019). Furthermore, incrementally increasing the number of phospho-mimetic mutations in the Hec1 tail domain coordinately reduces NDC80-microtubule binding affinity *in vitro* (Zaytsev et al., 2015). These studies have led to the idea that Hec1 tail domain phosphorylation directly reduces NDC80-microtubule binding affinity, which consequentially weakens kinetochore-microtubule attachments (reviewed in Wimbish and DeLuca, 2020).

The mechanistic basis for phospho-regulation of NDC80-microtubule interactions is not clear. One prominent model – referred to as the direct binding model – posits that Hec1 tail phosphorylation acidifies the otherwise basic tail domain and causes its electrostatic repulsion from the negatively charged microtubule lattice, thereby preventing NDC80 complex-microtubule binding (Tooley et al., 2011; Zaytsev et al., 2015; Wimbish and DeLuca, 2020). This model is challenged, however, by two key pieces of data

mentioned above: first, recombinant NDC80 complexes lacking the Hec1 tail bind to microtubules normally when oligomerized on an engineered scaffold (Huis in't Veld et al., 2019). Second, the Hec1 tail is dispensable for kinetochore-microtubule attachments in human cells and *C. elegans*, despite the fact that mimicking phosphorylation of the tail weakens attachments in both of these organisms (Cheerambathur et al., 2013; 2017; Wimbish et al., 2020). In the direct binding model, the phosphorylation-induced repulsion of the tail domain (and the NDC80 complex) from the microtubule lattice implies that a dephosphorylated tail domain is required for binding in the first place. Given that recent studies suggest that the Hec1/Ndc80 tail is dispensable for this activity (Cheerambathur et al., 2013; Huis in't Veld et al., 2019; Wimbish et al., 2020), the data imply that attachments are primarily mediated by the Hec1/Ndc80 CH domain. Thus, the mechanism by which a phosphorylated tail destabilizes CH domain-mediated attachments remains unclear.

Here, we investigate the requirements for force generation and attachment regulation by the Hec1 tail domain. We design length- and charge-specific Hec1 tail mutants to test the direct binding model and to determine how the Hec1 tail domain contributes to high-tension attachment generation. We find that NDC80 complexes with short Hec1 tails are not responsive to phospho-mimetic mutation, suggesting tail length and charge both play a role in attachment regulation. Furthermore, we find that blocking Aurora phosphorylation of short tail domains phenocopies expression of a phospho-blocked, full-length 9A-Hec1 mutant, suggesting that a full length Hec1 tail is not required for excess force generation. Finally, we engineer an extended tail Hec1 mutant that

generates excess tension at the kinetochore-microtubule interface, but regulates attachment strength normally and does not behave like previously characterized phospho-blocked Hec1 tail mutants. Collectively, these results suggest that the direct binding model does not fully explain the phospho-regulation of attachments, and suggest that the Hec1 tail exhibits different requirements for attachment regulation and tension generation.

### **3.2 Results**

#### **A 25 amino acid Hec1 tail rescues the tail deletion phenotype, but is defective in attachment regulation**

Our previous studies suggested that the Hec1 tail domain plays a role in force generation at the kinetochore: deletion of this small domain results in a metaphase arrest followed by spindle pole fragmentation and chromosome scattering, leading to a terminal phenotype of multipolar cells with unaligned chromosomes (Wimbish et al., 2020). To assess what tail length is sufficient for rescuing these defects, we expressed GFP-tagged Hec1 tail truncation mutants in HeLa cells and analyzed chromosome alignment phenotypes by fixed-cell microscopy. We reasoned that a Hec1 tail domain mutant that could rescue the force-deficiency of Hec1 tail deletion would not undergo spindle fragmentation and loss of chromosome alignment, and would thus present with aligned chromosomes by fixed-cell imaging. Cells were transfected with various GFP-tagged Hec1 variants, cold-treated prior to fixation, fixed, immunostained for tubulin and scored for their metaphase index based on DAPI staining. Expression of a Hec1 construct with a 25 amino acid tail largely rescued the tail deletion phenotype, resulting in chromosome alignment frequency similar to that observed for WT-Hec1 expressing

cells (Figure 3.1 A and B). This 25 amino acid tail mutant (25N-Hec1) is deleted for amino acids 1-55, thus retaining the 25 amino acids immediately proximal to the Hec1 CH domain (Figure 3.1 C). Importantly, this length of tail retains two Aurora phosphorylation sites and has a similar isoelectric point to the full length Hec1 tail domain (Figure 3.1 C). We next asked if this length of tail could negatively regulate kinetochore-microtubule attachments. We generated 25N<sup>D</sup>-Hec1, a version of the 25N-Hec1 mutant in which both Aurora phosphorylation sites (Ser 62 and Ser 69) are mutated to aspartic acid to mimic constitutive phosphorylation (Figure 3.1 C). This tail has an isoelectric point similar to a full length, completely phospho-mimetic tail (9D-Hec1), and expression of 9D-Hec1 results in dramatic chromosome alignment defects and a reduction in cold-stable kinetochore-microtubule attachments (DeLuca et al., 2011; Zaytsev et al., 2014; Wimbish et al., 2020). We therefore reasoned that if a 25 amino acid tail is long enough to negatively regulate attachments, expression of 25N<sup>D</sup>-Hec1 should phenocopy expression of 9D-Hec1. To our surprise, cells expressing 25N<sup>D</sup>-Hec1 exhibited a normal chromosome alignment phenotype, similar to WT- and 25N-Hec1 expressing cells and in contrast to cells expressing 9D-Hec1 (Figure 3.1 A and B). Similar to experiments in Chapter 2, we ensured selection of transgene-dominant cells by selecting cells with undetectable kinetochore fluorescence of phosphorylated Hec1 at Ser 69, a residue that is constitutively phosphorylated and which is not present in  $\Delta$ 80-, 9D-, and 25N<sup>D</sup>-Hec1 constructs (Figure 3.1 A, see also Methods). Taken with the fact that 25N<sup>D</sup>-Hec1 expression did not disrupt chromosome alignment (Figure 3.1 B), we hypothesized that a 25 amino acid Hec1 tail may not be sufficiently long to negatively regulate attachments in a manner similar to the full length

Hec1 tail. To investigate this, we analyzed cold-resistant kinetochore-microtubule attachments in early prometaphase cells. As shown previously, attachments are unstable in early mitotic cells expressing WT-Hec1 due to high tail phosphorylation by Aurora kinases (DeLuca et al., 2011; Wimbish et al., 2020). This phenotype can be reversed, however, upon expression of 9A-Hec1, in which all nine Aurora sites are blocked from phosphorylation by Ala mutation (see Figures 2.2 and 2.8 in this thesis). We reasoned that if a 25 amino acid Hec1 tail is too short to regulate attachments, both the “wild type” and phospho-mimetic versions of 25N-Hec1 should form attachments in early prometaphase. In agreement with the notion that a full length Hec1 tail can regulate attachments normally, cells expressing both WT- and 9D-Hec1 failed to form cold-stable attachments in early prometaphase (Figure 3.1 D and E). In contrast, kinetochores in cells expressing 25N- and 25N<sup>D</sup>-Hec1 formed robust attachments to microtubules, suggesting they are not able to properly promote high microtubule attachment turnover during early mitosis (Figure 3.1 D and E). Collectively, these results suggest that a 25 amino acid Hec1 tail rescues the force-generation defects associated with tail deletion, but that this length of tail is deficient in temporally regulating attachment strength.

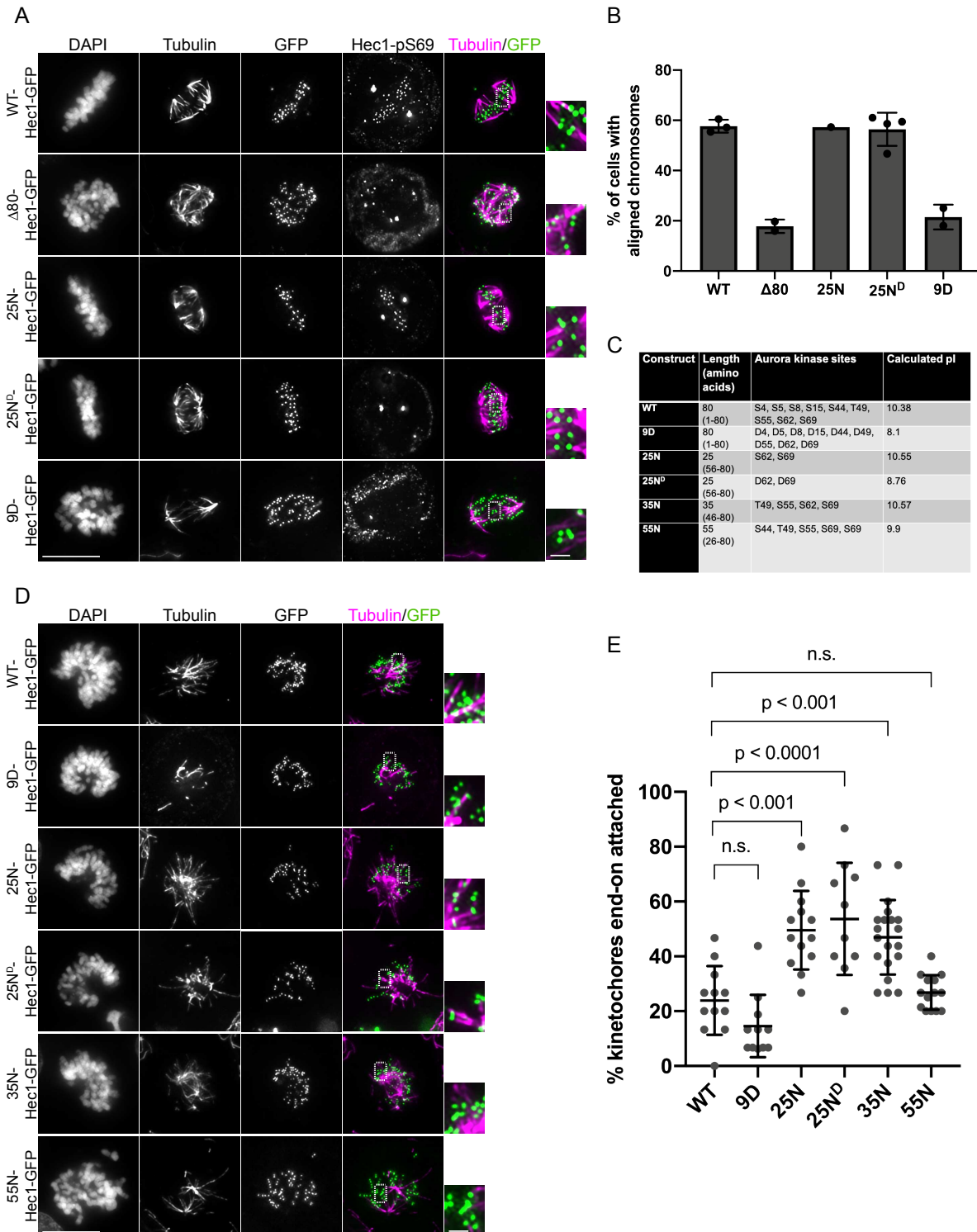


**Figure 3.1. A 25 amino acid Hec1 tail rescues the tail deletion phenotype, but is deficient in temporal attachment regulation.** (A) Immunofluorescence images of cold-treated HeLa cells expressing the indicated Hec1-GFP mutants. Cells were incubated in ice-cold DMEM for 12 min before fixation, permeabilized, fixed, and

immunostained with antibodies to phosphorylated Hec1 Ser 69 (Hec1-pS69) and tubulin. Insets (to show retention or depletion of cold-stable attachments) are enlargements of the region indicated by the dashed box. (B) Quantification of chromosome alignment frequency in Hec1-GFP expressing cells from the experiment in 3.1 A. Hec1-GFP expressing cells (depleted of kinetochore Hec1-pS69 signal for  $\Delta 80$ -, 9D-, and 25N<sup>D</sup> mutants) were scored as either “aligned” or “unaligned” based on signal from DAPI channel. Data for  $\Delta 80$ -Hec1 is from experiments in Chapter 2. Bar graph shows the average from all experiments with standard deviation (error bars) and individual averages from each experiment (black dots). (C) Table depicting Hec1-GFP mutants used in this study. Table shows overall tail length and amino acids present in tail, as well as Aurora kinase sites present in tail and calculated isoelectric point (pI) of tail. All isoelectric points were calculated using Isoelectric Point Calculator (Kozlowski, 2016). (D) Immunofluorescence images of early prometaphase cold-treated HeLa cells expressing the indicated Hec1-GFP mutants. Cells were incubated in ice-cold DMEM for 12 min before fixation, permeabilized, fixed, and stained using antibodies to tubulin. Insets are enlargements of the region indicated by the dashed box. (E) Quantification of end-on attachment in cold-treated cells expressing the indicated Hec1-GFP mutants. A one-way Anova was carried out to determine statistical significance. Each dot represents the number of end-on attachments for an entire cell. Scale bars: 10  $\mu\text{m}$  and 1  $\mu\text{m}$  for panels and insets, respectively. Total kinetochore, cell, and experimental replicate numbers for all experiments are provided in table 3.2.

### **A 55 amino acid Hec1 tail restores normal attachment regulation**

The regulation deficiencies in 25N-Hec1 expressing cells led us to ask what length of the Hec1 tail domain was sufficient for regulating attachment strength. We therefore generated Hec1 mutants with 35 and 55 amino acid tails (35N-Hec1 and 55N-Hec1) by deleting the preceding N-terminal amino acids, thus retaining the wild-type sequences of each tail truncation and all Aurora kinase sites therein (Figure 3.1 C). Analysis of metaphase Hec1-pS69 levels showed no difference in phosphorylation between any of the tail mutants and WT-Hec1, suggesting that truncation of the Hec1 tail domain does not impact its phosphorylation (Fig 3.2). Based on this observation we reasoned that if tail domains undergo normal phosphorylation, then a sufficiently long tail domain should inhibit attachment formation in early prometaphase. We therefore expressed 35N- and

55N-Hec1 in HeLa cells, cold-treated cells prior to fixation, stained with antibodies to tubulin, and measured end-on attachments in early prometaphase. We found that while both 25N- and 35N-Hec1 expression resulted in premature attachment formation, 55N-Hec1 expression restored attachments to wild-type levels (Figure 3.1 D and E). These findings demonstrate that a 55 amino acid tail is sufficient for normal kinetochore-microtubule attachment regulation.

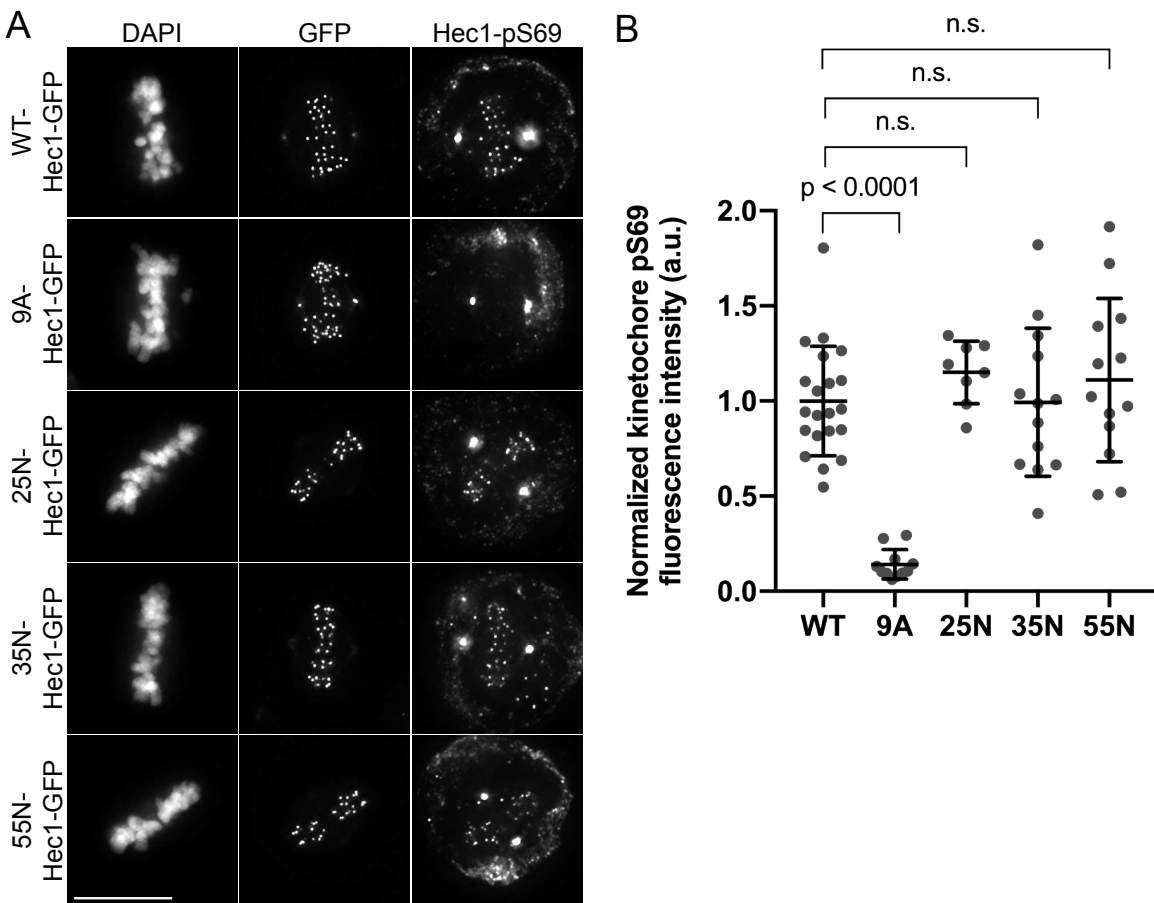


**Figure 3.2. Tail truncation mutants undergo normal Hec1-S69 phosphorylation.** (A) Immunofluorescence images of HeLa cells expressing the indicated Hec1-GFP mutants. Cells were permeabilized, fixed, and immunostained with antibodies to Hec1-pS69. (B) Quantification of kinetochore Hec1-pS69 signal in indicated Hec1-GFP expressing cells from experiment in 3.2 A. All kinetochore intensities were normalized to the average kinetochore fluorescence intensity of WT-Hec1. A one-way Anova was carried out to determine statistical significance. Each dot represents the average

kinetochore fluorescence intensity for an entire cell. Scale bar: 10  $\mu\text{m}$ . Total kinetochore, cell, and experimental replicate numbers for all experiments are provided in table 3.2.

### **NDC80-microtubule binding *in vitro* is less responsive to phospho-mimetic mutation of short Hec1 tail domains**

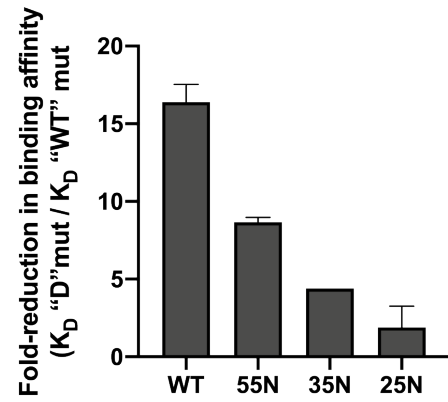
We next sought to assess the source of defective attachment regulation in cells expressing 35N- and 25N-Hec1. Several models for Hec1-mediated attachment regulation exist, and one prominent model is that Hec1 tail phosphorylation directly modulates NDC80-microtubule binding affinity by acidifying the otherwise basic Hec1 tail domain, causing its electrostatic repulsion from the negatively charged microtubule lattice (reviewed in section 1.8a, see also Alushin et al., 2010; Tooley et al., 2011; Zaytsev et al., 2014). This direct binding model of regulation predicts that mimicking phosphorylation of the Hec1 tail domain leads to weakened NDC80-microtubule binding regardless of tail length. We therefore set out to test this model *in vitro* using a TIRF microscopy-based microtubule binding assay (Wimbish et al., 2020). We purified recombinant human GFP-NDC80<sup>Bonsai</sup> complexes, in which the long coiled-coil region of the complex is truncated but the kinetochore- and microtubule-binding domains are intact (Ciferri et al., 2008). For all Hec1 tail lengths tested in cells, we expressed and purified the analogous NDC80<sup>Bonsai</sup> complexes with and without phospho-mimetic mutations at all Aurora kinase sites present, thereby generating both “wild-type” and phospho-mimetic versions of each respective tail length mutant. Notably, mimicking phosphorylation on all Hec1 tail lengths reduces the overall charge of the tail similar to that of the 9D-Hec1 tail, thus allowing us to analyze the effects of both charge and length on NDC80-microtubule binding (Figure 3.3 A). As controls, we purified WT-NDC80<sup>Bonsai</sup> and 9D-NDC80<sup>Bonsai</sup> complexes, since

we and others have previously shown that a full-length phospho-mimetic Hec1 tail significantly weakens the affinity of NDC80 complexes for microtubules *in vitro* (Umbreit et al., 2012; Zaytsev et al., 2015; Huis in't Veld et al., 2019). Fluorescently labeled, taxol-stabilized microtubules were adhered to coverslips and incubated with GFP-tagged NDC80 complexes, and GFP fluorescence intensity on microtubules was measured across a range of NDC80 complex concentrations to generate binding curves and calculate relative binding affinity. Similar to previous studies, we found that mimicking phosphorylation in the full length Hec1 tail dramatically weakened NDC80-microtubule binding affinity (~10-fold reduction, Fig 3.3 B). Performing the same experiment using NDC80 complexes with a 55 amino acid Hec1 tail resulted in a similar, but slightly smaller, reduction in microtubule binding affinity (~8-fold reduction, Fig 3.3 C), while mimicking phosphorylation on a 35 amino acid Hec1 tail even further minimized the effects of phospho-mimetic mutation on NDC80-microtubule binding (~5-fold reduction, Fig 3.3 D). Strikingly, NDC80<sup>Bonsai</sup> complexes with a 25 amino acid Hec1 tail bound microtubules almost identically with and without phospho-mimetic mutations (~1.5-fold reduction, Figure 3.3 E), leading to similar binding affinities for “wild-type” complexes and complexes containing phospho-mimetic Hec1. Collectively, our *in vitro* analyses show that shorter Hec1 tails are less efficient at phospho-regulating NDC80-microtubule interactions (Figure 3.3 F). These results suggest that both the length and charge of the Hec1 tail play important roles regulating NDC80-microtubule binding, which is consistent with experiments in Figure 3.1. Overall, these experiments imply that a simple electrostatic repulsion between the Hec1 tail and microtubule lattice may not completely explain how NDC80-microtubule interactions are phospho-regulated.

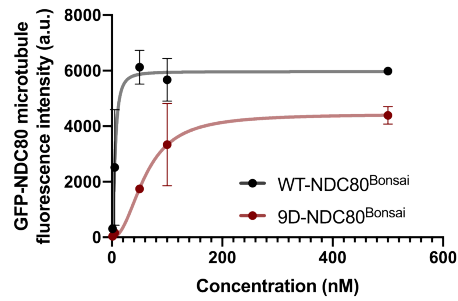
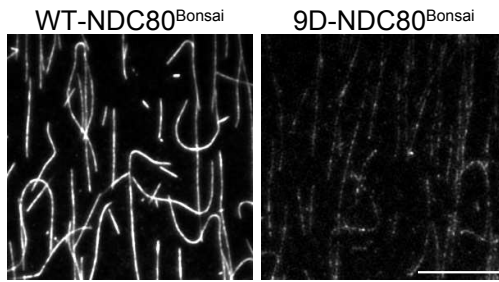
A

Construct	Tail length (amino acids)	Tail sequence	Calculated tail pI
25N	25 (56-80)	MLFGKRTSGHGSRNSQLGIFSSSEKI	10.55
25N <sup>D</sup>	25 (56-80)	MLFGKRTDGHGSRNDQLGIFSSSEKI	8.76
35N	35 (46-80)	MNKPTSERKVSFLFGKRTSGHGSRNSQLGIFSSSEKI	10.57
35N <sup>D</sup>	35 (46-80)	MNKPDSEKVDLFGKRTDGHGSRNSDQLGIFSSSEKI	8.46
55N	55 (26-80)	MKQGLYTPQTEKPTFGKLSINKPTSERKVSFLFGKRTSGHGSRNSQLGIFSSSEKI	9.9
55N <sup>D</sup>	55 (26-80)	MKQGLYTPQTEKPTFGKLDINKPDSERKVDLFGKRTDGHGSRNSDQLGIFSSSEKI	8.75
WT	80 (1-80)	MKRSSVSSGGAGRLSMQELRSQDVNKQGLYTPQTEKPTFGKLSINKPTSERKVSFLFGKRTSGHGSRNSQLGIFSSSEKI	10.38
9D	80 (1-80)	MKRDDVSDGGAGRLDMQELRSQDVNKQGLYTPQTEKPTFGKLDINKPDSERKVDLFGKRTDGHGSRNDQLGIFSSSEKI	8.1

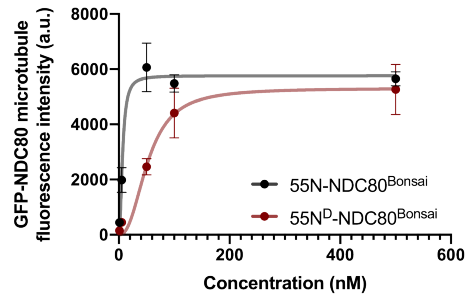
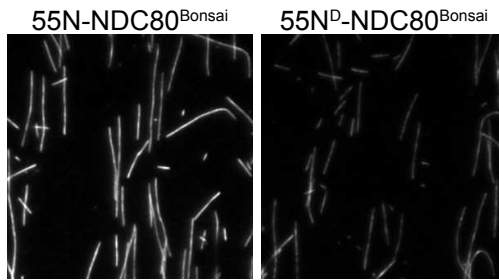
F



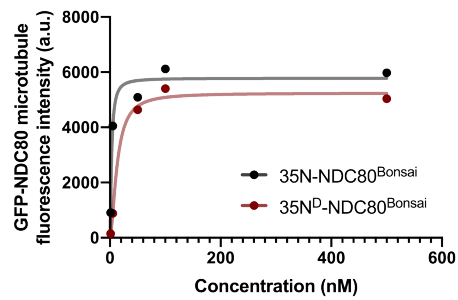
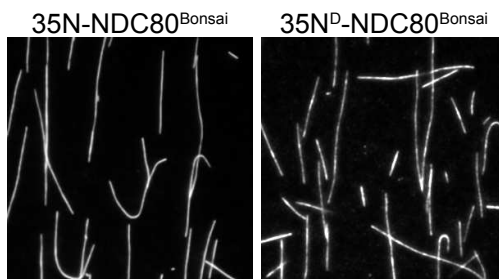
B



C



D



E

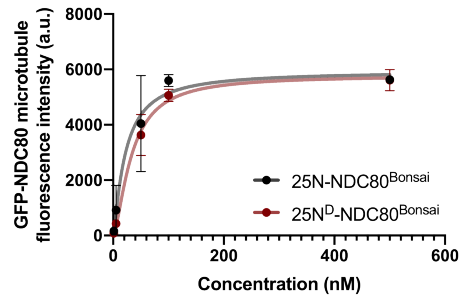
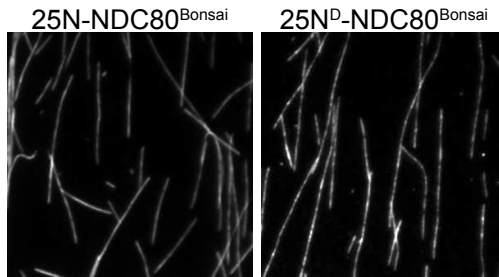


**Figure 3.3. Phospho-regulation of NDC80-microtubule interactions scales with Hec1 tail length *in vitro*.** (A) Table depicting Hec1 mutants incorporated into purified GFP-NDC80<sup>Bonsai</sup> complexes. Table shows overall tail length and amino acids present in tail, as well as the Hec1 tail sequences and calculated isoelectric point (pI) of tail. For phospho-mimetic variants, mutated aurora sites are highlighted in yellow. Isoelectric points were calculated using Isoelectric Point Calculator (Kozlowski, 2016). (B-E) representative images of the denoted 5 nM GFP-NDC80<sup>Bonsai</sup> variants binding to taxol-stabilized microtubules (left), and binding curves generated for respective mutants (right). On graphs, each dot represents the average fluorescence intensity on 30 microtubules from 10 different fields at that concentration. Error bars denote standard deviation from average of two experiments (except for 35N-NDC80<sup>Bonsai</sup>, which is one experiment). Curve fitting was done using a specific binding curve with Hill slope (see Methods for more detail). (F) Graph showing fold-reduction in binding affinity ( $K_D$ ) for respective Hec1 tail length NDC80 complexes upon phospho-mimetic mutation. The calculated  $K_D$  (from binding curve fit) for phospho-mimetic mutants was divided by the calculated  $K_D$  of “wild-type” mutants. Bar graph shows average fold-reduction with standard deviation (error bars) across individual replicates. Scale bar: 20  $\mu$ m. Total microtubule and experimental replicate numbers for all experiments are provided in table 3.2.

### **Chromosome alignment delays scale with Hec1 tail length for phospho-mimetic mutants**

Our *in vitro* analysis demonstrated that phospho-mimetic Hec1 tails modulate NDC80-microtubule binding in a length-dependent manner. In cells, chromosome alignment is directly impacted by kinetochore-microtubule attachment strength: perturbations that weaken attachments cause delays in chromosome alignment timing (Gaitanos et al., 2009; Sundin et al., 2011; Wimbish et al., 2020). Based on our finding short Hec1 tails are less efficient at phospho-regulating NDC80-microtubule interactions (Figure 3.3), we reasoned that short tails should not cause chromosome alignment delays in cells when made phospho-mimetic. To this end, we turned to live cell imaging experiments of cells expressing Hec1-GFP and mCherry-H2B to visualize chromosome dynamics. Cells were released from thymidine synchronization and filmed through mitosis, and timing from nuclear envelope breakdown to metaphase plate formation was scored. As mentioned

previously, all phospho-mimetic tail truncation mutants have isoelectric points similar to 9D-Hec1; however, based on *in vitro* experiments we predicted that chromosome alignment delays should increase with tail length. Indeed, cells expressing phospho-mimetic Hec1 tail domains experienced chromosome alignment delays in a length-dependent manner, with 25N<sup>D</sup>-Hec1 behaving nearly identically to WT-Hec1, but 35N<sup>D</sup>- and 55N<sup>D</sup>-Hec1 expression resulting in progressively longer alignment delays. Notably, 9D-Hec1 expression caused the longest delay, which is consistent with our finding that a full length tail phospho-regulates NDC80-microtubule binding most effectively (Figure 3.4). The observed alignment delays were dependent on the presence of phospho-mimetic mutations, as expression of the “wild type” versions of each tail truncation mutant did not alter chromosome alignment timing (Figure 3.5). These results further demonstrate that phospho-mimetic Hec1 tail domains impact kinetochore-microtubule attachment regulation in a length-dependent manner, providing additional evidence that regulation of kinetochore-microtubule attachments is not simply a function of Hec1 tail charge.

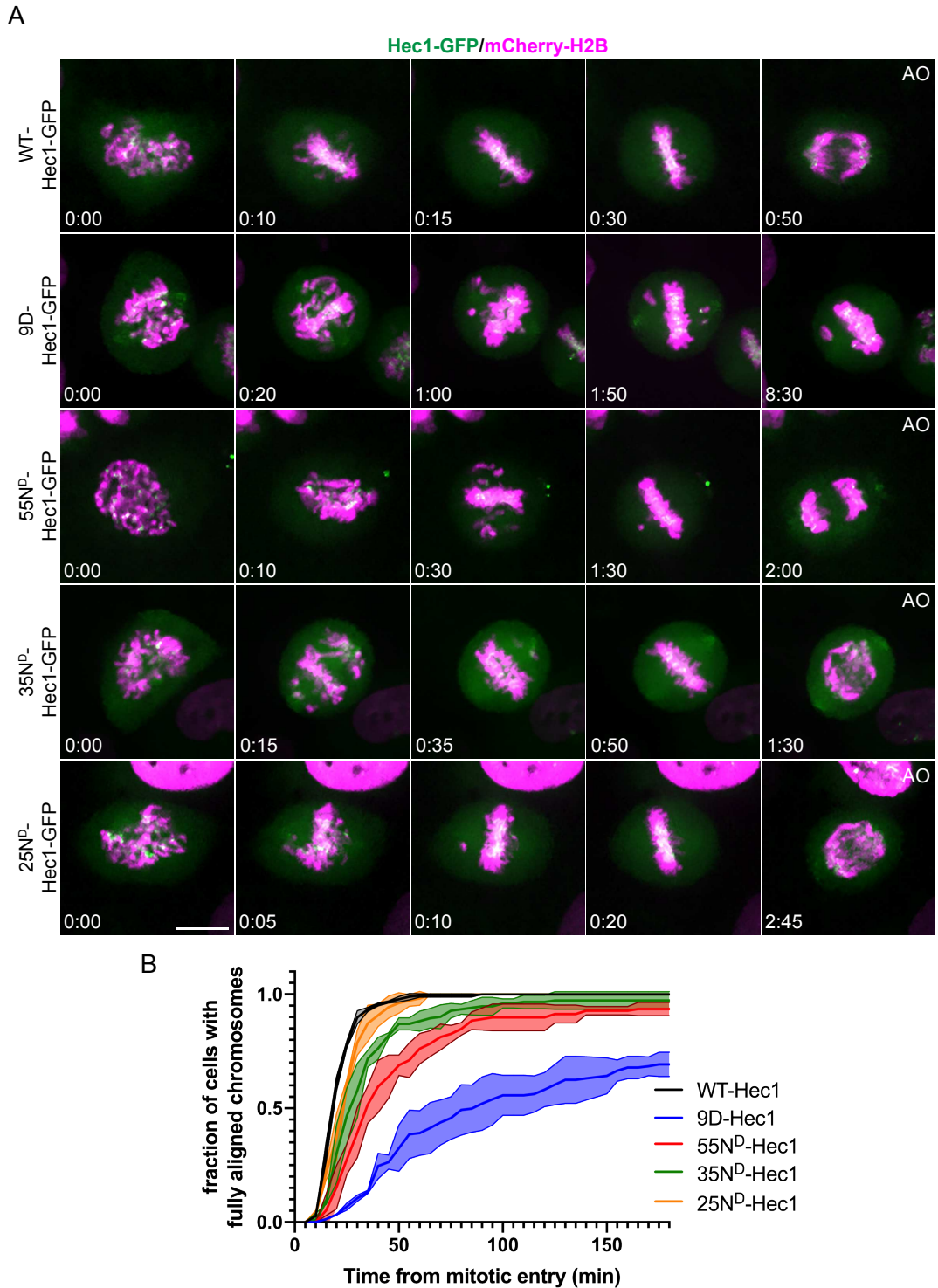


**Figure 3.4. Phospho-regulation of chromosome alignment scales with Hec1 tail length in cells.** (A) Still images from time-lapse experiments of cells expressing Hec1-GFP and mCherry-H2B. Cells were released from thymidine synchronization and filmed in 5-minute intervals. Time from nuclear envelope breakdown (NEBD) is denoted on bottom left corner of each image (hours: minutes), and anaphase onset (AO) is denoted for appropriate mutants. (B) Quantification of chromosome alignment timing in cells from

the experiment shown in panel 3.4 A. Cell fate was tracked after mitotic entry for 3 h, and cells were scored as “aligned” upon metaphase plate formation (as determined by Hec1-GFP and mCherry-H2B fluorescence). For all experiments, mean (bold line) timing is shown along with standard deviation of all experiments (shaded area). Scale bar: 10  $\mu$ m.

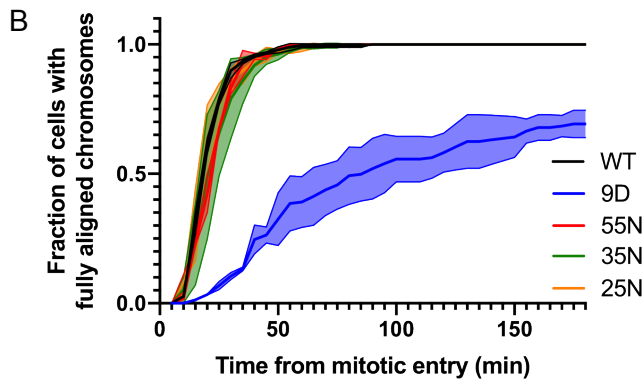
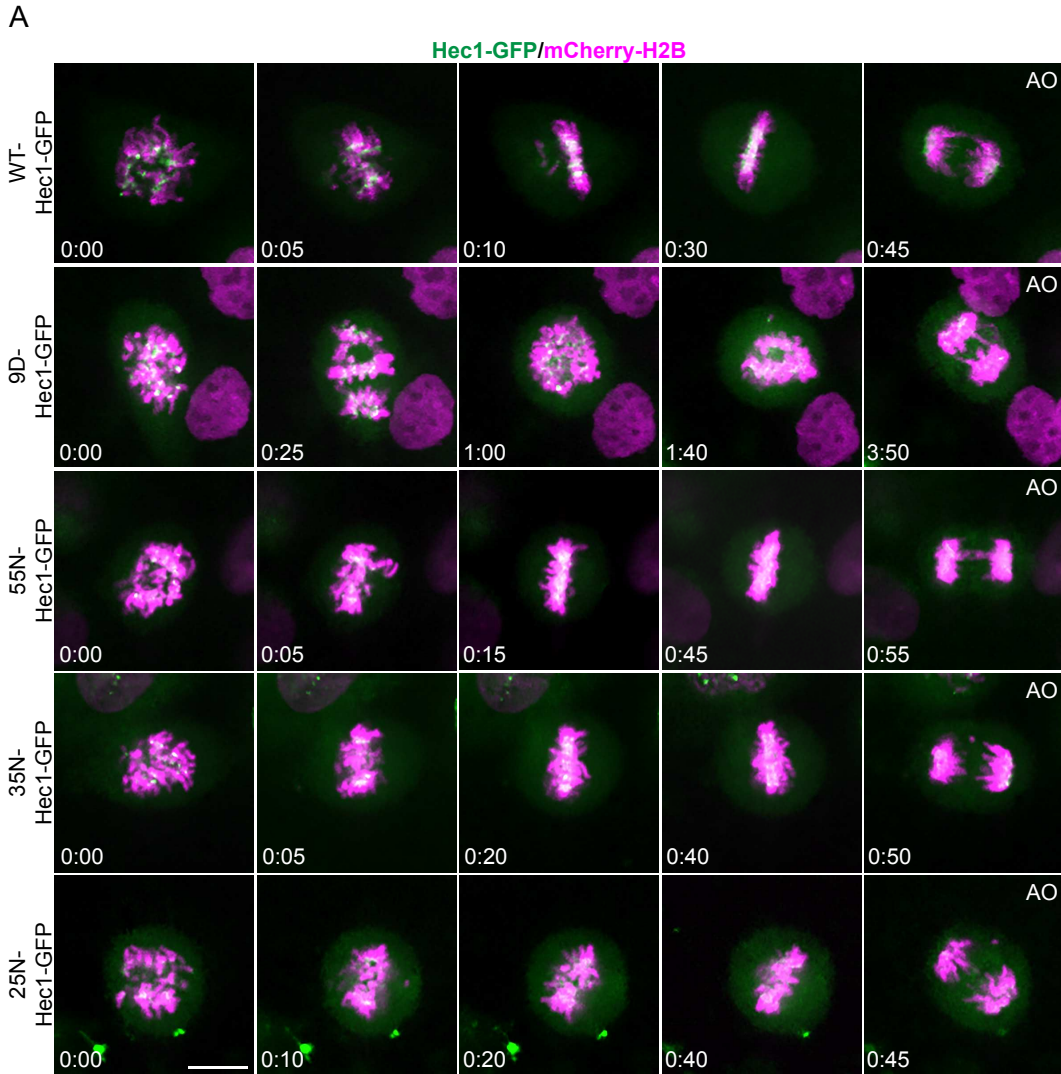


**Figure 3.5. Short, “wild-type” Hec1 tail-expressing cells align chromosomes normally.** (A) Still images from time-lapse experiments of cells expressing Hec1-GFP and mCherry-H2B. Cells were released from thymidine synchronization and filmed in 5-minute intervals. Time from nuclear envelope breakdown (NEBD) is denoted on bottom left corner of each image (hours: minutes), and anaphase onset (AO) is denoted. (B) Quantification of chromosome alignment timing in cells from the experiment shown in panel 3.5 A. Cell fate was tracked after mitotic entry for 3 h, and cells were scored as “aligned” upon metaphase plate formation (as determined by Hec1-GFP and mCherry-H2B fluorescence). For all experiments, mean (bold line) timing is shown along with standard deviation of all experiments (shaded area). Data shown for WT- and 9D-Hec1 are the same as the data shown in Figure 3.4. Scale bar: 10  $\mu$ m.

### **Blocking Aurora phosphorylation of short Hec1 tails causes high-tension attachment formation**

We next wanted to ask to what extent attachment regulation was lost for the tail truncation mutants. Loss of kinetochore-microtubule attachment regulation has been extensively studied in the context of 9A-Hec1, a regulation-deficient mutant where all 9 Aurora sites within the tail are blocked from phosphorylation by Ala mutation. Expression of this mutant precludes regulation of attachments by the Aurora kinase pathway, leading to accumulation of attachments in early mitosis, trapped polar chromosomes in metaphase, dampened chromosome oscillations, and high levels of chromosome mis-segregation in anaphase (Guimaraes et al., 2008; DeLuca et al., 2011; Zaytsev et al., 2014; Tauchman et al., 2015; Yoo et al., 2018; Wimbish et al., 2020). As our fixed cell chromosome alignment analysis did not reveal high levels of polar chromosomes in metaphase cells expressing 25N<sup>-</sup> or 25N<sup>D</sup>-Hec1 (Figure 3.1 A and B), we hypothesized that cells expressing short Hec1 tail mutants may not have lost attachment regulation with the same severity as cells expressing 9A-Hec1. Indeed, both 35N<sup>-</sup> and 25N<sup>-</sup>-Hec1 expression resulted in moderately elevated cold-stable kinetochore-microtubule attachments in prometaphase (~50% of kinetochores end-on attached; Figure 3.1 D and E), while

expression of 9A-Hec1 results in nearly metaphase levels of end-on attachments in prometaphase (~80% of kinetochores end-on attached; Figure 2.2; see also Figure 3.7). This led us to ask whether blocking phosphorylation of 35N- and 25N-Hec1 tail domains would exacerbate the regulation defects observed for these mutants. We therefore generated the analogous phospho-blocked versions of each tail mutant, where all Aurora sites present are mutated to Ala (Figure 3.6 A). We expressed these mutants in cells, cold-treated cells prior to fixation, immunostained with antibodies to tubulin, and measured end-on attachment formation in early prometaphase. To our surprise, expression of all tail length mutants resulted in a dramatic increase in attachment formation, similar to expression of 9A-Hec1 (Figure 3.6 B and C; Figure 3.7 E). Importantly, the amount of attachments observed for phospho-blocked short Hec1 tails was more than that observed for their “wild type” counterparts (compare 25N<sup>A</sup>- and 35N<sup>A</sup>-Hec1, Figure 3.6 C, to 25N- and 35N-Hec1, Figure 3.1 E). This suggested to us that blocking Hec1 tail phosphorylation leads to increased microtubule occupancy at kinetochores independently of loss of attachment regulation, and that blocking phosphorylation of regulation-deficient tail lengths may result in excess force generation at the kinetochore-microtubule interface in metaphase cells. To test this, we measured inter-kinetochore distances in cells expressing “wild-type” and phospho-blocked versions of 35- and 25N-Hec1 mutants, as these tail lengths are deficient in attachment regulation (Figure 3.1 D and E). If loss of attachment regulation in early mitosis directly causes elevated force generation in metaphase, kinetochores in cells expressing 35N- and 25N-Hec1 should be under higher tension than kinetochores in cells expressing WT-Hec1. Contrary to this hypothesis, metaphase inter-kinetochore distances were similar in WT-,

25N-, and 35N-Hec1 expressing cells (Figure 3.6 D and E). In contrast, expression of 35N<sup>A</sup>- and 25N<sup>A</sup>-Hec1 caused significant increases in inter-kinetochore distances, more similar to 9A-Hec1 expression (Figure 3.6 D and E). Given that 25N- and 35N-Hec1 expression results in premature kinetochore-microtubule attachment formation in early prometaphase, but does not increase inter-kinetochore distance, it is likely that loss of attachment regulation does not directly result in excess force-generating attachments. Rather, the experiments in early prometaphase cells suggest that blocking Hec1 tail phosphorylation significantly increases microtubule occupancy, which in turn leads to excess tension generation. Cumulatively, these experiments demonstrate that a full length Hec1 tail is not required for generation of high-strength attachments when blocked from Aurora phosphorylation.

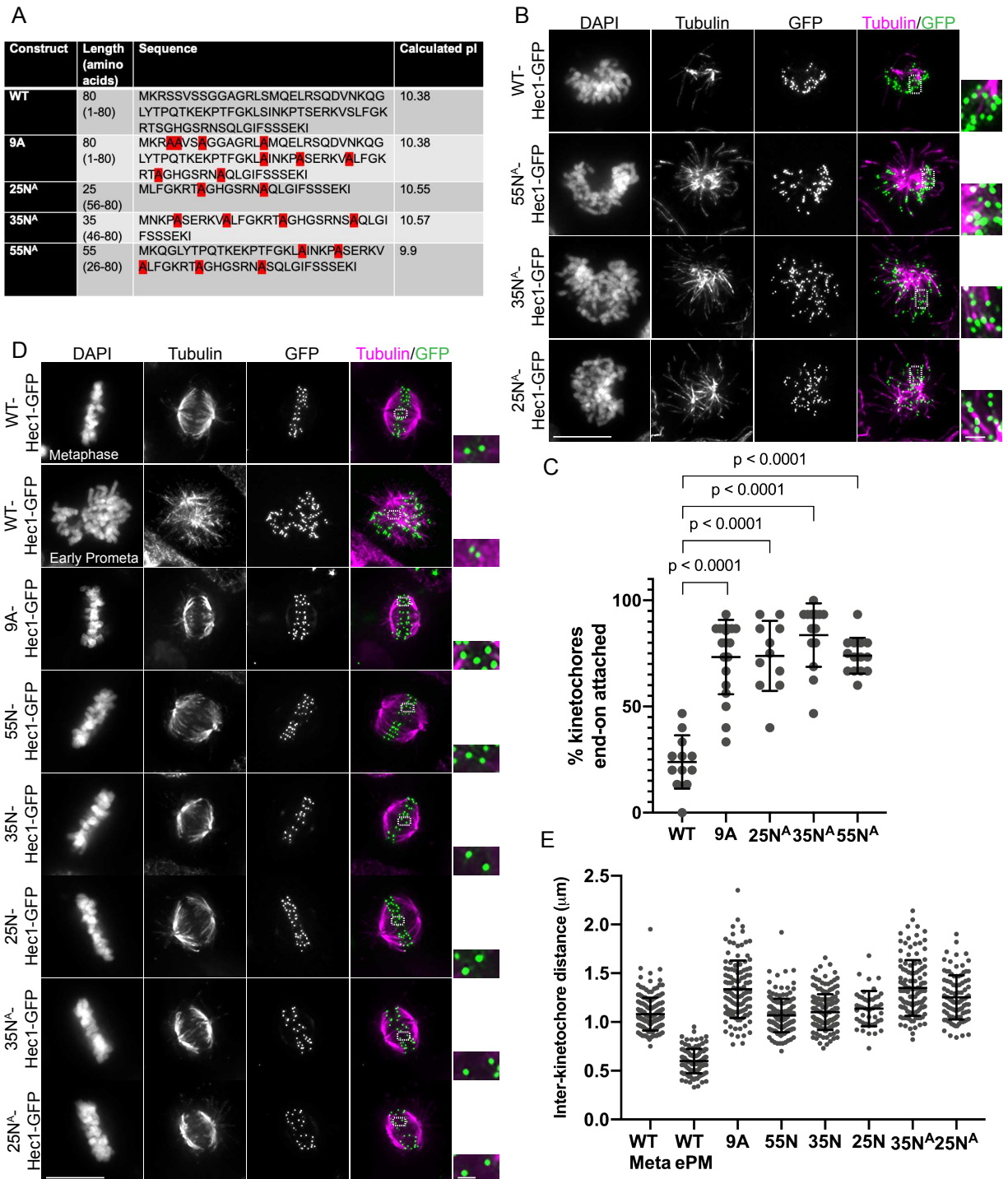


**Figure 3.6. Expression of short, phospho-blocked Hec1 tails phenocopies expression of full-length, phospho-blocked Hec1 tails.** (A) Table depicting phospho-blocked Hec1 mutants used in experiments. Table shows overall tail length and amino acids present in tail, as well as the Hec1 tail sequences and calculated isoelectric point (pI) of tail. For phospho-blocked variants, mutated Aurora sites are highlighted in red. Isoelectric points were calculated using Isoelectric Point

Calculator (Kozlowski, 2016). (B) Immunofluorescence images of early prometaphase cold-treated HeLa cells expressing the indicated Hec1-GFP mutants. Cells were incubated in ice-cold DMEM for 12 min before fixation, permeabilized, fixed, and stained using antibodies to tubulin. Insets are enlargements of the region indicated by the dashed box. (C) Quantification of end-on attachment in cold-treated cells expressing the indicated Hec1-GFP mutants. A one-way Anova was carried out to determine statistical significance. Each dot represents the percent of end-on attachments for an entire cell. (D) Immunofluorescence images of HeLa cells expressing the indicated Hec1-GFP mutants. Cells were permeabilized, fixed, and stained with antibodies to tubulin. Insets are enlargements of the region indicated by the dashed box. (E) Quantification of inter-kinetochore distances in metaphase and prometaphase cells expressing WT-Hec1-GFP, and cells expressing denoted Hec1-GFP mutants. P-values from one-way ANOVA analysis are presented in table 3.1. Each dot represents the distance measured for a single kinetochore pair. Scale bars: 10  $\mu$ m and 1  $\mu$ m for panels and insets, respectively. Total kinetochore, cell, and experimental replicate numbers for all experiments are provided in table 3.2.

**Table 3.1. Statistical analysis of IKD data in Figure 3.6 E.** Table shows calculated p-values from one-way ANOVA analysis of inter-kinetochore distance data in Figure 3.6 E. Note that 25N-Hec1 is excluded from analysis due to only being one technical replicate (N=1).

Hec1 mutant	p-value vs WT meta	p-value vs 9A
WT meta	n/a	<0.0001
WT ePM	<0.0001	<0.0001
9A	<0.0001	n/a
55N	0.9992	<0.0001
35N	0.964	<0.0001
35N <sup>A</sup>	<0.0001	0.9993
25N <sup>A</sup>	<0.0001	0.0205

### Force generation and attachment regulation by the Hec1 tail domain are uncoupled

It was particularly surprising that blocking phosphorylation of short Hec1 tails led to elevated inter-kinetochore distances and cold-stable attachment formation in early prometaphase, even for tail lengths that were already deficient in attachment regulation

in their “wild type” state (Figure 3.1 D and E, and Figure 3.6 D and E). It has been previously hypothesized that the Hec1 tail domain contributes to kinetochore-mediated force generation by providing an extra microtubule binding site within the NDC80 complex (Huis in’t Veld et al., 2019; Wimbish et al., 2020). We speculated that blocking phosphorylation of short Hec1 tails may increase the contact frequency between tail domains and the microtubule, whereas the persistent phosphorylation of Hec1-Ser 69 may keep these interactions more transient (DeLuca et al., 2018). Indeed, phosphorylation of the Hec1 tail reduces tail-microtubule contact frequency *in silico*, and a single phospho-mimetic mutation in the Hec1 tail weakens NDC80-microtubule binding affinity *in vitro* (Zaytsev et al., 2015). In this scenario, blocking phosphorylation of short Hec1 tail domains would lead to robust tail-microtubule interactions, causing accumulation of early attachments and elevated inter-kinetochore distances. We were curious if we could increase tail-microtubule interactions without perturbing Aurora kinase sites. We hypothesized that we may be able to increase Hec1 tail-microtubule contact frequency by increasing the length of the tail domain. To this end, we generated a Hec1 mutant with an extended tail, in which we added amino acids 1-12 of the human Hec1 tail domain immediately following amino acids 1-80 and preceding the CH domain, thus retaining the tail’s wild-type charge without mutations to the native Aurora kinase sites (92N-Hec1, Figure 3.7 A). We speculated that expression of this mutant may result in a larger binding interface between the tail and the microtubule lattice, therefore generating a higher force attachment site. Indeed, we found that metaphase cells expressing 92N-Hec1 had significantly higher inter-kinetochore distances than cells expressing WT-Hec1 (Figure 3.7 B and C). The 92N Hec1 tail retains all 9 native Aurora kinase sites, and also

has three additional predicted sites within the 12 amino acid extension (Figure 3.7 A). Based on this, we hypothesized that this mutant should not preclude normal kinetochore-microtubule attachment regulation. In line with this prediction, we found that expression of 92N-Hec1 led to wild-type levels of cold-stable attachments in early prometaphase, in contrast to 9A-Hec1 expression (Figure 3.7 D and E). Additionally, live cell imaging revealed that chromosome alignment and mitotic transit timing were unaffected for 92N-Hec1 expressing cells, whereas 9A-Hec1 expressing cells experienced delays in both (Figure 3.8 A-C). Finally, cells expressing 92N-Hec1 did not undergo significant loss of spindle bipolarity or exhibit increased levels of chromosome mis-segregation, in contrast to cells expressing 9A-Hec1 (Figure 3.8 D and E). Cumulatively, these data show that 92N-Hec1 does not phenocopy 9A-Hec1, despite the fact that it forms high-tension attachments in metaphase. This suggests that the defects associated with blocking Hec1 tail phosphorylation are not simply a consequence of excess tension generation. From these experiments, we conclude that the requirements for force generation and negative attachment regulation within the Hec1 tail domain are separable, as 92N-Hec1 expression did not preclude normal attachment regulation.

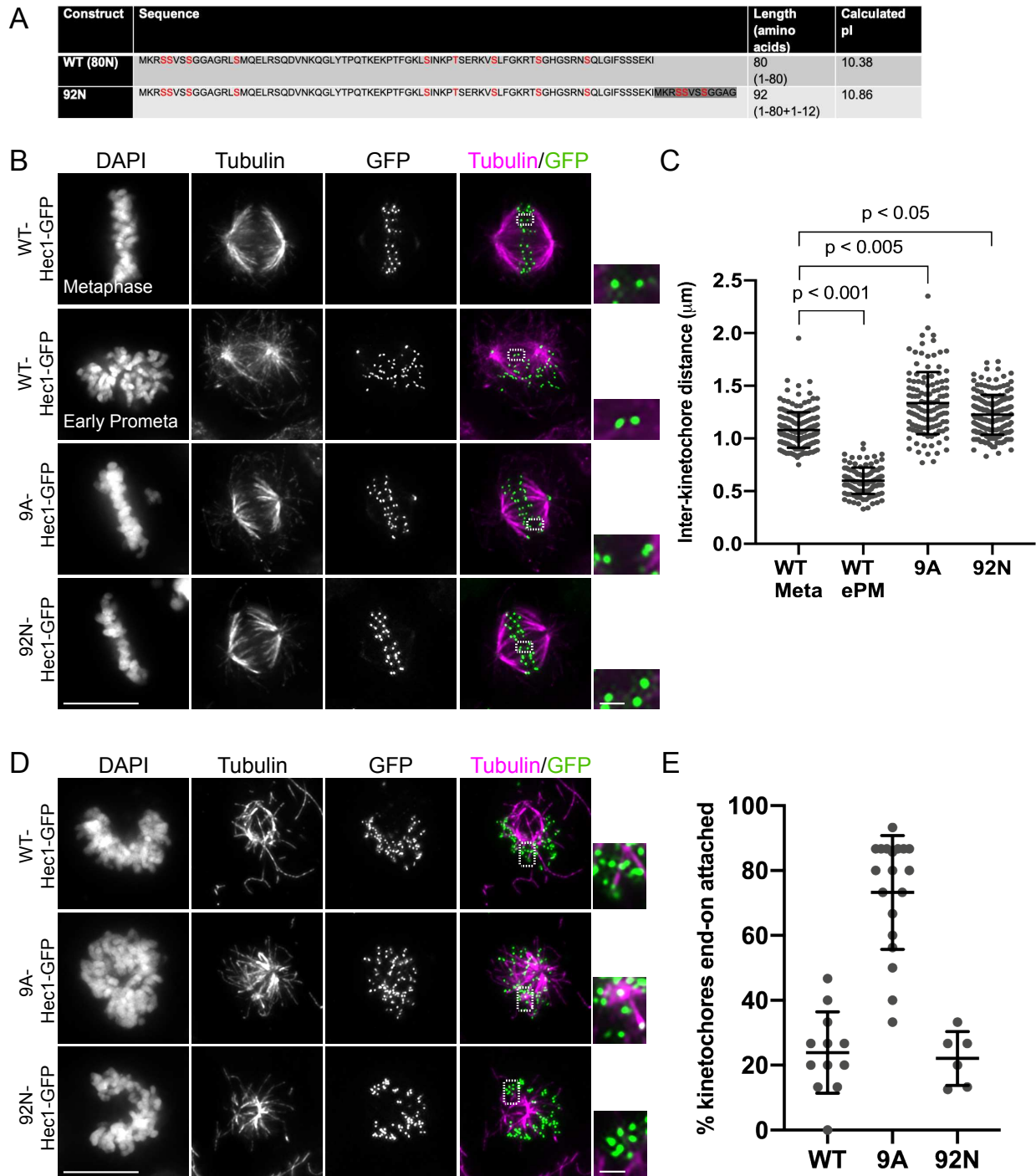


**Figure 3.7. Force generation and attachment regulation by the Hec1 tail domain are uncoupled.** (A) Table depicting 92N-Hec1 mutant used in experiments. Table shows overall tail length and amino acids present in tail, as well as the Hec1 tail sequences and calculated isoelectric point (pI) of tail. Aurora kinase sites are in red text, and tail extension of 92N-Hec1 (amino acids 1-12) are highlighted dark gray. Isoelectric points were calculated using Isoelectric Point Calculator (Kozlowski, 2016). (B) Immunofluorescence images of HeLa cells expressing the indicated Hec1-

GFP mutants. Cells were permeabilized, fixed, and stained with antibodies to tubulin. Insets are enlargements of the region indicated by the dashed box. (C) Quantification of inter-kinetochore distances in metaphase and prometaphase cells expressing WT-Hec1-GFP, and cells expressing denoted Hec1-GFP mutants. Statistical significance was determined using a one-way Anova. Each dot represents the distance measured for a single kinetochore pair. (D) Immunofluorescence images of early prometaphase cold-treated HeLa cells expressing the indicated Hec1-GFP mutants. Cells were incubated in ice-cold DMEM for 12 min before fixation, permeabilized, fixed, and stained using antibodies to tubulin. Insets are enlargements of the region indicated by the dashed box. (E) Quantification of end-on attachment in cold-treated cells expressing the indicated Hec1-GFP mutants. Data for 9A-Hec1 are from the experiments shown in Chapter 2. Each dot represents the percent of end-on attachments for an entire cell. Scale bars: 10  $\mu\text{m}$  and 1  $\mu\text{m}$  for panels and insets, respectively. Total kinetochore, cell, and experimental replicate numbers for all experiments are provided in table 3.2.

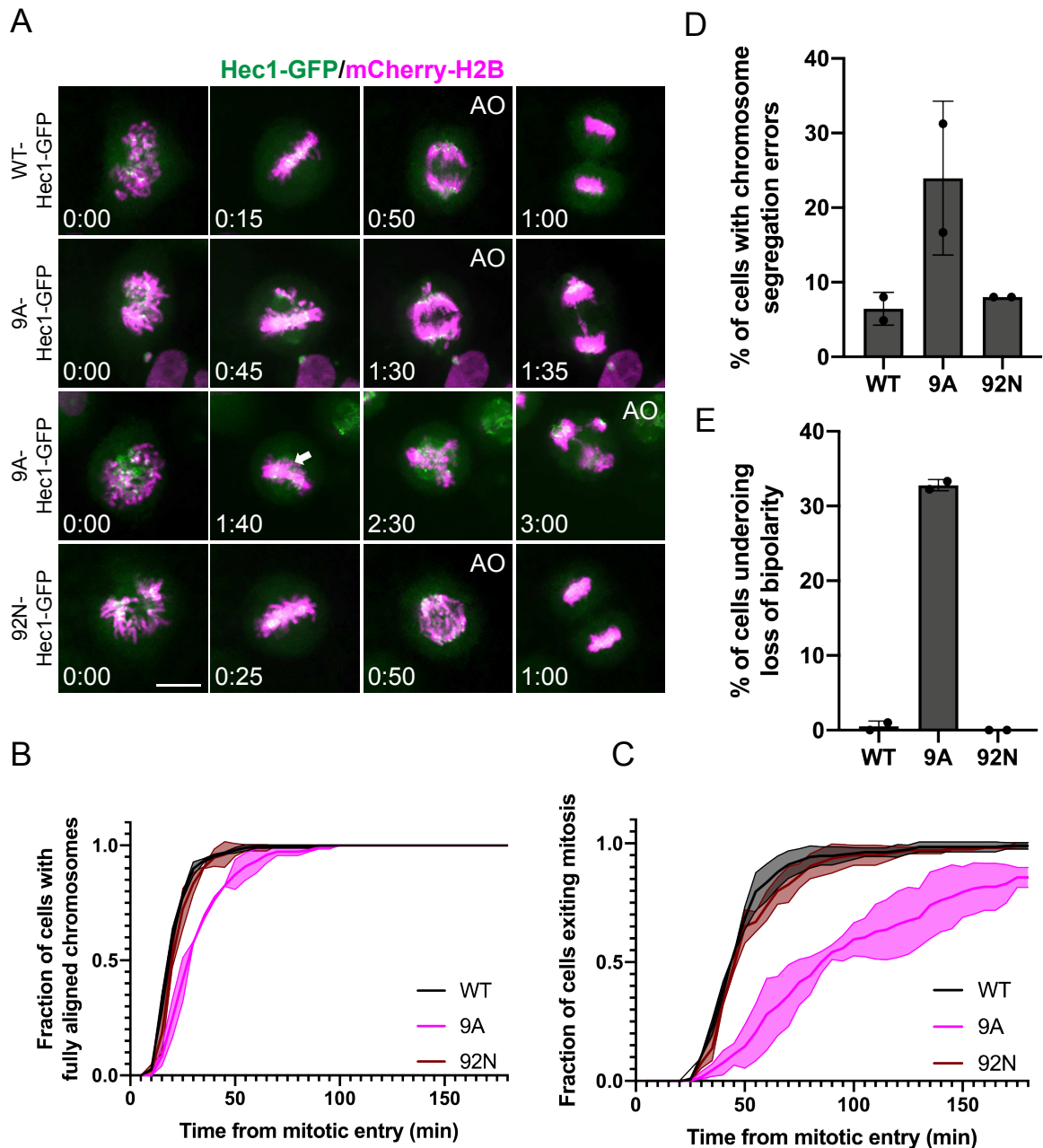


**Figure 3.8. Generation of excess tension by 92N-Hec1 expression does not cause mitotic defects** (A) Still images from time-lapse experiments of cells expressing Hec1-GFP and mCherry-H2B. Cells were released from thymidine synchronization and filmed in 5-minute intervals. Time from nuclear envelope breakdown (NEBD) is denoted on bottom left corner of each image (hours: minutes), and anaphase onset (AO) is denoted for appropriate mutants. Note that for 9A-Hec1, two examples of cells are shown depicting the two most prominent cell fates: chromosome segregation errors (top) and loss of bipolarity (bottom). White arrow on 9A-Hec1 panel denotes un-congressed chromosomes near area where spindle fragmentation originates. (B) Quantification of chromosome alignment timing in cells from the experiment shown in panel 3.8 A. Cell

fate was tracked after mitotic entry for 3 h, and cells were scored as “aligned” upon metaphase plate formation (as determined by Hec1-GFP and mCherry-H2B fluorescence). For all experiments, mean (bold line) timing is shown along with standard deviation of all experiments (shaded area). (C) Quantification of mitotic exit timing in cells from the experiment shown in panel 3.8 A. Cell fate was tracked after mitotic entry for 3 h, and cells were scored as exiting mitosis upon anaphase onset. For all experiments, mean (bold line) timing is shown along with standard deviation of all experiments (shaded area). (D) Graph showing chromosome segregation errors. Cells were scored as having segregation errors of bridging chromatin was visible in anaphase that was not resolved prior to anaphase B (see Methods). Graph shows average across experiments, and black dots are individual replicates. (E) Graph showing loss of bipolarity. Cells were scored as losing bipolarity if, after reaching metaphase, an obvious “splitting” in metaphase plate was detected (see example in 3.8 A, see also Methods). All data for WT-Hec1 on all graphs are from experiments depicted in Figure 3.4. Total cell and experimental replicate numbers for all experiments are provided in table 3.2. Scale bar: 10  $\mu$ m.

### 3.3 Discussion

#### **The Hec1 tail deletion phenotype is rescued with a 25 amino acid tail domain**

The 80 amino acid Hec1 tail domain contributes to kinetochore-microtubule attachment regulation and force generation during mitosis (DeLuca et al., 2006; Cheeseman et al., 2006; Zaytsev et al., 2014; 2015; Suzuki et al., 2016; Long et al., 2017; Helgeson et al., 2018; Huis in't Veld et al., 2019; Wimbish et al., 2020). Recombinant NDC80 complexes lacking the tail are deficient in resisting force on and tracking with dynamic microtubule ends *in vitro*, and expression of tailless Hec1 mutants in cells leads to loss of spindle bipolarity, chromosome scattering and resting-length inter-kinetochore distances for kinetochores that retain end-on attachments (Helgeson et al., 2018; Huis in't Veld et al., 2019; Wimbish et al., 2020). We found here that the pleiotropic mitotic defects associated with Hec1 tail deletion could be rescued upon expression of 25N-Hec1, a mutant that retains the 25 amino acids of the tail domain most proximal to the CH domain. It has been speculated that the Hec1 tail provides an extra microtubule interaction site within the

kinetochore, and that the tail-microtubule interaction is specifically important on depolymerizing (curved) microtubule ends, while the Hec1 CH domain is the primary microtubule binding site on polymerizing (straight) protofilaments (Ciferri et al., 2008; Alushin et al., 2012; Umbreit et al., 2012; Huis in't Veld et al., 2019). Our results suggest that this interaction can be facilitated by a tail domain that is less than a third of the wild-type length in human cells. This observation brings up the question of whether a full-length Hec1 tail domain confers any advantages in microtubule end-tracking to NDC80 complexes. Although we did not do a thorough comparison of microtubule binding by NDC80 complexes with a Hec1 tail truncations, the 25N-NDC80<sup>Bonsai</sup> mutant appears to bind to microtubules more weakly than complexes with a full-length tail (Figure 3.3), in line with the observation that the tail domain is required for high-affinity microtubule binding to NDC80 complexes *in vitro* (Ciferri et al., 2008; Miller et al., 2008; Umbreit et al., 2012; Zaytsev et al., 2015; Wimbish et al., 2020). It is possible that truncation of the Hec1 tail domain causes mitotic defects in cells that were not resolved by our assays: while 25N-Hec1 expression rescues the terminal phenotype of  $\Delta$ 80-Hec1 expression and does not alter chromosome alignment dynamics, we did not carry out analysis of whether chromosome oscillation dynamics or microtubule tracking *in vitro* were impacted for Hec1 tail truncation mutants. Interestingly, expression of all Hec1 tail length mutants resulted in a moderate increase in chromosome segregation errors (Figure 3.9). The cause of these defects is not immediately clear, although an attractive explanation is that the loss of prometaphase regulation associated with these mutants results in accumulation of erroneous attachments that cause segregation errors in anaphase. Puzzlingly, expression of 55N-Hec1 – which regulates attachments normally – may still result in

chromosome segregation errors, although further experiments need to be conducted to verify this phenotype (Figure 3.9). As shown in Figure 3.3, a 55 amino acid tail is only ~50% as efficient as a full length tail in regulating NDC80-microtubule binding *in vitro*; thus, it is possible that expression of 55N-Hec1 causes some level of regulation loss that is undetectable in the early prometaphase assay, but that still results in merotelic attachment formation. An alternative explanation is that tail truncation mutants exhibit defects in tracking dynamic microtubules, and that these defects lead to segregation errors in anaphase. Altered chromosome oscillation dynamics have been previously correlated with chromosome segregation errors (DeLuca et al., 2018); thus, it will be important to measure tracking dynamics for tail truncation mutants. A thorough characterization of the effects of Hec1 tail truncation on NDC80-microtubule binding dynamics *in vitro* will also be helpful in addressing this question.

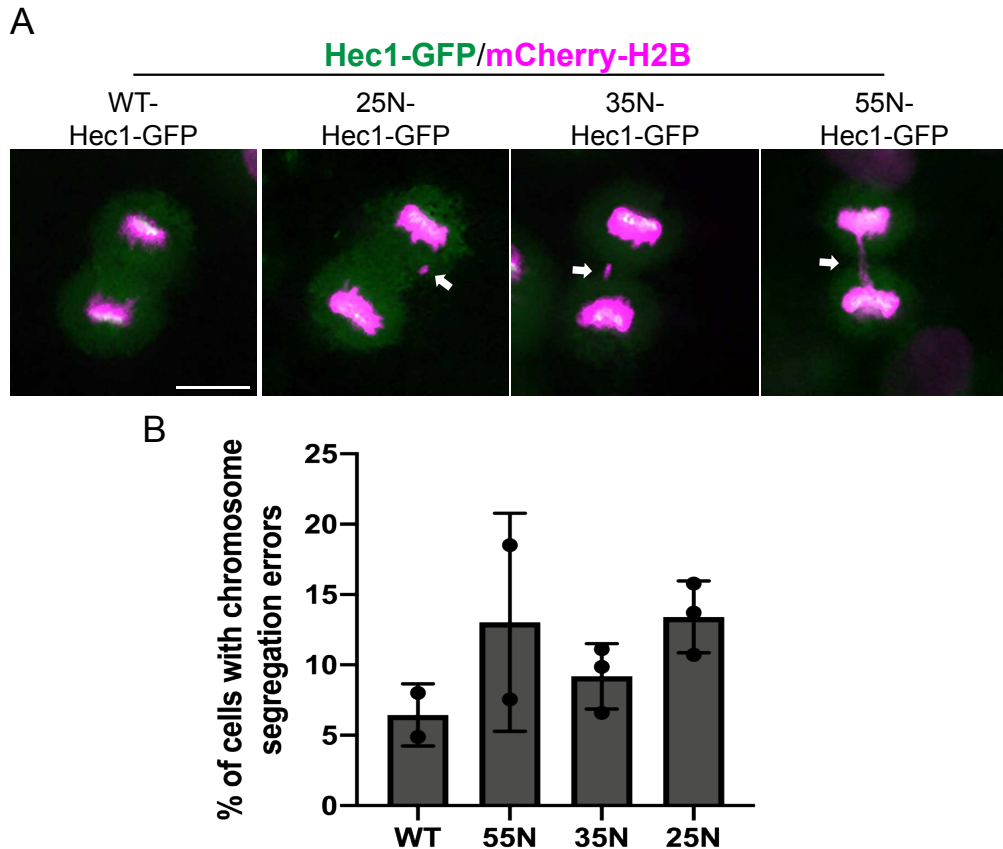


**Figure 3.9. Expression of Hec1 tail truncation mutants leads to higher chromosome segregation errors.** A) Still images of cells in anaphase B from time-lapse experiments of cells expressing Hec1-GFP and mCherry-H2B. White arrows denote lagging chromosomes. (B) Graph showing chromosome segregation errors. Cells were scored as having segregation errors of bridging chromatin was visible in anaphase that was not resolved prior to anaphase B (see Methods). Graph shows average across experiments, and black dots are individual replicates. Total cell and experimental replicate numbers for all experiments are provided in table 3.2. Scale bar: 10  $\mu$ m.

### Short Hec1 tail domains are deficient in regulation of NDC80-microtubule binding *in vitro* and kinetochore-microtubule attachment regulation in cells

Perhaps the most well documented function of the Hec1 tail domain in human cells is its role in kinetochore-microtubule attachment regulation. As discussed in Chapter 1, the tail is a key target of Aurora kinase phosphorylation at the kinetochore, and this pathway is used to temporally regulate kinetochore-microtubule attachment strength to prevent

chromosome mis-segregation (see Section 1.3 and Figures 1.1 and 1.2). One explanation for the mechanism of Hec1-mediated phospho-regulation of attachments is that the reduced charge of a phosphorylated Hec1 tail causes electrostatic repulsion of the NDC80 complex from the negatively charged microtubule lattice, resulting in weakened kinetochore-microtubule attachments (see Section 1.8a). Contrary to this model, we found here that kinetochores in cells expressing short Hec1 tail domain mutants formed cold-stable attachments in early prometaphase, even when phospho-mimetic mutations were introduced in the tails to reduce their charge similar to a full-length phospho-mimetic tail. Normal attachment regulation was restored upon expression of a 55 amino acid Hec1 tail, suggesting that specific length requirements exist for phospho-regulation of kinetochore-microtubule attachments. Notably, we were able to recapitulate these findings *in vitro*: the microtubule-binding affinity of recombinant NDC80 complexes was more impacted by phospho-mimetic mutation for complexes with longer Hec1 tails, whereas short-tail containing NDC80 complexes were almost unaffected by phospho-mimetic mutation. To further verify the length-dependency of attachment regulation, we expressed phospho-mimetic Hec1 tail truncation mutants in cells and tracked chromosome alignment dynamics by live cell imaging. Consistent with our fixed cell and *in vitro* results, these experiments demonstrated that longer delays in chromosome alignment scaled with longer phospho-mimetic tail length. Collectively, our in-cell and *in vitro* experiments with “wild type” and phospho-mimetic Hec1 tail mutants conflict with the model that Hec1 tail phosphorylation regulates kinetochore-microtubule attachments simply through electrostatic repulsion of NDC80 complexes from the microtubule lattice

(Figure 1.3a). Rather, they demonstrate that both charge and length requirements exist for Hec1 tail-mediated regulation of attachments.

An important question is why short Hec1 tail domains cannot regulate attachments normally. The answer to this question may lie in the highly conserved, well ordered CH domains of Hec1 and Nuf2. The globular CH domains of Hec1/Nuf2 directly bind to microtubules, with the Hec1 portion containing the key binding site for tubulin (Ciferri et al., 2008). Both CH domains contain many positively charged residues that are required for NDC80 complex-microtubule binding *in vitro*: collectively, 12 residues facilitate the NDC80-microtubule interaction, and they are well distributed throughout the surface of the Hec1-Nuf2 CH domains (Ciferri et al., 2008). Many of these residues have been shown to be important for chromosome alignment and kinetochore-microtubule attachments in cells, demonstrating the importance of a positively charged surface for NDC80-microtubule interactions (Sundin et al., 2011; Tooley et al., 2011). Notably, the combined mutation of multiple residues has a more dramatic impact on NDC80-microtubule binding *in vitro* and chromosome alignment in cells than single point mutations, in line with the idea that multiple sites within the Hec1-Nuf2 CH domains contact the microtubule lattice (Ciferri et al., 2008; Tooley et al., 2011). Ciferri and colleagues (2008) proposed a model in which Hec1 tail phosphorylation promoted a tail-CH domain interaction which would block the CH domain from binding to the microtubule lattice. While this model has yet to be directly tested, it was supported by data from Umbreit et al. (2012) using recombinant NDC80 complexes with dynamic microtubules *in vitro*: the authors found that both wild-type and tail-less NDC80 complexes promoted

microtubule rescue, where a microtubule switches from depolymerization to polymerization, with high frequency. This led the authors to speculate that microtubule rescue was promoted by the CH domain of NDC80 complexes binding to depolymerizing microtubules and causing them to “straighten”, thus slowing depolymerization. In contrast to the case for wild-type and tail-less complexes, NDC80 complexes containing a completely phospho-mimetic Hec1 tail domain could not promote high levels of rescue, leading the authors to conclude that a 9D-Hec1 tail must inhibit the ability of the CH domain to bind to microtubules and cause rescue (Umbreit et al., 2012). Our results in this study support the autoinhibition model for regulation of NDC80-microtubule interactions. Because many positively charged residues are involved in NDC80-microtubule interactions, it is likely that a longer tail could interact with more of these residues, thereby preventing microtubule binding more effectively. Conversely, shorter Hec1 tail domains cannot extend as far, and therefore would be unable to bind to as large of a surface area of the CH domains, therefore less effectively inhibiting CH domain-microtubule interactions. In our studies, short tail mutants are unable to effectively regulate NDC80-microtubule interactions *in vitro* or kinetochore-microtubule interactions in cells. A key step in validating or refuting the autoinhibition model will be to investigate whether a phospho-mimetic tail interacts with the CH domain *in vitro*. If an interaction is detected, it will be important to investigate which residues of the CH domain are important for this interaction by performing the same interaction assay with point mutants of charged residues in the CH domain.

It is important to mention that our results do not refute the notion that phosphorylation of the Hec1 tail weakens its interaction with the microtubule lattice. Due to the presence of the acidic C-terminal extensions of tubulin subunits, the microtubule lattice is highly negatively charged (Ponstingl et al., 1979; Sackett, 1995; Nogales et al., 1998). As the Hec1 tail is highly basic, it follows that its acidification should weaken its interaction with microtubules by reducing the ionic strength of this interaction; indeed, this has been shown for purified phospho-mimetic Hec1 tail fragments *in vitro* (Alushin et al., 2010). Furthermore, our observation that regulation-deficient Hec1 mutants can form more robust attachments when phospho-blocked suggests that the persistence of phosphorylation within the tail keeps attachments weaker than a completely dephosphorylated tail (discussed in the next section). Taken together, the available data suggest that acidification of the Hec1 tail weakens tail-microtubule interactions; however, based on our studies here and a previous study (Umbreit et al., 2012), it is likely that this is not the sole determinant of binding regulation.

### **Force generation and attachment regulation by the Hec1 tail are functionally uncoupled**

As mitosis progresses, the Hec1 tail becomes dephosphorylated and microtubule occupancy at kinetochores increases, leading to attachments that generate higher forces and are robust enough to move chromosomes (DeLuca et al., 2006; DeLuca et al., 2011; Yoo et al., 2018). The consequences of Hec1 tail dephosphorylation have been studied using 9A-Hec1, a mutant in which all nine Aurora kinase sites are mutated to Ala to prevent phosphorylation. Expression of 9A-Hec1 results in premature kinetochore-

microtubule attachment formation, hyper-stretched inter-kinetochore distances, trapped polar chromosomes, dampened chromosome oscillations, and chromosome mis-segregation (Guimaraes et al., 2008; DeLuca et al., 2011; Zaytsev et al., 2014; Long et al., 2017; Wimbish et al., 2020). It has been speculated that blocking Hec1 tail phosphorylation prevents phospho-regulation of attachments, and that loss of regulation causes the aforementioned defects. Contrary to this hypothesis, we found here that expression of Hec1 mutants with short tails – which are deficient in attachment regulation – does not result in elevated inter-kinetochore distances or trapped polar chromosomes, suggesting loss of attachment regulation does not directly cause the phenotypes associated with 9A-Hec1 expression. However, when short tails are blocked from Aurora kinase phosphorylation, we observed an increase in inter-kinetochore distance and cold-stable end-on attachments more similar to what has been observed upon 9A-Hec1 expression. This result may initially seem counter-intuitive, as the Hec1 tail has been posited to be an extra microtubule binding site for the NDC80 complex and one might assume this function to be length-dependent (Guimaraes et al., 2008; Miller et al., 2008; Tooley et al., 2011; Huis in't Veld et al., 2019). However, the behavior of the tail domain *in silico* may provide insight into its length-dependency: molecular dynamics simulations have suggested that a full length tail, while highly dynamic in solution, occupies a small volume with a similar radius of gyration to that of the beta tubulin monomer (Zaytsev et al., 2015). In these simulations, the Hec1 tail domain only contacts one to two C-terminal tails of tubulin. As mentioned above, an 80 amino acid peptide chain should be able to linearly extend ~28 nm; thus, a fully extended tail could, in theory, longitudinally reach across roughly 3 tubulin dimers and interact with up to 6 tubulin tails. Our data showing

that blocking phosphorylation of a 25 amino acid Hec1 tail phenocopies blocking phosphorylation of a full length tail suggest that this is not the case, and agree with molecular dynamics simulations predicting that the tail is more compact and interacts with tubulin subunits more proximal to the CH domains of the NDC80 complex (Zaytsev et al., 2015).

We were somewhat surprised at the finding that short, phospho-blocked Hec1 tail domains elicit similar phenotypes to 9A-Hec1 expression. This result suggests that for all tail lengths, maintenance of Ser 69 phosphorylation in metaphase is critical for maintaining “wild type” attachments, with this modification holding tail-microtubule interactions more dynamic. Several lines of evidence support this idea: (a) expressing a phospho-blocked Ser 69 mutant (with all other sites left intact) leads to dampened chromosome oscillations, increased segregation errors, and accelerated chromosome alignment (DeLuca et al., 2018), and (b) expressing a completely phospho-blocked Hec1 tail mutant results in hyper-recruitment of the Ska complex, a protein known to load to kinetochores with higher microtubule occupancy, whereas a Hec1 tail mutant where all sites except for Ser 69 are phospho-blocked rescues this defect (Wimbish et al., 2020). It will be important to determine if subtle differences in attachment phenotypes exist for phospho-blocked tails that scale with length. Additionally, a key future experiment is to understand the biochemical basis for the high-force attachments generated upon complete tail dephosphorylation. Determining the microtubule-binding characteristics of recombinant NDC80 complexes with single phospho-mimetic mutations at Ser 69

compared to complexes with non-phospho-mimetic tails under force would be helpful in addressing this question.

### **Implications for high-tension attachments from 92N-Hec1 expression**

In our attempt to understand whether a higher Hec1 tail-microtubule contact frequency leads to stronger attachments, we generated a Hec1 mutant with an extended, 92 amino acid tail domain. Expression of this mutant resulted in metaphase attachments that were under excess tension. However, as 92N-Hec1 has all Aurora kinase sites intact, its expression did not preclude normal kinetochore-microtubule attachment regulation and did not result in the pleiotropic mitotic defects associated with 9A-Hec1 expression. This result suggests that the previously documented phenotypes for 9A-Hec1 – including trapped polar chromosomes in metaphase, high chromosome mis-segregation, and multipolarity – are not solely due to excess tension generation in metaphase. Similarly, the observation that regulation-deficient tail mutants do not generate excess tension suggests that the 9A-Hec1 phenotype is not solely due to loss of regulation. It is likely that these defects are a combination, rather, of high-tension attachment generation and loss of attachment regulation.

How does the addition of a 12 amino acid extension cause high-tension attachments? As mentioned above, the 80 amino acid tail is simulated to be relatively compact (Zaytsev et al., 2015). However, it is possible that it is sterically unfavorable for the tail to compact further, and that the additional 12 amino acids in our 92N-Hec1 mutant protrude out from the compacted 80 amino acids, therefore interacting with a larger surface area of the

microtubule. Alternatively, addition of the tail extension could disrupt the compaction of the native 80 amino acids, causing a change in the overall volume that the tail occupies and causing it to interact with a higher surface area of the microtubule. Performing molecular dynamics simulations of extended Hec1 tails may shed light on the reason for high-tension attachments for tail extension mutants. Additionally, it will be important to generate mutants with longer tail extensions to see if they can exacerbate the force-generation increase caused by the 92N-Hec1 mutant.

One interesting aspect of the 9A-Hec1 phenotype we report here is the frequency with which cells expressing this mutant undergo loss of bipolarity. This defect was previously observed in our lab, but its origin remains unclear (DeLuca et al., 2011). While we have previously noted that weak microtubule-binding Hec1 variants cause loss of spindle bipolarity (see  $\Delta 80$ -, 9D, and ML-Hec1; Figures 2.8), 9A-Hec1 expression causes robust kinetochore-microtubule interactions and therefore is unlikely to exhibit its multipolar phenotype as a consequence of weak kinetochore-based forces. In a study using an N-terminally tagged GFP-Hec1 construct, Mattiuzo and colleagues (2011) noted that cells expressing this mutant accumulated a high incidence of lateral kinetochore-microtubule attachments and exhibited a high frequency of multipolarity. The authors concluded that in this scenario, uncongressed (polar) chromosomes accumulate faulty kinetochore-microtubule interactions which disrupt inter-spindle forces, leading to pole fragmentation (Mattiuzo et al., 2011). An alternative explanation in the case of 9A-Hec1 expressing cells is that “trapped” polar chromosomes sterically block the HSET/NuMA-driven efforts of motor-mediated spindle focusing, leading to loss of the architectural integrity of the

spindle (Manning and Compton, 2007). We note that for 9A-Hec1 expressing cells that lose bipolarity, many of the apparent pole fragmentation events originate near an uncongressed chromosome (white arrow in top panel, Figure 3.8 A).

Overall, our results suggest that kinetochore-microtubule attachment regulation and tension generation are not functionally coupled. Furthermore, they demonstrate that the length requirements for generation of high-tension attachments in metaphase are different from the length requirements for negatively regulating attachments in prometaphase. An important goal in the future is to thoroughly characterize the consequences of loss of attachment regulation and generation of excess tension.

**Table 3.2. Table depicting n-values for all experiments in Chapter 3.** Relevant figures (shaded dark grey, white text) are denoted, and for each Hec1/NDC80 complex mutant in that figure (light grey) the relevant cell, kinetochore, and microtubule numbers are given. Total biological replicates performed for each experiment (N replicates) is also shown. Abbreviations: KT = kinetochore, MT = microtubule, meta = metaphase, ePM = early prometaphase.

<b>3.1 B</b>			
<b>Hec1 mutant</b>	<b>n Cells</b>	<b>N replicates</b>	
WT	300	3	
$\Delta 80$	200	2	
25N	75	1	
25N <sup>D</sup>	199	4	
9D	200	2	
<b>3.1 E</b>			
<b>Hec1 mutant</b>	<b>n KTs</b>	<b>n Cells</b>	<b>N replicates</b>
WT	180	12	2
9D	169	11	2
25N	152	10	2
25N <sup>D</sup>	189	13	2

35N	307	20	3
55N	212	14	2
<b>3.2 B</b>			
<b>Hec1 mutant</b>	<b>n KTs</b>	<b>n Cells</b>	<b>N replicates</b>
WT	420	21	3
9A	220	11	2
25N	160	8	1
35N	260	13	2
55N	260	13	2
<b>3.3 B-F</b>			
<b>NDC80 mutant</b>	<b>n MTs</b>	<b>N replicates</b>	
WT	60	2	
9D	60	2	
55N	60	2	
55N <sup>D</sup>	60	2	
35N	30	1	
35N <sup>D</sup>	30	1	
25N	60	2	
25N <sup>D</sup>	60	2	
<b>3.4 B</b>			
<b>Hec1 mutant</b>	<b>n Cells</b>	<b>N replicates</b>	
WT	182	2	
9D	150	2	
55N <sup>D</sup>	104	2	
35N <sup>D</sup>	155	2	
25N <sup>D</sup>	121	3	
<b>3.5 B</b>			
<b>Hec1 mutant</b>	<b>n Cells</b>	<b>N replicates</b>	
WT	182	2	
9D	150	2	
55N	107	2	
35N	225	3	
25N	145	3	
<b>3.6 C</b>			
<b>Hec1 mutant</b>	<b>n KTs</b>	<b>n Cells</b>	<b>N replicates</b>
WT	180	12	2
55N <sup>A</sup>	165	11	2

35N <sup>A</sup>	210	14	2
25N <sup>A</sup>	210	14	2
<b>3.6 E</b>			
<b>Hec1 mutant</b>	<b>n KT pairs</b>	<b>n Cells</b>	<b>N replicates</b>
WT meta	221	23	3
WT ePM	116	13	2
9A	118	13	2
55N	155	18	2
35N	161	18	2
25N	46	5	1
35N <sup>A</sup>	118	14	2
25N <sup>A</sup>	100	11	2
<b>3.7 C</b>			
<b>Hec1 mutant</b>	<b>n KT pairs</b>	<b>n Cells</b>	<b>N replicates</b>
WT meta	221	23	3
WT ePM	116	13	2
9A	118	13	2
92N	182	19	3
<b>3.7 E</b>			
<b>Hec1 mutant</b>	<b>n KTs</b>	<b>n Cells</b>	<b>N replicates</b>
WT	180	12	2
9A	285	19	3
92N	90	6	1
<b>3.8 B-E</b>			
<b>Hec1 mutant</b>	<b>n Cells</b>	<b>N replicates</b>	
WT	182	2	
9A	137	2	
92N	125	2	

### 3.4 Methods

#### Cell culture, treatments and transfections

HeLa Kyoto cells were grown in Dulbecco's Modified Eagle Medium (DMEM) supplemented with 10% fetal bovine serum (FBS) and a 1% antibiotic/antimycotic

solution. Cells were maintained in T-25 flasks in a 5% CO<sub>2</sub> incubator at 37°C. For all fixed cell experiments, cells were seeded onto acid-washed, sterile 22 x 22 mm coverslips 24 hours prior to lipid transfections. For live cell experiments, cells were seeded into custom built glass-bottom 35 mm dishes 24 hours prior to lipid transfections. For all DNA transfections were done using Lipofectamine 2000 (Thermo Fisher Scientific) in Optimem (Life Technologies) according to the manufacturer's instructions. For live cell experiments in cells co-expressing Hec1-GFP and H2B-mCherry, cells were transfected with plasmids encoding Hec1-GFP (2 µg) and H2B-mCherry (200 ng) 24 hours after seeding. At 8 hours post-transfection, cells were arrested in S-phase by adding 2 mM thymidine to transfection media for 16 hours. Subsequently, cells were washed out of thymidine extensively with DMEM, and 9 hours post-washout were filmed for 16 hours. For fixed cell studies, cells were processed for immunofluorescence 24 hours after transfection. For analysis of cold-stable kinetochore-microtubule attachments, cells were incubated in ice-cold DMEM on ice for 12 minutes prior to fixation. For all nucleic acid transfections, cells in Optimem were supplemented with 10% FBS 8 hours post-transfection.

### **Live cell imaging**

For all live cell experiments, cells were filmed in Leibovitz's L-15 medium (Invitrogen) supplemented with 10% FBS, 4.5 g/l glucose, and 7 mM HEPES pH 7.0. Approximately 9 hours after thymidine washout, cells were imaged for 16 hours using a 0.6 NA 40X objective on a Nikon Ti-E microscope equipped with a spinning disk confocal scanner unit (CSUX1; Yokogawa) and Piezo Z-control (Physik Instrumente). Cells were maintained at 37°C using a stage-top incubation system (Okolab). Hec1-GFP and H2B-mCherry were

filmed by exciting the respective fluorophores with 488 nm and 594 nm lasers using a 488/594 filter cube, and images were taken with a iXon DU888 EM-CCD camera (Andor). For each experiment, 20 different fields were imaged taking 2  $\mu\text{m}$  Z-steps for a depth of 8  $\mu\text{m}$  (5 total Z-steps) at 5 minute intervals for 16 hours.

### **Immunofluorescence processing and fixed-cell imaging**

All cell processing for immunofluorescence microscopy was carried out as follows: prior to fixation, cells were quickly rinsed in PHEM buffer (60 mM PIPES, 25 mM HEPES, 10 mM EGTA, 4 mM  $\text{MgCl}_2$ , pH 7.0), and subsequently permeabilized in lysis buffer (PHEM + 1% Triton-X 100) at 37°C for 5 minutes. Following lysis, cells were fixed in 4% paraformaldehyde (diluted in PHEM buffer) for 20 minutes at room temperature. Following fixation, coverslips were transferred to a custom-built humid chamber (protected from light), and washed three times with PHEM-T (PHEM buffer + 0.1% Triton-X 100) for 5 minutes per wash at room temperature. All following steps were performed in humid chambers protected from the light. Coverslips were quickly washed in PHEM, and blocked in 10% boiled donkey serum (BDS; diluted in PHEM) for 1 hour at room temperature. Subsequently, coverslips were incubated in primary antibodies overnight at 4°C. All primary antibodies were diluted in 5% BDS (diluted in PHEM). Concentrations used were as follows: mouse anti-tubulin (DM1a) at 1:600 (Sigma-Aldrich) and rabbit anti-phosphorylated Hec1-Ser 69 (pS69) at 1:3000 (DeLuca et al., 2018). Following primary antibody incubation, coverslips were washed three times with PHEM-T (5 minutes per wash) at room temperature, and quickly washed in PHEM. Secondary antibodies conjugated to Cy3 or Alexa 647 dyes (Jackson ImmunoResearch) were diluted 1:1000 (in

5% BDS), and subsequently added to coverslips. Secondary antibodies were incubated at room temperature for 45 minutes, and unbound antibody was washed off with PHEM-T (two washes at 5 minutes each). After a brief PHEM wash, coverslips were incubated in a 2 ng/ml solution of 4',6-diamidino-2-phenylindole (DAPI; diluted in PHEM) for 30 seconds at room temperature. Unbound DAPI was washed off with two PHEM-T washes for 5 minutes each. Coverslips were briefly washed in PHEM, and subsequently mounted onto glass slides with an antifade mounting solution (90% glycerol + 0.5% *N*-propyl gallate). To prevent drying out, coverslip edges were sealed with nail polish, and slides were stored in the dark at 4°C prior to imaging. Fixed cell imaging was performed on a DeltaVision Personal DV Imaging system (GE Healthcare) using an IX71 inverted microscope (Olympus) with SoftWoRx software (GE Healthcare). Fixed cell coverslips were imaged using a 1.42 NA, 60X Plan Achromat oil immersion lens (Olympus) using a standard DAPI-FITC-TRITC-647 filter cube to excite and capture emissions for DAPI, GFP, Cy3, and Alexa 647 fluorophores, respectively. Images were acquired using a CoolSNAP HQ2 camera (Photometrics/Roper Technologies) with a final magnification of 107 nm/pixel.

### **Protein expression and purification**

Glutathione-S-transferase (GST)-NDC80<sup>Bonsai</sup> (Ciferri et al., 2008) was a generous gift from Andrea Musacchio (Max Planck Institute of Molecular Physiology, Dortmund, Germany). Tail truncation NDC80<sup>Bonsai</sup> constructs were cloned by PCR from the parent vector (tail truncation Hec1 mutants generated for in-cell expression by Isothermal Assembly) with sufficient overlap with the Spc25 fragment for isothermal assembly.

Cloned Hec1-Spc25 fragments were subsequently cloned back into the cut GST-NDC80<sup>Bonsai</sup> vector. Expression and purification of all NDC80<sup>Bonsai</sup> proteins was carried out as follows: BL21-DE3 cells were transformed with plasmids encoding NDC80<sup>Bonsai</sup>, and cultures were grown to a moderate density ( $OD_{600} \sim 0.5$ ) before induction of protein expression with 400  $\mu$ M isopropyl  $\beta$ -d-1-thiogalactopyranoside. Induced cultures were shaken at 200 rpm for 16 hours at 18°C. All of the following steps were carried out at 4°C. Cells were harvested by centrifugation and resuspended in lysis buffer (25 mM Tris, pH 7.6, 300 mM NaCl, 1 mM EDTA) supplemented with protease inhibitors (Pierce Protease Inhibitor tablets; Thermo Scientific), 1 mM phenylmethylsulfonyl fluoride (dissolved in isopropyl alcohol), and 1 mM DTT (Gold Bio). The resuspended cell mixture was lysed by running the mixture extensively through a microfluidic chamber at 80 psi. The lysed mixture was cleared of cell debris by centrifugation at 35,000 rpm for 45 min in a Beckman L8-70M ultracentrifuge using a TY70-TI rotor. The resulting supernatant was applied to a glutathione-agarose resin slurry (Pierce resin; Thermo Scientific) that had been pre-equilibrated in lysis buffer, and the mixture was rocked gently for 2 h. The resin was extensively washed with lysis buffer, and resin-bound protein was eluted by overnight by cleaving the GST tag with human rhinovirus 3C protease (HRV-3C protease, expressed and purified in-house). Elutions were pooled and concentrated in a 30 kDa molecular weight cutoff concentrator, and run on a Superose 6 Increase 10/300 GL sizing column (GE Healthcare Life Sciences) in lysis buffer supplemented with 5% glycerol and 1 mM DTT. Protein fractions were pooled and concentrated in a 30 kDa molecular weight cutoff concentrator, and glycerol was added to 20% final volume before small aliquots were snap-frozen in liquid nitrogen and stored at  $-80^{\circ}\text{C}$ .

## **TIRF microscopy**

For each experiment, “wild type” and phospho-mimetic NDC80<sup>Bonsai</sup> complexes of a single tail length were assessed for microtubule binding on the same day. The morning of the experiment, NDC80<sup>Bonsai</sup> aliquots were flash-thawed and centrifuged at  $90,000 \times g$  to remove large aggregates. The concentration of the resulting supernatant was measured by Bradford assay, and the aliquot at the highest concentration was diluted to the same extent as the lowest concentration aliquot in lysis buffer supplemented with 20% glycerol to ensure that all protein was in the same buffering environment. TIRF microscopy (TIRFM) binding assays were performed as described in section 2.4, except that the buffer used was BRB20 (20 mM PIPES, 1 mM EGTA, 1 mM MgCl<sub>2</sub>). For all experiments, GFP-NDC80 complexes were added to the flowchamber and incubated for 90 seconds per addition. Three total additions were performed at each concentration point, and following the third addition images were acquired of 10 different fields at various, random locations on the coverslip. All TIRFM images were collected at room temperature using a 1.49 NA 100 X Plan Apo TIRF oil immersion lens on a Nikon Ti-E inverted microscope equipped with an iXon3 DU897 EM-CCD camera (Andor) for a final pixel size of 160 nm/pixel.

## **Data analysis**

For all in-cell studies of Hec1-GFP expression, only cells with moderate to high levels of kinetochore GFP signal were analyzed. For fixed-cell studies of mutants lacking a Ser at position 69 in the Hec1 tail (all “A” and “D” mutants), kinetochore staining of Hec1-pS69 was qualitatively assessed and only cells with undetectable levels were analyzed.

Quantitative analysis of kinetochore Hec1-pS69 fluorescence intensity in fixed cells was carried out on non-deconvolved, non-compressed images using a custom program in MatLab (Mathworks) courtesy of X. Wan (University of North Carolina at Chapel Hill; Wan *et al.*, 2009). Measurement of end-on attachment was carried out in early prometaphase cells on deconvolved images using SoftWoRx Explorer software (GE Healthcare Life Sciences). In early prometaphase cells (as determined by DAPI staining), cold-stable attachment was analyzed by selecting random kinetochores in the GFP channel and then subsequently overlaying the tubulin channel (647) and scoring whether spindle microtubules terminated at the preselected kinetochores (ambiguous and lateral attachments were not quantified). Inter-kinetochore distances were analyzed on non-deconvolved images in ImageJ (National Institutes of Health) by measuring the distance between the approximate centroids of Hec1-GFP signals from two kinetochores in a sister pair in the same z-plane. For chromosome alignment analysis, Hec1-GFP expressing cells post-nuclear envelope breakdown were scored as either aligned (metaphase plate with <5 chromosomes off the plate) or unaligned (no metaphase plate, or metaphase plate with five or more chromosomes off the plate) based on kinetochore signal and DAPI signal. Cells containing tilted (off-axis) spindles were discarded from analysis.

Analysis of NDC80<sup>Bonsai</sup>-microtubule binding in vitro was carried out using ImageJ as described in section 2.4. The fluorescent signal from GFP-NDC80 along the microtubule axis was measured by creating a length- and shape-specific mask for each microtubule, and background GFP intensity was measured in a region in close proximity to the microtubule to account for unevenness of the TIRF field. Background signal was subtracted from microtubule-localized signal for each microtubule, and the average

corrected signal intensity was taken for 30 microtubules from 10 fields for each concentration point per experiment. The average signal-corrected GFP fluorescence for each concentration point was plotted against concentration in Prism (Graphpad), and binding curves were fit using a Specific binding curve with a Hill fit.

Analysis of live cell experiments was carried out in NIS-Elements software (Nikon Instruments). Cells were discarded from analysis if they entered mitosis <3 hours from the end of the filming period, and cells were discarded from analysis if they entered mitosis with multipolar spindles or obvious micronuclei to avoid quantifying mitotic defects that arose from a previous cell division or from the S-phase arrest. Only cells with moderate to high levels of mCherry-H2B and Hec1-GFP fluorescence were analyzed. Timing was scored for chromosome alignment, metaphase to anaphase transition, and total mitotic transit based on apparent nuclear envelope breakdown (as judged by change in nuclear shape and subsequent mitotic entry), metaphase plate formation, and anaphase onset (as judged by obvious separation of sister chromatids). For analysis of chromosome segregation errors, only cells for which lagging chromosomes persisted into anaphase B (as determined by cell morphology) were scored as erroneous to ensure that resolved laggings were not quantified. For 9A-Hec1 expressing cells, chromosome segregation errors were not quantified in cells that lost bipolarity during the experiment, as nearly every multipolar anaphase resulted in lagging chromatin and the effects of spindle multipolarity likely convolute an accurate comparison to bipolar cells.

## CHAPTER 4: CONCLUSIONS AND FUTURE STUDIES

### **4.1 Summary and relevance**

In these studies, we have conducted biochemical and cell biological analyses of the means by which human kinetochores regulate their attachment to the mitotic spindle. Our focus has been on the mechanisms that underlie Aurora kinase mediated phosphorylation of the Hec1 tail domain to regulate NDC80-microtubule interactions, and how this mechanism contributes to the fine-tuning of kinetochore-microtubule attachment. Understanding the mechanisms that kinetochores use to regulate their attachments to the spindle is critical to our insight into how these attachments can be mis-regulated, leading to chromosome segregation errors that can be catastrophic to cellular and organismal health. As such, studies that broaden our understanding of the molecular basis for chromosome segregation have implications in aneuploidy-driven diseases that can arise from chromosome mis-segregation events.

### **4.2 Insight into NDC80-Ska complex coordination and future directions**

A key goal of our experiments from Chapter 2 was to understand how the Aurora kinase pathway regulates the coordination of NDC80 and Ska complexes. We found that Hec1 phospho-regulation impacts kinetochore-microtubule attachment stability independently of the Ska complex, suggesting that Ska complex loading to kinetochores is likely a consequence of increased kinetochore-microtubule binding upon Hec1 tail dephosphorylation. We also mapped the domains of the NDC80 complex required for Ska complex kinetochore localization in cells and Ska-NDC80 complex coordination *in*

*vitro*. These studies clear up outstanding discrepancies regarding several conflicting models in the field regarding Aurora-mediated phospho-regulation of attachments: namely, they demonstrate that phosphorylation of the Hec1 tail does not regulate attachments through recruitment of the Ska complex as previously suggested (Cheerambathur et al., 2017; Wimbish and DeLuca, 2020). Furthermore, our experiments resolve conflicting reports regarding the domain requirements for NDC80-Ska complex coordination (Zhang et al., 2012; Janczyk et al., 2017; Zhang et al., 2017; Helgeson et al., 2018; Huis in't Veld et al., 2019). Finally, they substantiate the longstanding model that Hec1 tail phosphorylation affects kinetochore-microtubule attachment stability by directly affecting NDC80 complex-microtubule binding (Cheeseman et al., 2006; DeLuca et al., 2006; Guimaraes et al., 2008; Zaytsev et al., 2014; 2015).

Several key questions arose from our studies of NDC80 and Ska complexes which should be addressed in the future. First, we demonstrated that a pool of Ska complex exists at kinetochores prior to nuclear envelope breakdown, and that Ska complexes progressively load onto kinetochores with increased microtubule occupancy. It is becoming increasingly clear that the Ska complex itself is highly modified by both CDK1 and Aurora kinases: While CDK1 phosphorylation of Ska promotes its interaction with NDC80 complexes, Aurora phosphorylation of Ska complexes antagonizes their kinetochore localization (Chan et al., 2012; Abad et al., 2016; Zhang et al., 2017; Huis in't Veld et al., 2019; Zhang et al., 2020). An important task for the future is to determine the dynamics of Ska complex phosphorylation and dephosphorylation to understand

how the Aurora modifications are preferentially reversed while the CDK1 modifications are left intact. Using phospho-specific antibodies to Aurora and CDK1 sites in the Ska complex at different stages of mitosis, or generating fragmented antibodies to these sites that can be used for live cell imaging (Morisaki et al., 2016), will be an important step towards this goal.

A second major question pertains to the contribution of Ska complexes to kinetochore-microtubule attachments. We and others have shown that the Ska complex enhances NDC80-microtubule binding *in vitro*, and that depletion of this complex from human cells weakens kinetochore-microtubule attachments (Gaitanos et al., 2009; Schmidt et al., 2012; Helgeson et al., 2018; Wimbish et al., 2020). Importantly, several additional microtubule-associated proteins (MAPs) at kinetochores serve similar functions, including the Astrin-SKAP complex and Cdt1 (Dunsch et al., 2011; Varma et al., 2012; Kern et al., 2017; Conti et al., 2019). Biochemical studies have shown that Ska complexes, Cdt1, and Astrin-SKAP complexes bind to microtubules synergistically with NDC80 complexes, and recent efforts have elucidated critical details about the domains of these MAPs that are required for this cooperativity (Varma et al., 2012; Abad et al., 2014; Kern et al., 2017; Helgeson et al., 2018; Huis in't Veld et al., 2019; Wimbish et al., 2020). While each of these MAPs individually coordinate with NDC80 complexes to enhance microtubule binding, the distinct contributions of these proteins to a mature kinetochore-microtubule attachment is less clear. Why does the human kinetochore-microtubule interface encompass multiple MAPs with seemingly overlapping roles? A thorough biochemical analysis of microtubule tip-tracking and load-

bearing by recombinant human Cdt1, Ska and Astrin-SKAP complexes would help address this question. Additionally, assessing the ability of these complexes to confer increased microtubule binding affinity and/or tip-tracking ability to NDC80 complexes – both in the context of each individual MAP and combinations of them – would likely uncover new details about distinctions and/or overlaps in these proteins' functions.

Along a similar line, it will be important to determine how Ska and Astrin-SKAP complexes contribute to kinetochore-microtubule attachments in human cells. Depletion of either protein complex results in pleiotropic mitotic defects including mitotic arrest, weakened kinetochore-microtubule attachments, uncongressed chromosomes, and multipolar spindles (Gaiatanos et al., 2009; Theis et al., 2009; Kern et al., 2017). The phenotypes associated with Astrin-SKAP or Ska complex depletion are further complicated by the fact that both proteins play a role in recruitment of protein phosphatase 1 (PP1) to kinetochores; therefore it is likely that Astrin-SKAP/Ska complex depletion impacts spindle assembly checkpoint silencing independently of their contributions to kinetochore-microtubule attachment stability (Sivakumar et al., 2016; Conti et al., 2019). Because of these varied defects, it has been difficult to home in on the specific contributions of these complexes to microtubule-attachment stability. Selective inactivation or degradation of kinetochore-localized Ska and Astrin-SKAP complexes (perhaps by utilizing an optogenetic degron; Renicke et al., 2013), while leaving spindle-localized complexes unperturbed, could be helpful in addressing this question.

### **4.3 Insight into Hec1 loop domain function and future directions**

Another interesting observation from our experiments in Chapter 2 was that mutation of the Hec1 loop domain plays a Ska complex-independent role in kinetochore-microtubule attachments. The 40 amino acid Hec1 loop was originally identified in a cross-linking mass spectrometry study as a brief interruption in the extended coiled-coil domains of the NDC80 complex, and its precise function has been elusive since its discovery (Maiolica et al., 2007). Critically, the loop domain is required for kinetochore-microtubule attachments, as deleting this region or reversing its sequence results in chromosome alignment and kinetochore-microtubule attachment defects nearly as severe as depleting Hec1 from cells altogether (Zhang et al., 2012; Varma et al., 2012; Wimbish et al., 2020). It has been hypothesized that the loop domain is a critical interaction region for multiple essential microtubule-stabilizing factors including the Ska complex and Cdt1 (Varma et al., 2012; Zhang et al., 2012; Zhang et al., 2017; Zhang et al., 2018). We found, however, that cells expressing Hec1 with both a mutant loop and phospho-blocked tail could not form kinetochore-microtubule attachments, whereas Ska complex-depleted cells expressing a phospho-blocked Hec1 tail could. These results suggest that the loop domain plays a Ska complex-independent role in attachments, though this role currently remains unclear. By systematic mutagenesis of short stretches in the loop domain, we found that regions with a high local charge density were critical for the loop function: mutations of highly charged sections phenocopied full loop mutation in a chromosome alignment assay, while mutating uncharged regions had no effect. It is not

clear why these high-charge regions are critical, although it is likely that altering their charge changes the hydrophilicity of the loop, thereby affecting its conformation in a way that precludes normal function.

The role of the loop domain in kinetochore-microtubule attachment formation is further obscured by the fact that recombinant NDC80 complexes bind microtubules with wild-type affinity *in vitro* (Zhang et al., 2012; Wimbish et al., 2020). Recently, studies using purified NDC80 complex from *S. cerevisiae* have shown that the loop imparts an important flexibility to the NDC80 complex, and that this domain may act as a “hinge” region that allows bending of the tetrameric complex (Scarborough et al., 2019). This is consistent with electron microscopy observations from the Nilsson lab (2012), who noted that recombinant human NDC80 complexes lacking the loop were less likely to “kink” than their wild-type counterparts (Zhang et al., 2012). Interestingly, a recent study used FRET sensors and microtubule poisons to demonstrate that the NDC80 complex adopts different conformations depending on the attachment state of the kinetochore: unattached kinetochores lead to a tight “jackknifed”, or kinked, conformation of NDC80 complexes, while attachments under tension lead to a more elongated conformation (Roscioli et al., 2020). Collectively, these studies implicate the loop as an effector of NDC80 complex conformation. An interesting hypothesis is that in the context of a kinetochore where NDC80 complexes are anchored in place, mutation of the loop forces this “jackknifing”, which precludes kinetochore-microtubule attachment formation. In such a scenario, soluble NDC80 complexes *in vitro* would not be sensitive to loop mutation, as they are not anchored to a scaffold. Analyzing the behavior of reconstituted

kinetochore particles containing loop-mutant NDC80 complexes (discussed in section 4.4) may provide insight into the discrepancies between the *in vitro* and in-cell effects of Hec1 loop mutation.

#### **4.4 Insight into Hec1 tail domain function and future directions**

Perhaps the most surprising observation from our experiments in Chapter 2 was that cells expressing  $\Delta 80$ -Hec1 formed cold-stable kinetochore microtubule attachments. This finding is especially important as it unifies the view of Hec1/Ndc80 tail function across species and emphasizes the importance of the CH domain as the key microtubule binding site within NDC80 complexes. Additionally, our finding that the tail plays a role in force generation at kinetochores is reminiscent of recent biochemical studies using human NDC80 complexes and recent findings in *S. cerevisiae* using FRET sensors (Suzuki et al., 2016; Huis in't Veld et al., 2019).

The phenotype we observe in cells expressing Hec1 tail deletion mutants is dramatic, with cells experiencing a metaphase arrest followed by fragmentation of spindles and loss of chromosome alignment. We hypothesize that these defects are a consequence of defective force generation at the kinetochore (Logarinho et al., 2014). However, it is possible that the Hec1 tail domain is important for silencing the spindle assembly checkpoint, and that prolonged metaphase arrest leads to the spindle pole fragmentation phenotype. Additionally, we cannot rule out that the multipolarity we observe is a consequence of defective interactions between Hec1 and Hice1, a centrosomal protein important for spindle structure (Wu et al., 2009). In the case of the latter hypothesis, it

would be interesting to selectively tether  $\Delta 80$ -Hec1 to Hice1 using an inducible anchoring system such as the FRB-FKBP system previously described (Robinson et al., 2010). Doing such an experiment in otherwise unperturbed cells (with endogenous Hec1 at kinetochores) might allow one to specifically analyze the effects of tail deletion on Hec1's function at spindle poles.

As noted in the previous section, an important goal for the future is to understand the discrepancies between biochemical and in-cell studies regarding NDC80 complex function. Notably, recombinant NDC80 complexes from human, *S. cerevisiae*, and *C. elegans* systems require the Hec1/Ndc80 tail domain for high affinity microtubule binding *in vitro*, as discussed in Chapter 1 (Wei et al., 2007; Ciferri et al., 2008; Cheerambathur et al., 2013). Despite this, cells from these organisms are competent to form kinetochore-microtubule attachments when expressing tail-less Hec1/Ndc80 mutants (Kemmler et al., 2009; Demirel et al., 2012; Lampert et al., 2013; Cheerambathur et al., 2013; Suzuki et al., 2016; Wimbish et al., 2020). Therefore, caution must be used when interpreting *in vitro* findings with NDC80 complexes in the context of kinetochores. One interesting possibility is that the Hec1/Ndc80 tail domain is a critical effector of the on-rate of NDC80 complexes for microtubules. For example, the tail domain may be important for soluble NDC80 molecules to “land” on microtubules and bring the CH domain in close enough proximity to “find” its binding site. In this scenario, the tail would be less important in cells, where microtubules are delivered directly to the kinetochore. Efforts to reconstitute entire kinetochores *in vitro* will be a significant advance for the field, as it will allow for analysis of mutation-specific defects in the context of kinetochore-microtubule binding. Exciting

progress towards this goal has been made for both yeast and human kinetochores, and already these studies are elucidating new details about both kinetochore assembly and microtubule binding characteristics (Pesenti et al., 2018; Hamilton et al., 2020).

#### **4.5 Insight into regulation of attachment strength by the Hec1 tail domain and future directions**

Our experiments in Chapter 3 demonstrate that the Hec1 tail has specific length requirements for regulating kinetochore-microtubule attachment strength in cells and NDC80-microtubule binding *in vitro*. This finding may contradict the direct binding model for regulation and begs the question of how a phosphorylated Hec1 tail domain inhibits NDC80-microtubule interactions. One interesting possibility is through the autoinhibition model mentioned in section 3.3, where a phosphorylated Hec1 tail domain may interfere with the CH domain-microtubule interaction. This idea was originally proposed by Ciferri and colleagues (2008) over a decade ago and substantiated by biochemical data examining the effects of NDC80 complexes on microtubule dynamics (Umbreit et al., 2012; discussed in section 3.3 of this thesis). Our in-cell and biochemical studies from Chapter 2 support the autoinhibition model for phospho-regulation of attachments; however, further experiments will be important to validate or refute this model. Specifically, it will be important to measure a direct interaction between recombinant Hec1 CH domains and phosphorylated/phospho-mimetic Hec1 tails *in vitro*, and to investigate whether wild type Hec1 tail domains are less efficient in facilitating this interaction. If a direct interaction can be detected between a phospho-mimetic Hec1 tail and CH domain, one could parse out which specific residues within the CH domain are

required for this interaction by systematically neutralizing positively charged residues (through Ala mutagenesis, for example) and determining whether the tail-CH domain interaction is reduced when specific residues within the CH domain are neutralized. Furthermore, the functional implications of a tail-CH domain interaction could be examined by testing its relevance in the context of microtubules. If phosphorylation of the Hec1 tail inhibits the CH domain from binding to microtubules, this could potentially be observed *in vitro*. For example, one could allow GFP-NDC80 complexes to bind to microtubules in a flow chamber, then subsequently add recombinant 9D-Hec1 tails and determine whether the tails competed the bound NDC80 complexes from the microtubules (by measuring GFP fluorescence intensity with and without the addition of 9D-Hec1 tails). Performing these experiments will be an important step in validating or refuting the autoinhibition model for kinetochore-microtubule attachment regulation.

#### **4.6 Insight into the effects of blocking Hec1 tail phosphorylation and future directions**

Blocking Hec1 tail phosphorylation has been widely shown to cause hyper-stable kinetochore-microtubule attachment formation, but the length requirements for this function of the tail were not known (DeLuca et al., 2006; Guimaraes et al., 2008; DeLuca et al., 2011). We found in Chapter 3 that blocking phosphorylation of a 25 amino acid tail elicits a 9A-Hec1-like phenotype, where high levels of attachments are formed in early mitosis and metaphase kinetochores are under excess tension. As discussed in section 3.3, these results point to maintenance of a phosphorylated Hec1 tail as a key modulator of attachment dynamics, consistent with previous studies

(DeLuca et al., 2018). Indeed, a recent study using FRET sensors in metaphase cells showed that the fraction of microtubule-bound NDC80 complexes nearly doubles for 9A-Hec1 expressing cells compared to WT-Hec1 expressing cells (Yoo et al., 2018). Taken together, the available data suggest that maintaining high levels of Ser 69 phosphorylation keeps NDC80-microtubule binding more labile, thereby promoting normal kinetochore-microtubule interactions. Investigating the effects of Ser 69 phosphorylation on microtubule binding, diffusion, and force-coupling by NDC80 complexes *in vitro* is an important step in understanding the dramatic phenotypic differences between WT- and 9A-Hec1 expression in cells.

An important question is how short of a tail can interact with the microtubule lattice and generate the forces necessary for proper chromosome segregation. Although a 25 amino acid tail rescued the tail deletion phenotype, it is likely that too short of a tail does not sufficiently interact with microtubules and therefore fails to rescue the tail deletion phenotype. We did not study tails shorter than 25 amino acids, but this will be an important experiment to answer this question. Furthermore, it will be important to show that the specific tail truncation variants used in Chapter 3 do not result in their respective phenotypes due to differences in tail sequence. It has been proposed that two key sub-domains exist in the tail that differentially regulate microtubule binding and NDC80 complex oligomerization (Alushin et al., 2012; see also Section 1.8b of this thesis). Although there is mounting evidence *in vitro* that this is not the case (Zaytsev et al., 2014; 2015), it will be important to verify that our tail truncation mutants are not perturbing regulation and force generation in a sequence-specific manner. Generating

mutants of the same tail length (25, 35, and 55 amino acids) using different portions of the tail should resolve this issue.

Finally, an outstanding question for future investigation is how extending tail length impacts force generation at the kinetochore-microtubule interface. We found that extending the tail by 12 amino acids did not preclude attachment regulation, but led to elevated inter-kinetochore distances in metaphase, suggesting higher microtubule occupancy. Here, a key experiment is to investigate whether the tail extension phenotype can be exacerbated with longer tails. To this end, analysis of inter-kinetochore distances in cells expressing Hec1 mutants with progressively longer tails will be important (for example, measurements in cells expressing a 120N- or 140N-Hec1 mutant). Finally, validating these findings biochemically is an important step in understanding how the tail influences force coupling. Measuring binding of bead-bound, Hec1 tail extension-containing NDC80 complexes in an optical trap may yield interesting information about whether longer Hec1 tails increase the binding force of NDC80 complexes for microtubules.

#### **4.7 Evolutionary perspective on Hec1/Ndc80 tail function**

Our results from this study have uncovered new details about how the small, disordered Hec1 tail domain makes significant contributions to the formation and regulation of kinetochore-microtubule attachments in human cells. It will be interesting in the future to investigate how conserved these functions are across eukaryotes. As discussed in Chapter 1, deletion of this domain impacts kinetochore-derived force generation in both

budding yeast and human cells (Suzuki et al., 2016; Wimbish et al., 2020). Despite this similarity, the mechanism of phospho-regulation of attachments appears to be divergent: while human and *C. elegans* cells regulate their attachments through Hec1 tail phosphorylation, budding yeast appear to primarily regulate attachments through phosphorylation of the ring-forming Dam1 complex (Guimaraes et al., 2008; Kemmler et al., 2009; Akiyoshi et al., 2009; Cheerambathur et al., 2013; Zaytsev et al., 2014; Cheerambathur et al., 2017). Although the reason for this difference is not entirely clear, an attractive explanation may lie in the architecture of the budding yeast kinetochore, which binds to only a single microtubule (as opposed to the 15-20 bound by a human kinetochore) and for which the fungi-specific Dam1 complex is the primary force-coupling machinery (Miranda et al., 2005; Tien et al., 2010; Lampert et al., 2010; Kim et al., 2017). In this case, phosphorylation of the Hec1/Ndc80 tail may be a less effective means of weakening attachments, as the NDC80-Dam1 complex interaction may act as a bridge between the budding yeast kinetochore and microtubule, and this interaction is regulated through the phosphorylation of Dam1 complex subunits (Kim et al., 2017). In metazoan cells lacking the Dam1 complex, an analogous NDC80-microtubule “bridge” may be absent, and phosphorylation of the Hec1 tail would be the most effective way to weaken attachments. It is not clear why the Hec1/Ndc80 tail in budding yeast contains Aurora/Ipl1 kinase sites, several of which are confirmed to be phosphorylated in cells (Cheeseman et al., 2002; Akiyoshi et al., 2009). As kinetochore proteins are reported to undergo rapid evolution (van Hooff et al., 2017), one possibility is that these sites are a remnant from an evolutionary ancestor, given that their phosphorylation does not impact mitotic progression to the same severity as Dam1 complex phosphorylation (Akiyoshi et

al., 2009; Kemmler et al., 2009; Kalantzaki et al., 2015; Jin et al., 2017). Comparing the effects of Hec1/Ndc80 tail phosphorylation on NDC80-microtubule binding affinity in the presence and absence of organism-specific MAPs (for example, Dam1 complex in budding yeast and Ska complex in human cells) *in vitro* may provide interesting insight into this question.

Further insight into Hec1 tail function may be gained by studying its contribution to non-mitotic processes. It has recently come to light that the KMN network plays a role in specifying neurite morphology in developing neurons (Norket et al., 2019). Specifically, Zhao et al. (2019) detected neuron-specific expression of KMN proteins in *Drosophila melanogaster*, and found that knockdown of Mis12, KNL1/Spc105, and Hec1/Ndc80 resulted in aberrant neurite outgrowth and defective synaptic morphology. This group also demonstrated that knockdown of Mis12 in rat hippocampal neurons caused alterations in dendrite morphology, demonstrating a conservation in function for KMN proteins in neuronal development (Zhao et al., 2019). Similarly, Cheerambathur et al. (2019) detected expression of KNL1 and Hec1/Ndc80 in post-mitotic neurons of the developing *C. elegans* embryo, and found similar morphological defects to Zhao and colleagues upon depletion of these proteins. Interestingly, the *C. elegans* study found that expressing Hec1/Ndc80 lacking the N-terminal tail or with a mutant CH domain (using a silence-rescue expression system) resulted in the same defects as depleting Hec1/Ndc80 altogether, implicating the microtubule-binding moieties of the NDC80 complex in its neuronal function (Cheerambathur et al., 2019). Both groups speculated that the role of KMN proteins during neuron development may be to facilitate synaptic

microtubule stabilization, as destabilization of microtubules during this process has been reported to cause similar dendritic defects to those that the authors observed (Borgen et al., 2017; Cheerambathur et al., 2019; Zhao et al., 2019). These studies raise many interesting questions regarding the expression and regulation of KMN proteins during neuronal development (Cheerambathur et al., 2019). They may also provide insight into the evolution of these proteins – namely, certain domain(s) of the NDC80 complex, for example, may be specialized more for its neuronal functions than its functions at the kinetochore, and vice-versa. Furthermore, investigation of neuronal NDC80 complex function may elucidate cell type-specific differences in post-translational modifications. For example, DeLuca et al. (2011) generated phospho-specific antibodies to 6 sites in the Hec1 tail, and found that two of them (Ser 8 and Ser 62) did not recognize human kinetochores – one could speculate that these sites may be phosphorylated in neurons, but not in mitotic cells. Given that Aurora kinase activity is implicated in neuronal function (Takitoh et al., 2012; Gwee et al., 2018), it will be interesting to determine whether NDC80-microtubule binding is phospho-regulated in a manner that impacts dendrite organization. Similarly, it will be interesting to assess whether phosphorylation of Ser 69 is maintained for neuronal Hec1 proteins. Given that this modification persists in high levels throughout mitosis (DeLuca et al., 2018), a key question has been why evolution has not selected for an acidic amino acid at this site. An attractive hypothesis would be that this site may not be phosphorylated in neurons, and that maintenance of Ser at this position allows for its cell type-specific phosphorylation. Cumulatively, the study of KMN protein regulation and function in

neurons is an exciting new avenue that may provide new details about both the mitotic and neuronal functions of these rapidly evolving proteins.

## REFERENCES

1. Abad MA, Medina B, Santamaria A, Zou J, Plasberg-Hill C, Madhumalar A, Jayachandran U, Redli PM, Rappsilber J, Nigg EA, Jeyaprakash AA. (2014). Structural basis for microtubule recognition by the human kinetochore Ska complex. *Nature Commun.* 2964.
2. Abad MA, Zou J, Medina-Pritchard B, Nigg EA, Rappsilber J, Santamaria A, Jeyaprakash AA. (2016). Ska3 Ensures timely mitotic progression by interacting directly with microtubules and Ska1 microtubule binding domain. *Sci Rep* 34042.
3. Akiyoshi B., Nelson C. R., Ranish J. A., Biggins S. (2009). Analysis of Ipl1-mediated phosphorylation of the Ndc80 kinetochore protein in *Saccharomyces cerevisiae*. *Genetics* 183 1591–1595. 10.1534/genetics.109.109041
4. Alushin G. M., Musinipally V., Matson D., Tooley J., Stukenberg P. T., Nogales E. (2012). Multimodal microtubule binding by the Ndc80 kinetochore complex. *Nat. Struct. Mol. Biol.* 19 1161–1167. 10.1038/nsmb.2411
5. Alushin G. M., Ramey V. H., Pasqualato S., Ball D. A., Grigorieff N., Musacchio A., et al. (2010). The Ndc80 kinetochore complex forms oligomeric arrays along microtubules. *Nature* 467 805–810. 10.1038/nature09423
6. Amin MA, McKenney RJ, Varma D. (2018). Antagonism between the dynein and Ndc80 complexes at kinetochores controls the stability of kinetochore-microtubule attachments during mitosis [published correction appears in *J Biol Chem.* 2018 Jul 6;293(27):10825]. *J Biol Chem.* 293(16):5755-5765. 10.1074/jbc.RA117.001699
7. Auckland P., Clarke N. I., Royle S. J., McAinsh A. D. (2017). Congressing kinetochores progressively load Ska complexes to prevent force-dependent detachment. *J. Cell Biol.* 216 1623–1639. 10.1083/jcb.201607096
8. Bakhoun S. F., Thompson S. L., Manning A. L., Compton D. A. (2009). Genome stability is ensured by temporal control of kinetochore-microtubule dynamics. *Nat. Cell Biol.* 11 27–35. 10.1038/ncb1809
9. Bakhoun S. F., and Compton D. A. (2012). Kinetochores and disease: keeping microtubule dynamics *in check!* *Curr. Opin. Cell. Biol.* 24:64-70
10. Bakhoun S. F., and Compton, D. A. (2012). Chromosomal instability and cancer: a complex relationship with therapeutic potential. *J. Clin. Invest.* 122:1138-1143.
11. Barr A. R., Gergely F. (2007). Aurora-A: the maker and breaker of spindle poles. *J. Cell Sci.* 120 2987–2996. 10.1242/jcs.013136
12. Biggins S., Severin F. F., Bhalla N., Sassoon I., Hyman A. A., Murraray A. W. (1999). The conserved protein kinase Ipl1 regulates microtubule binding to kinetochores in budding yeast. *Genes Dev* 13 532–544. 10.1101/gad.13.5.532
13. Borgen MA, Wang D, Grill B. (2017). RPM-1 regulates axon termination by affecting growth cone collapse and microtubule stability. *Development.* 144(24):4658-4672
14. Caldas G. V., DeLuca K. F., DeLuca J. G. (2013). KNL1 facilitates phosphorylation of outer kinetochore proteins by promoting Aurora B kinase activity. *J. Cell Biol.* 203 957–969. 10.1083/jcb.201306054

15. Campbell C. S., Desai A. (2013). Tension sensing by Aurora B kinase is independent of survivin-based centromere localization. *Nature* 497 118–121. 10.1038/nature12057
16. Carmena M., Ruchaud S., Earnshaw W. C. (2009). Making the Auroras glow: regulation of Aurora A and B kinase function by interacting proteins. *Curr. Opin. Cell Biol.* 21 796–805. 10.1016/j.ceb.2009.09.008
17. Carmena M., Wheelock M., Funabiki H., Earnshaw W. C. (2012). The chromosomal passenger complex (CPC): from easy rider to the godfather of mitosis. *Nat. Rev. Mol. Cell Biol.* 13 789–803. 10.1038/nrm3474
18. Chan YW, Jeyaprakash AA, Nigg EA, Santamaria A. (2012). Aurora B controls kinetochore-microtubule attachments by inhibiting Ska complex-KMN network interaction. *J Cell Biol* , 563–571.
19. Cheerambathur D. K., Gassmann R., Cook B., Oegema K., Desai A. (2013). Crosstalk between microtubule attachment complexes ensures accurate chromosome segregation. *Science* 342 1239–1242. 10.1126/science.1246232
20. Cheerambathur D. K., Prevo B., Hattersley N., Lewellyn L., Corbett K. D., Oegema K., et al. (2017). Dephosphorylation of the Ndc80 tail stabilizes kinetochore-microtubule attachments via the Ska complex. *Dev. Cell* 41 424.e4.–437.e4. 10.1016/j.devcel.2017.04.013
21. Cheerambathur DK, Prevo B, Chow TL, et al. (2019) The Kinetochore-Microtubule Coupling Machinery Is Repurposed in Sensory Nervous System Morphogenesis. *Dev Cell.* 48(6):864-872
22. Cheeseman I. M., Anderson S., Jwa M., Green E. M., Kang J. S., Yates J. R., III, et al. (2002). Phospho-regulation of kinetochore-microtubule attachments by the Aurora kinase Ipl1p. *Cell* 111 163–172. 10.1016/s0092-8674(02)00973-x
23. Cheeseman I. M., Brew C., Wolyniak M., Desai A., Anderson S., Muster N., et al. (2001). Implication of a novel multiprotein Dam1p complex in outer kinetochore function. *J. Cell Biol.* 155 1137–1145. 10.1083/jcb.200109063
24. Cheeseman I. M., Chappie J. S., Wilson-Kubalek E. M., Desai A. (2006). The conserved KMN network constitutes the core microtubule-binding site of the kinetochore. *Cell* 127 983–997. 10.1016/j.cell.2006.09.039
25. Chmátal L., Yang K., Schultz R. M., Lampson M. A. (2015). Spatial regulation of kinetochore microtubule attachments by destabilization at spindle poles in meiosis I. *Curr. Biol.* 25 1835–1841. 10.1016/j.cub.2015.05.013
26. Ciferri C., DeLuca J. G., Monzani S., Ferrari K. J., Ristic D., Wyman C., et al. (2005). Architecture of the human Ndc80-Hec1 complex, a critical constituent of the outer kinetochore. *J. Biol. Chem.* 280 29088–29095. 10.1074/jbc.M504070200
27. Ciferri C., Pasqualato S., Screpanti E., Varetto G., Santaguida S., Dos Reis G., et al. (2008). Implications for Kinetochore-Microtubule Attachment from the Structure of an Engineered Ndc80 Complex. *Cell* 133 427–439. 10.1016/j.cell.2008.03.020
28. Cimini D., Wan X., Hirel C. B., Salmon E. D. (2006). Aurora kinase promotes turnover of kinetochore microtubules to reduce chromosome segregation errors. *Curr. Biol.* 16 1711–1718. 10.1016/j.cub.2006.07.022

29. Conti D, Gul P, Asifa I, Martín-Durán JM, Pickersgill RW, Draviam VM. (2019). Kinetochores attached to microtubule-ends are stabilized by Astrin bound PP1 to ensure proper chromosome segregation. *eLife*, e49325.
30. Daum J. R., Wren J. D., Daniel J. J., Sivakumar S., Mcavoy J. N., Potapova T. A., et al. (2009). Ska3 is required for spindle checkpoint silencing and the maintenance of chromosome cohesion in mitosis. *Curr. Biol.* 19 1467–1472. 10.1016/j.cub.2009.07.017
31. Daum JR, Potapova TA, Sivakumar S, Daniel JJ, Flynn JN, Rankin S, Gorbsky GJ. (2011). Cohesion fatigue induces chromatid separation in cells delayed at metaphase. *Curr Biol* , 1018–1024.
32. De Wulf P., Montani F., Visintin R. (2009). Protein phosphatases take the mitotic stage. *Curr. Opin. Cell Biol.* 21 806–815. 10.1016/j.ceb.2009.08.003
33. DeLuca J. G. (2017). Aurora A kinase function at kinetochores. *Cold Spring Harb. Symp. Quan. Biol.* 82 91–99. 10.1101/sqb.2017.82.034991
34. DeLuca J. G., Gall W. E., Ciferri C., Cimini D., Musacchio A., Salmon E. D. (2006). Kinetochores microtubule dynamics and attachment stability are regulated by Hec1. *Cell* 127 969–982. 10.1016/j.cell.2006.09.047
35. DeLuca JG, Musacchio A. (2012). Structural organization of the kinetochore-microtubule interface. *Curr Opin Cell Biol* , 48–56.
36. DeLuca K. F., Lens S. M., DeLuca J. G. (2011). Temporal changes in Hec1 phosphorylation control kinetochore-microtubule attachment stability during mitosis. *J. Cell Sci.* 124 622–634. 10.1242/jcs.072629
37. DeLuca K. F., Meppelink A., Broad A. J., Mick J. E., Peersen O. B., Petkas S., et al. (2018). Aurora A kinase phosphorylates Hec1 to regulate metaphase kinetochore-microtubule dynamics. *J. Cell Biol.* 217 163–177. 10.1083/jcb.201707160
38. Demirel P. B., Keyes B. E., Chatterjee M., Remington C. E., Burke D. J. (2012). A redundant function for the N-Terminal Tail of Ndc80 in kinetochore-microtubule interaction in *Saccharomyces cerevisiae*. *Genetics* 192 753–756. 10.1534/genetics.112.143818
39. Ditchfield C., Johnson V. L., Tighe A., Ellston R., Haworth C., Johnson T., et al. (2003). Aurora B couples chromosome alignment with anaphase by targeting BubR1, Mad2, and Cenp-E to kinetochores. *J. Cell Biol.* 161 267–280. 10.1083/jcb.200208091
40. Dunsch A. K., Linnane E., Barr F. A., Gruneberg U. (2011). The astrin-kinastrin/SKAP complex localizes to microtubule plus ends and facilitates chromosome alignment. *J. Cell Biol.* 192 959–968. 10.1083/jcb.201008023
41. Ecklund KH, Morisaki T, Lammers LG, Marzo MG, Stasevich TJ, Markus SM. (2017). She1 affects dynein through direct interactions with the microtubule and the dynein microtubule-binding domain. *Nat Commun* , 2151.
42. Espeut J., Cheerambathur D. K., Krenning L., Oegema K., Desai A. (2012). Microtubule binding by KNL-1 contributes to spindle checkpoint silencing at the kinetochore. *J. Cell Biol.* 196 469–482. 10.1083/jcb.201111107
43. Etemad B., Kuijt T. E., Kops G. J. (2015). Kinetochores-microtubule attachment is sufficient to satisfy the human spindle assembly checkpoint. *Nat. Commun.* 6:8987. 10.1038/ncomms9987

44. Etemad B., Vertesy A., Kuijt T. E. F., Sacristan C., van Oudenaarden A., Kops G. J. P. L. (2019). Spindle checkpoint silencing at kinetochores with submaximal microtubule occupancy. *J. Cell Sci.* 132:jcs231589. 10.1242/jcs.231589
45. Fischböck-Halwachs J., Singh S., Potocnjak M., Hagemann G., Solis-Mezarino V., Woike S., et al. (2019). The COMA complex interacts with Cse4 and positions Sli15/Ipl1 at the budding yeast inner kinetochore. *eLife* 8:e42879. 10.7554/eLife.42879
46. Francisco L., Wang W., Chan C. S. (1994). Type 1 protein phosphatase acts in opposition to Ipl1 protein kinase in regulating yeast chromosome segregation. *Mol. Cell. Biol.* 7 4731–4740. 10.1128/mcb.14.7.4731
47. Funabiki H., Wynne D. J. (2013). Making an effective switch at the kinetochore by phosphorylation and dephosphorylation. *Chromosoma* 122 135–158. 10.1007/s00412-013-0401-5
48. Gaiatanos T. N., Santamaria A., Jeyaprakash A. A., Wang G., Conti E., Nigg E. A. (2009). Stable kinetochore-microtubule interactions depend on the Ska complex and its new component Ska3/C13Orf3. *EMBO J.* 28 1375–1377. 10.1038/emboj.2009.96
49. García-Rodríguez L. J., Kasciukovic T., Denninger V., Tanaka T. U. (2019). Aurora B-INCENP localization at centromeres/inner kinetochores is required for chromosome Bi-orientation in budding yeast. *Curr. Biol.* 29 1536–1544. 10.1016/j.cub.2019.03.051
50. Godek K. M., Kabeche L., Compton D. A. (2015). Regulation of kinetochore-microtubule attachments through homeostatic control during mitosis. *Nat. Rev. Mol. Cell Biol.* 16 57–64. 10.1038/nrm3916
51. Guimaraes G. J., DeLuca J. G. (2009). Connecting with Ska, a key complex at the kinetochore-microtubule interface. *EMBO J.* 28 1442–1452. 10.1038/emboj.2009.124
52. Guimaraes G. J., Dong Y., McEwen B. F., DeLuca J. G. (2008). Kinetochore-microtubule attachment relies on the disordered N-Terminal tail domain of Hec1. *Curr Biol* 18 1778–1784. 10.1016/j.cub.2008.08.012
53. Gwee SSL, Radford RAW, Chow S, Syal MD, Morsch M, Formella I, Lee A, Don EK, Badrock AP, Cole NJ, West AK, Cheung SNS, Chung RS. (2018). Aurora kinase B regulates axonal outgrowth and regeneration in the spinal motor neurons of developing zebrafish. *Cell Mol Life Sci.* 75(23):4269-4285.
54. Hamilton GE, Helgeson LA, Noland CL, Asbury CL, Dimitrova YN, and Davis TN. (2020). Reconstitution reveals two paths of force transmission through the kinetochore. *eLife.* 10.7554/eLife.56582
55. Hanisch A., Sillje H. H. W., Nigg E. A. (2006). Timely anaphase onset requires a novel spindle and kinetochore complex comprising Ska1 and Ska2. *EMBO J.* 25 5504–5515. 10.1038/sj.emboj.7601426
56. Hara M., Ariyoshi M., Okumura E. I., Hori T., Fukagawa T. (2018). Multiple phosphorylations control recruitment of the KMN network onto kinetochores. *Nat. Cell Biol.* 20 1378–1388. 10.1038/s41556-018-0230-0
57. Hauf S., Cole R. W., LaTerra S., Zimmer C., Schnapp G., Walter R., et al. (2003). The small molecule Hesperadin reveals a role for Aurora B in correcting

- kinetochore-microtubule attachment and in maintaining the spindle assembly checkpoint. *J. Cell Biol.* 161 281–294. 10.1083/jcb.200208092
58. Helgeson L. A., Zelter A., Riffle M., Maccoss M. J., Asbury C. L., Davis T. N. (2018). Human Ska complex and Ndc80 complex interact to form a load-bearing assembly that strengthens kinetochore-microtubule attachments. *PNAS* 115 2740–2745. 10.1073/pnas.1718553115
59. Hengeveld R. C. C., Vromans M. J. M., Vleugel M., Hadders M. A., Lens S. M. A. (2017). Inner centromere localization of the CPC maintains centromere cohesion and allows mitotic checkpoint silencing. *Nat. Commun.* 8 15542. 10.1038/ncomms15542
60. Hindriksen S., Lens S. M. A., Hadders M. A. (2017). The Ins and outs of Aurora B inner centromere localization. *Fron.t Cell Dev. Biol.* 5:112. 10.3389/fcell.2017.00112
61. Huis in't Veld P. J., Jeganathan S., Petrovic A., Singh P., John J., Krenn V., et al. (2016). Molecular basis of outer kinetochore assembly on CENP-T. *eLife* 5:e21007. 10.7554/eLife.21007
62. Huis in't Veld P. J., Volkov V. A., Stender I., Musacchio A., Dogterom M. (2019). Molecular determinants of the Ska-Ndc80 interaction and their influence on microtubule tracking and force-coupling. *eLIFE* 8 e49539. 10.7554/eLife.49539
63. Janczyk P., Skorupka K. A., Tooley J. G., Matson D. R., Kestner C. A., West T., et al. (2017). Mechanism of Ska recruitment by Ndc80 complexes to kinetochores. *Dev. Cell* 41 438.e4–449.e4. 10.1016/j.devcel.2017.04.020
64. Janke C., Ortiz J., Tanaka T. U., Lechner K., Schiebel E. (2002). Four new subunits of the Dam1-Duo1 complex reveal novel functions in sister kinetochore biorientation. *EMBO J.* 21 181–193. 10.1093/emboj/21.1.181
65. Jeyaprakash A. A., Santamaria A., Jayachandran U., Chan Y. W., Benda C., Nigg E. A., et al. (2012). Structural and functional organization of the Ska complex, a key component of the kinetochore-microtubule interface. *Mol. Cell* 46 274–286. 10.1016/j.molcel.2012.03.005
66. Jin F., Bokros M., Wang Y. (2017). The phosphorylation of a kinetochore protein Dam1 by Aurora B/Ipl1 kinase promotes chromosome bipolar attachment in yeast. *Sci. Rep.* 7:11880. 10.1038/s41598-017-12329-z
67. Jones M. H., He X., Giddings T. H., Winey M. (2001). Yeast Dam1p has a role at the kinetochore in assembly of the mitotic spindle. *PNAS* 98 13675–13680. 10.1073/pnas.241417098
68. Kalantzaki M., Kitamura E., Zhang T., Mino A., Novak B., Tanaka T. U. (2015). Kinetochore-microtubule error correction is driven by differentially regulated interaction modes. *Nat. Cell Biol.* 17 421–433. 10.1038/ncb3128
69. Kallio M. J., McClelland M. L., Stukenberg P. T., Gorbsky G. J. (2002). Inhibition of Aurora B kinase blocks chromosome segregation, overrides the spindle checkpoint, and perturbs microtubule dynamics in mitosis. *Curr. Biol.* 12 900–905. 10.1016/s0960-9822(02)00887-4
70. Kemmler S., Stach M., Knapp M., Ortiz J., Pfannstiel J., Ruppert T., et al. (2009). Mimicking Ndc80 phosphorylation triggers spindle assembly checkpoint signaling. *EMBO J.* 28 1099–1110. 10.1038/emboj.2009.62

71. Kettenbach A. N., Schweppe D. K., Faherty B. K., Pechenick D., Pletnev A. A., Gerber S. (2011). Quantitative phosphoproteomics identifies substrates and functional modules of Aurora and polo-like kinase activities in mitotic cells. *Sci. Signal.* 179 rs5. 10.1126/scisignal.2001497
72. Kim H., Stumpff J. (2018). Kif18A promotes Hec1 dephosphorylation to coordinate chromosome alignment with kinetochore microtubule attachment. *Biorxiv* [Preprint].
73. Kim J. O., Zelter A., Umbreit N. T., Bollozos A., Riffle M., Johnson R., et al. (2017). The Ndc80 complex bridges two Dam1 complex rings. *eLife* 6:e21069. 10.7554/eLife.21069
74. Kim Y., Holland A. J., Lan W., Cleveland D. W. (2010). Aurora kinases and protein phosphatase 1 mediate chromosome congression through regulation of CENP-E. *Cell* 142 444–455. 10.1016/j.cell.2010.06.039
75. Koch A., Krug K., Pengelley S., Macek B., Hauf S. (2011). Mitotic substrates of the kinase Aurora with roles in chromatin regulation identified through quantitative phosphoproteomics of fission yeast. *Sci. Signal.* 4:rs6. 10.1126/scisignal.2001588
76. Krenn V., Musacchio A. (2015). The Aurora B kinase in chromosome Bi-Orientation and spindle checkpoint signaling. *Front. Oncol.* 5:225. 10.3389/fonc.2015.00225
77. Kruse T., Zhang G., Larsen M. S. Y., Llschetti T., Streicher W., Nielsen T. K., et al. (2013). Direct binding between BubR1 and B56-PP2A phosphatase complexes regulate mitotic progression. *J. Cell Sci.* 126 1086–1092. 10.1242/jcs.122481
78. Kuhn J., Dumont S. (2019). Mammalian kinetochores count attached microtubules in a sensitive and switch-like manner. *J. Cell Biol.* 218 3583–3596. 10.1083/jcb.201902105
79. Lampert F., Hornung P., Westermann S. (2010). The Dam1 complex confers microtubule plus end-tracking activity to the Ndc80 kinetochore complex. *J. Cell Biol.* 189 641–649. 10.1083/jcb.200912021
80. Lampert F., Mieck C., Alushin G. M., Nogales E., Westermann S. (2013). Molecular requirements for the formation of a kinetochore-microtubule interface by Dam1 and Ndc80 complexes. *J. Cell Biol.* 200 21–30. 10.1083/jcb.201210091
81. Lampson M. A., Cheeseman I. M. (2011). Sensing centromere tension: Aurora B and the regulation of kinetochore function. *Trends Cell Biol.* 21 133–140. 10.1016/j.tcb.2010.10.007
82. Lampson M. A., Renduchitala K., Khodjakov A., Kapoor T. M. (2004). Correcting improper chromosome-spindle attachments during cell division. *Nat. Cell Biol.* 6 232–237. 10.1038/ncb1102
83. Liu D., Vader G., Vromans M. J., Lampson M. A., Lens S. M. (2009). Sensing chromosome bi-orientation by spatial separation of Aurora B kinase from kinetochore substrates. *Science* 323 1350–1353. 10.1126/science.1167000
84. Liu D., Vleugel M., Backer C. B., Hori T., Fukagawa T., Cheeseman I. M., et al. (2010). Regulated targeting of protein phosphatase 1 to the outer kinetochore by

- KNL1 opposes Aurora B kinase. *J. Cell Biol.* 188 809–820.  
10.1083/jcb.201001006
85. London N., Ceto S., Ranish J. A., Biggins S. (2012). Phosphoregulation of Spc105 by Mps1 and PP1 regulates Bub1 localization to kinetochores. *Curr. Biol.* 22 900–906. 10.1016/j.cub.2012.03.052
  86. Long A. F., Udy D. B., Dumont S. (2017). Hec1 tail phosphorylation differentially regulates mammalian kinetochore coupling to polymerizing and depolymerizing microtubules. *Curr. Biol.* 27 1692–1699. 10.1016/j.cub.2017.04.058
  87. Löwe J., Li H., Downing K. H., Nogales E. (2001). Refined structure of alpha beta-tubulin at 3.5 Å resolution. *J. Mol. Biol.* 313 1045–1057.  
10.1006/jmbi.2001.5077
  88. Maia A. F., Feijão T., Vromans M. J., Sunkel C. E., Lens S. M. (2010). Aurora B kinase cooperates with CENP-E to promote timely anaphase onset. *Chromosoma* 119 405–413. 10.1007/s00412-010-0265-x
  89. Maiato H, Logarinho E. (2014). Mitotic spindle multipolarity without centrosome amplification. *Nat Cell Biol* , 386–394.
  90. Maiolica A., Cittaro D., Borsotti D., Sennels L., Ciferri C., Tarricone C., et al. (2007). Structural analysis of multiprotein complexes by cross-linking, mass spectrometry, and database searching. *Mol. Cell Proteomics* 6. 12 2200–2211.  
10.1074/mcp.M700274-MCP200
  91. Malvezzi F., Litos G., Schleiffer A., Heuck A., Mechtler K., Clausen T., et al. (2013). A structural basis for kinetochore recruitment of the Ndc80 complex via two distinct centromere receptors. *EMBO J.* 32 409–423.  
10.1038/emboj.2012.356
  92. Manic G., Corradi F., Sistigu A., Siteni S., Vitale I. (2017). Molecular regulation of the spindle assembly checkpoint by kinases and phosphatases. *Int. Rev. Cell Mol. Biol.* 328 105–161. 10.1016/bs.ircmb.2016.08.004
  93. Manning AL, Compton DA. (2007). Mechanisms of spindle-pole organization are influenced by kinetochore activity in mammalian cells. *Curr Biol* , 260–255.
  94. Manning A. L., Bakhoun S. F., Maffini S., Correia-Melo C., Maiato H., Compton D. A. (2010). CLASP1, Astrin, and Kif2b form a molecular switch that regulates kinetochore-microtubule dynamics to promote mitotic progression and fidelity. *EMBO J.* 29 3531–3543. 10.1038/emboj.2010.230
  95. Mattiuzzo M, Vargiu G, Totta P, Fiore M, Ciferri C, Musacchio A, Degrossi F. (2011). Abnormal kinetochore-generated pulling forces from expressing a N-terminally modified Hec1. *PLoS One* , e16307.
  96. McIntosh J. R., Grishchuk E. L., Morphew M. K., Efremov A. K., Zhudenkov K., Volkov V. A., et al. (2008). Fibrils connect microtubule tips with kinetochores: a mechanism to couple tubulin dynamics to chromosome motion. *Cell* 135 322–333. 10.1016/j.cell.2008.08.038
  97. Meadows J. C., Shepperd L. A., Vanoosthuyse V., Lancaster T. C., Sochaj A. M., Buttrick G. J., et al. (2011). Spindle checkpoint silencing requires association of PP1 to both Spc7 and kinesin-8 motors. *Dev. Cell* 20 739–750.  
10.1016/j.devcel.2011.05.008

98. Meraldi P., Honda R., Nigg E. A. (2004). Aurora kinases link chromosome segregation and cell division to cancer susceptibility. *Curr. Opin. Genet. Dev.* 14 29–36. 10.1016/j.gde.2003.11.006
99. Miller S. A., Johnson M. L., Stukenberg P. T. (2008). Kinetochore attachments require an interaction between unstructured tails on microtubules and Ndc80Hec1. *Curr. Biol.* 18 1785–1791. 10.1016/j.cub.2008.11.007
100. Miranda J. J., De Wulf P., Sorger P. K., Harrison S. C. (2005). The yeast DASH complex forms closed rings on microtubules. *Nat. Struct. Mol. Biol.* 12 138–143. 10.1038/nsmb896
101. Morisaki T., Lyon K, DeLuca KF, DeLuca JG, English BP, Zhang Z, Lavis LD, Grimm JB, Viswanathan S, Looger LL, Lionnet T, and Stasevich TJ. (2016). Real-time quantification of single RNA translation dynamics in living cells. *Science* 352: 1425-1429.
102. Murata-Hori M., Wang Y. L. (2002). The kinase activity of Aurora B is required for kinetochore-microtubule interactions during mitosis. *Curr. Biol.* 12 894–899. 10.1016/s0960-9822(02)00848-5
103. Nijenhuis W., Vallardi G., Teixeira A., Kops G. J., Saurin A. T. (2014). Negative feedback at kinetochores underlies a responsive spindle checkpoint signal. *Nat. Cell Biol.* 16 1257–1264. 10.1038/ncb3065
104. Nishino T., Rago F., Hori T., Tomii K., Cheeseman I. M., Fukagawa T. (2013). CENP-T provides a structural platform for outer kinetochore assembly. *EMBO J.* 32 424–436. 10.1038/emboj.2012.348
105. Nogales E., Whittaker M., Milligan R. A., Downing K. H. (1999). High-resolution model of the microtubule. *Cell* 96 79–88. 10.1016/s0092-8674(00)80961-7
106. Nogales E., Wolf S. G., Downing K. H. (1998). Structure of the alpha beta tubulin dimer by electron crystallography. *Nature* 391 199–203. 10.1038/34465
107. Norkett R, Lu W, Gelfand VI. (2019). Repurposing Kinetochore Microtubule Attachment Machinery in Neurodevelopment. *Dev Cell.* 48(6):746-748.
108. Nousiainen M., Sillje H., Sauer G., Nigg E. A., Korner R. (2006). Phosphoproteome analysis of the human mitotic spindle. *PNAS* 103 5391–5396. 10.1073/pnas.0507066103
109. Ohashi S., Sakashita G., Ban R., Nagasawa M., Matsuzaki H., Murata Y., et al. (2006). Phospho-regulation of human protein kinase Aurora-A: analysis using anti-phospho-Thr288 monoclonal antibodies. *Oncogene* 25 7691–7702. 10.1038/sj.onc.1209754
110. Pesenti ME, Prumbaum D, Auckland P, Smith CM, Faesen AC, Petrovic A, Erent M, Maffini S, Pentakota S, Weir JR, Lin YC, Raunser S, McAinsh AD, and Musacchio A. (2018) Reconstitution of a 26-Subunit Human Kinetochore Reveals Cooperative Microtubule Binding by CENP-OPQR and NDC80. *Molecular Cell* 71: 923-939.e10
111. Petrovic A., Pasqualato S., Dube P., Krenn V., Santaguida S., Cittaro D., et al. (2010). The MIS12 complex is a protein interaction hub for outer kinetochore assembly. *J. Cell Biol.* 190 835–852. 10.1083/jcb.201002070
112. Pinsky B. A., Nelson C. R., Biggins S. (2009). Protein phosphatase 1 regulates exit from the spindle checkpoint in budding yeast. *Curr. Biol.* 19 1182–1187. 10.1016/j.cub.2009.06.043

113. Ponstingl H., Little M., Krauhs E., Kempf T. (1979). Carboxy-terminal amino acid sequence of alpha-tubulin from porcine brain. *Nature* 282 423–425. 10.1038/282423a0
114. Posch M., Khoukoli G. A., Swift S., King E. M., DeLuca J. G., Swedlow J. R. (2010). Sds22 regulates Aurora B activity and microtubule-kinetochore interactions at mitosis. *J. Cell Biol.* 191 61–74. 10.1083/jcb.200912046
115. Powers A. F., Franck A. D., Gestaut D. R., Cooper J., Graczyk B., Wei R. R., et al. (2009). The Ndc80 kinetochore complex forms load-bearing attachments to dynamic microtubule tips via biased diffusion. *Cell* 136 865–875. 10.1016/j.cell.2008.12.045
116. Raaijmakers J. A., Tanenbaum M. E., Maia A. F., Medema R. H. (2009). RAMA1 is a novel kinetochore protein involved in kinetochore-microtubule attachment. *J. Cell Sci.* 122 2436–2445. 10.1242/jcs.051912
117. Renicke C, Schuster D, Usherenko S, Essen LO, and Taxis S. (2013) A LOV2 Domain-Based Optogenetic Tool to Control Protein Degradation and Cellular Function. *Chemistry and Biology.* 20:4 619-626
118. Robinson MS, Sahlender DA, and Foster SD. (2010). Rapid Inactivation of Proteins by Rapamycin-Induced Rerouting to Mitochondria. *Dev. Cell* 18(2-3): 324-331.
119. Roll-Mecak A. (2015). Intrinsically disordered tubulin tails: complex tuners of microtubule functions? *Semin. Cell Dev. Biol.* 37 11–19. 10.1016/j.semcdb.2014.09.026
120. Roscioli E, Germanova TE, Smith CA, Embacher PA, Erent M, Thompson AI, Burroughs NJ, McAinsh AD. (2019). Ensemble-level organization of human kinetochores and evidence for distinct tension and attachment sensors. *BioRxiv.*
121. Rosenberg J. S., Cross F. R., Funabiki H. (2011). KNL1/Spc105 recruits PP1 to silence the spindle assembly checkpoint. *Curr. Biol.* 21 942–947. 10.1016/j.cub.2011.04.011
122. Sackett D. L. (1995). Structure and function in the tubulin dimer and the role of the acidic carboxyl terminus. *Subcell. Biochem.* 24 255–302. 10.1007/978-1-4899-1727-0\_9
123. Salmon E. D., Cimini D., Cameron L. A., DeLuca J. G. (2005). Merotelic kinetochores in mammalian tissue cells. *Philos. T. R. Soc. Lond.* 360 553–568. 10.1098/rstb.2004.1610
124. Santaguida S., and Amon A. (2015). Short- and long-term effects of chromosome mis-segregation and aneuploidy. *Nat. Rev. Mol. Cell Biol.* 16: 473-485.
125. Saurin A. T. (2018). Kinase and phosphatase cross-talk at the kinetochore. *Front. Cell Dev. Biol.* 6:62. 10.3389/fcell.2018.00062
126. Schmidt J. C., Arthanari H., Boeszoermenyi A., Natalia M., Wilson-Kubalek E. M., Monnier N., et al. (2013). The kinetochore-bound Ska1 complex tracks depolymerizing microtubules and binds to curved protofilaments. *Dev. Cell* 23 968–980. 10.1016/j.devcel.2012.09.012
127. Schmidt J. C., Kiyomitsu T., Hori T., Backer C. B., Fukagawa T., Cheeseman I. M. (2010). Aurora B kinase controls the targeting of the Astrin-SKAP complex to bioriented kinetochores. *J. Cell Biol.* 191 269–280. 10.1083/jcb.201006129

128. Shang C., Hazbun T. R., Cheeseman I. M., Aranda J., Fields S., Drubin D. G., et al. (2003). Kinetochore protein interactions and their regulation by the Aurora kinase Ipl1p. *Mol. Biol. Cell* 14 3342–3355. 10.1091/mbc.e02-11-0765
129. Shrestha R. L., Conti D., Tamura N., Braun D., Ramalingam R. A., Cieslinski K., et al. (2017). Aurora-B kinase pathway controls the lateral to end-on conversion of kinetochore-microtubule attachments in human cells. *Nat. Commun.* 8:150. 10.1038/s41467-017-00209-z
130. Sivakumar S., Janczyk P. L., Qu Q., Brautigam C. A., Stukenberg P. T., Yu H., et al. (2016). The human SKA complex drives the metaphase-anaphase cell cycle transition by recruiting protein phosphatase 1 to kinetochores. *eLife* 5:e12902. 10.7554/eLife.12902
131. Sjöblom B., Ylänne J., Djinović-Carugo K. (2008). Novel structural insights into F-actin-binding and novel functions of calponin homology domains. *Curr. Opin. Struc. Biol.* 18 702–708. 10.1016/j.sbi.2008.10.003
132. Slep K. C., Rogers S. L., Elliott S. L., Ohkura H., Kolodziej P. A., Vale R. D. (2005). Structural determinants for EB1-mediated recruitment of APC and spectraplakins to the microtubule plus end. *J. Cell Biol.* 168 587–598. 10.1083/jcb.200410114
133. Smith R. J., Cordeiro M. H., Davey N. E., Vallardi G., Ciliberto A., Gross F., et al. (2019). PP1 and PP2A Use opposite phospho-dependencies to control distinct processes at the kinetochore. *Cell Rep.* 28 2206–2219. 10.1016/j.celrep.2019.07.067
134. Stevens D, Gassman R, Oegema K, Desai A. (2011). Uncoordinated loss of chromatid cohesion is a common outcome of extended metaphase arrest. *PLoS One* , e22969.
135. Suijkerbuijk S. J., Vleugel M., Teixeira A., Kops G. J. (2012). Integration of kinase and phosphatase activities by BUBR1 ensures formation of stable kinetochore-microtubule attachments. *Developmental Cell* 23 745–755. 10.1016/j.devcel.2012.09.005
136. Sundin L. J. R., Guimaraes G. J., DeLuca J. G. (2011). The NDC80 complex proteins Nuf2 and Hec1 make distinct contributions to kinetochore-microtubule attachment in mitosis. *Mol. Biol. Cell* 22 759–768. 10.1091/mbc.E10-08-0671
137. Suzuki A., Badger B. L., Haase J., Ohashi T., Erickson H. P., Salmon E. D., et al. (2016). How the kinetochore couples microtubule force and centromere stretch to move chromosomes. *Nat. Cell Biol.* 18 382–392. 10.1038/ncb3323
138. Suzuki A, Long SK, Salmon ED. (2018). An optimized method for 3D fluorescence co-localization applied to human kinetochore protein architecture. *eLife* , e32418.
139. Takitoh T, Kumamoto K, Wang C, Sato M, Toba S, Wynshaw-Boris A, and Hirotsune S. (2012). Activation of Aurora-A is essential for neuronal migration via modulation of microtubule organization. *J. Neurosci.* 32: 11050-66
140. Tauchman EC, Boehm FJ, DeLuca JG. (2015). Stable kinetochore-microtubule attachment is sufficient to silence the spindle assembly checkpoint in human cells. *Nat Commun* , 10036.
141. Tanaka T. U., Rachidi N., Janke C., Pereira G., Galova M., Schiebel E., et al. (2002). Evidence that the Ipl1-Sli15 (Aurora kinase-INCENP) complex promotes

- chromosome bi-orientation by altering kinetochore-spindle pole connections. *Cell* 108 317–329. 10.1016/s0092-8674(02)00633-5
142. Theis M., Slabicki M., Junqueira M., Paszkowski-Rogacz M., Sontheimer J., Kittler R., et al. (2009). Comparative profiling identifies C13orf3 as a component of the Ska complex required for mammalian cell division. *EMBO J.* 28 1453–1465. 10.1038/emboj.2009.114
  143. Tien J. F., Umbreit N. T., Gestaut D. R., Franck A. D., Cooper J., Wordeman L., et al. (2010). Cooperation of the Dam1 and Ndc80 kinetochore complexes enhances microtubule coupling and is regulated by Aurora B. *J. Cell Biol.* 189 713–723. 10.1083/jcb.200910142
  144. Tooley J. G., Miller S. A., Stukenberg P. T. (2011). The Ndc80 complex uses a tripartite attachment point to couple microtubule depolymerization to chromosome movement. *Mol. Biol. Cell* 22 1217–1226. 10.1091/mbc.E10-07-0626
  145. Trinkle-Mulcahy L., Andrews P. D., Wickramasinghe S., Sleeman J., Prescott A., Lam Y. W., et al. (2003). Time-lapse imaging reveals dynamic relocalization of PP1gamma throughout the mammalian cell cycle. *Mol. Biol. Cell* 14 107–117. 10.1091/mbc.e02-07-0376
  146. Umbreit N. T., Gestaut D. R., Tien J. F., Vollmar B. S., Gonen T., Asbury C. L. (2012). The Ndc80 kinetochore complex directly modulates microtubule dynamics. *PNAS* 109 16113–16118. 10.1073/pnas.1209615109
  147. Vader G., Lens S. M. (2008). The Aurora kinase family in cell division and cancer. *Biochim. Biophys. Acta* 1786 60–72. 10.1016/j.bbcan.2008.07.003
  148. Valverde R., Ingram J., Harrison S. C. (2016). Conserved tetramer junction in the kinetochore ndc80 complex. *Cell Rep.* 17 1915–1922. 10.1016/j.celrep.2016.10.065
  149. Van Hooff J JE, Tromer E, van Wijk LM, Snel B, and Kops G JPL. (2017). Evolutionary dynamics of the kinetochore network in eukaryotes as revealed by comparative genomics. *EMBO Rep.* 18: 1559-1571.
  150. Vanoosthuysen V., Hardwick K. G. (2009). A novel protein phosphatase 1-dependent spindle checkpoint silencing mechanism. *Curr. Biol.* 19 1176–1181. 10.1016/j.cub.2009.05.060
  151. Varma D., Chandrasekaran S., Sundin L. J. R., Reidy K. T., Wan X., Chasse D. A. D., et al. (2012). Recruitment of the human Cdt1 replication licensing protein by the loop domain of Hec1 is required for stable kinetochore-microtubule attachment. *Nat. Cell Biol.* 14 593–603. 10.1038/ncb2489
  152. Volkov V. A., Huis in't Veld P. J., Dogterom M., Musacchio A. (2018). Multivalency of NDC80 in the outer kinetochore is essential to track shortening microtubules and generate forces. *eLife* 7:e36764. 10.7554/eLife.36764
  153. Wan X, O'Quinn RP, Pierce HL, Joglekar AP, Gall WE, DeLuca JG, Carroll CW, Liu ST, Yen TJ, McEwen BF, et al. (2009). Protein architecture of the human kinetochore microtubule attachment site. *Cell* , 672–684.
  154. Wang H., Long S., Ciferri C., Westermann S., Drubin D., Barnes G., et al. (2008). Architecture and flexibility of the yeast Ndc80 kinetochore complex. *J. Mol. Biol.* 383 894–903. 10.1016/j.jmb.2008.08.077

155. Wei R. R., Al-Bassam J., Harrison S. C. (2007). The Ndc80/HEC1 complex is a contact point for kinetochore-microtubule attachment. *Nat. Struct. Mol. Biol.* 14 54–59. 10.1038/nsmb1186
156. Wei R. R., Schnell J. R., Larsen N. A., Sorger P. K., Chou J. J., Harrison S. C. (2006). Structure of a central component of the yeast kinetochore: the Spc24p/Spc25p globular domain. *Structure* 14 1003–1009. 10.1016/j.str.2006.04.007
157. Wei R. R., Sorger P. K., Harrison S. C. (2005). Molecular organization of the Ndc80 complex, an essential kinetochore component. *PNAS* 102 5363–5367. 10.1073/pnas.0501168102
158. Welburn JPI, Grishchuk EL, Backer CB, Wilson-Kubalek EM, Yates JR, III, Cheeseman IM. (2009). The human kinetochore Ska1 complex facilitates microtubule depolymerization-coupled motility. *Dev Cell* , 374–385.
159. Welburn J. P., Vleugel M., Liu D., Yates J. R., III, Lampson M. A., Fukagawa T., et al. (2010). Aurora B phosphorylates spatially distinct targets to differentially regulate the kinetochore-microtubule interface. *Mol. Cell* 38 383–392. 10.1016/j.molcel.2010.02.034
160. Westermann S., Avila-Sakar A., Wang H. W., Niederstrasser H., Wong J., Drubin D. G., et al. (2005). Formation of a dynamic kinetochore-microtubule interface through assembly of the Dam1 ring complex. *Mol. Cell* 17 277–290. 10.1016/j.molcel.2004.12.019
161. Wilson-Kubalek E. M., Cheeseman I. M., Yoshioka C., Desai A., Milligan R. A. (2008). Orientation and structure of the Ndc80 complex on the microtubule lattice. *J. Cell Biol.* 182 1055–1061. 10.1083/jcb.200804170
162. Wimbish R. T., DeLuca K. F., Himes J., Mick J. E., Sanchez I. J., Jeyaprakash A. A., et al. (2019). Coordination of the NDC80 and Ska complexes at the kinetochore-microtubule interface in human cells. *BioRxiv* [Preprint].
163. Wimbish RT, DeLuca JG. (2020). Hec1/Ndc80 tail domain function at the kinetochore-microtubule interface. *Front Cell Dev Biol* , 43.
164. Wu G, Wei R, Cheng E, Ngo B, Lee WH. (2009). Hec1 contributes to mitotic centrosomal microtubule growth for proper spindle assembly through interaction with Hice1. *Mol Biol Cell* , 4686–4695.
165. Xu P., Raetz E. A., Kitagawa M., Virshup D. M., Lee S. H. (2013). BUBR1 recruits PP2A via the B56 family of targeting subunits to promote chromosome congression. *Biol Open.* 2 479–486. 10.1242/bio.20134051
166. Ye A. A., Deretic J., Hoel C. M., Hinman A. W., Cimini D., Welburn J. P., et al. (2015). Aurora a kinase contributes to a pole-based error correction pathway. *Curr. Biol.* 25 1842–1851. 10.1016/j.cub.2015.06.021
167. Yoo T. Y., Choi J., Conway W., Yu C., Pappu R. V., Needleman D. J. (2018). Measuring NDC80 binding reveals the molecular basis of tension-dependent kinetochore-microtubule attachments. *Elife* 7 1–34. 10.7554/eLife.36392
168. Yue Z., Carvalho A., Xu Z., Yuan X., Cardinale S., Ribeiro S., et al. (2008). Deconstructing Survivin: comprehensive genetic analysis of Survivin function by conditional knockout in a vertebrate cell line. *J. Cell Biol.* 183 279–296. 10.1083/jcb.200806118

169. Zaytsev A. B., Mick J. E., Maslennikov E., Nikashin B., DeLuca J. G., Grishchuk E. L. (2015). Multisite phosphorylation of the NDC80 complex gradually tunes its microtubule-binding affinity. *Mol. Biol. Cell* 26 1829–1844. 10.1091/mbc.E14-11-1539
170. Zaytsev A. V., Sundin L. J. R., DeLuca K. F., Grishchuk E. L., DeLuca J. G. (2014). Accurate phosphoregulation of kinetochore-microtubule affinity requires unconstrained molecular interactions. *J. Cell Biol.* 206 45–59. 10.1083/jcb.201312107
171. Zhai Y., Kronebusch P. J., Borisy G. G. (1995). Kinetochore microtubule dynamics and the metaphase-anaphase transition. *J. Cell Biol.* 131 721–734. 10.1083/jcb.131.3.721
172. Zhang G, Kelstrup CD, Hu X, Hansen MJK, Singleton MR, Olsen JV, Nilsson J. (2012). The Ndc80 internal loop is required for recruitment of the Ska complex to establish end-on microtubule attachment to kinetochores. *J. Cell Sci.* 3243–3253.
173. Zhang Q., Sivakumar S., Chen Y., Gao H., Yang L., Yuan Z., et al. (2017). Ska3 phosphorylated by Cdk1 Binds Ndc80 and recruits Ska to kinetochores to promote mitotic progression. *Curr. Biol.* 27 1477–1484. 10.1016/j.cub.2017.03.060
174. Zhang Q, Chen Y, Yang L, Liu H. (2018). Multitasking Ska in chromosome segregation: its distinct pools might specify various functions. *BioEssays* 1700176.
175. Zhao G., Cheng Y., Gui P., Cui M., Liu W., Wang W., et al. (2019). Dynamic acetylation of the kinetochore-associated protein HEC1 ensures accurate microtubule-kinetochore attachment. *J. Biol Chem.* 294 576–592. 10.1074/jbc.RA118.003844
176. Zhao G, Oztan A, Ye Y, and Schwarz TL. (2019) Kinetochore Proteins Have a Post-Mitotic Function in Neurodevelopment. *Developmental Cell* 48: 873-882.